

AEDC-TR-70-92



**STUDY OF AN UNCOOLED NOZZLE
THROAT FOR A LARGE
HYPERSONIC WIND TUNNEL**

**P. B. Hasselquist, K. W. Smith, and D. G. DeCoursin
FluidDyne Engineering Corporation**

May 1970

This document has been approved for public release and
sale; its distribution is unlimited.

**ARNOLD ENGINEERING DEVELOPMENT CENTER
AIR FORCE SYSTEMS COMMAND
ARNOLD AIR FORCE STATION, TENNESSEE**

NOTICES

When U. S. Government drawings specifications, or other data are used for any purpose other than a definitely related Government procurement operation, the Government thereby incurs no responsibility nor any obligation whatsoever, and the fact that the Government may have formulated, furnished, or in any way supplied the said drawings, specifications, or other data, is not to be regarded by implication or otherwise, or in any manner licensing the holder or any other person or corporation, or conveying any rights or permission to manufacture, use, or sell any patented invention that may in any way be related thereto.

Qualified users may obtain copies of this report from the Defense Documentation Center.

References to named commercial products in this report are not to be considered in any sense as an endorsement of the product by the United States Air Force or the Government.

STUDY OF AN UNCOOLED NOZZLE
THROAT FOR A LARGE
HYPERSONIC WIND TUNNEL

P. B. Hasselquist, K. W. Smith, and D. G. DeCoursin
Fluidyne Engineering Corporation

This document has been approved for public release and
sale; its distribution is unlimited.

FOREWORD

The work reported herein was sponsored by Arnold Engineering Development Center (AEDC), Air Force Systems Command (AFSC), under Program Element 62402F, Project 3012, Task 07. Technical monitoring at AEDC was under the direction of Mr. Gottfried M. Arnold and Mr. Forrest B. Smith.

The research was performed by Fluidyne Engineering Corporation, Minneapolis, Minnesota, under Contract AF 40 (600)-1186.

One subcontract - for the development of a computer program for thermal stress computation - was let to the Illinois Institute of Technology Research Institute. IITRI Final Report M6201, Analysis of Thermal Stresses in Rectangular Blocks, summarizes their work. This report is included as Appendix I.

This technical report has been reviewed and is approved.

Forrest B. Smith, Jr.
Research Division
Directorate of Plans
and Technology

Harry L. Maynard
Colonel, USAF
Director of Plans
and Technology

ABSTRACT

A study was made of the feasibility of an uncooled throat for a large hypersonic wind tunnel facility using currently available materials. Maximum fullscale stagnation conditions would be: 2000 psi, 4400°R, 1500 lb/sec air flow, and throat diameter 10.5-inches. The basic throat concept was that of a ceramic insulation layer, composed of small pieces, that would form a protective liner within a metal structure. High resistance to thermal spalling was the material characteristic of greatest importance. Tests were made of several zirconia materials and two zirconium diboride compositions by exposing them to hot air flow in a sonic throat at maximum conditions of 800 psi and 3550°R. Behavior of the zirconia materials ranged from minor cracking to complete fragmentation. The zirconium-diborides did not crack and were oxidation resistant at these conditions. In addition, the thermal stress distribution was studied for the individual blocks that would form the throat insulation. For this purpose the three-dimensional stress distribution was calculated for mechanically unrestrained blocks having one-dimensional temperature distributions. Effects of temperature distribution, block size and block shape were determined. The computer program is included with the report. It was concluded that currently available materials are not satisfactory for a throat that would be used with no cooling. Some of the materials tested may be satisfactory if the thermal shock conditions were reduced by use of film cooling (less than that required for a back-side cooled throat) and by preheating with a flow of air through the throat during heater pressurization. A major problem in use of zirconia would be the attachment of the insulation layer to the backup structure. Use of zirconium-diboride would require a design concept that would be compatible with its high thermal conductivity. Both materials might be used to advantage in a single design.

TABLE OF CONTENTS

	Page
FOREWORD	ii
ABSTRACT	iii
LIST OF TABLES	vi
LIST OF FIGURES	vii
I. INTRODUCTION	1
II. PRELIMINARY CONSIDERATIONS	2
2.1 Mach 7 Nozzle and Valve	2
2.2 Uncooled Throat Concept	3
2.3 Heat Transfer Reduction	3
2.4 Test Program and Analysis	4
III. TEST PROGRAM	6
3.1 Facility and Test Apparatus	6
3.2 Test Specimens	7
3.3 Test Procedures	9
3.4 Test Results	10
3.4.1 Phase I Tests	10
3.4.2 Phase II Tests	13
3.5 Conclusions From Test Results	15
IV. THERMAL STRESS ANALYSIS	17
4.1 Introduction	17
4.2 Thermal Stress Parameters	18
4.2.1 Temperature Distributions	18
4.2.2 Block Shape and Size	19
4.3 Computer Program	20
4.3.1 Assumptions	20
4.3.2 Problem Specifications and Input - Output Data	21
4.4 Calculation Results	22
4.4.1 Effect of Curvature of Temperature Profile	23

	Page
4.4.2 Effect of Block Size and Shape	24
4.4.3 Variation of Stresses with Time During Run	25
4.4.4 Principal Stresses and Maximum Shear Stresses	25
4.4.5 Variation of Stresses with Material Properties	26
4.4.6 Computer Program Use	26
4.5 Conclusions From Stress Analysis	27
V. CONCLUSIONS	29
REFERENCES	31
APPENDIX I - ANALYSIS OF THERMAL STRESSES IN RECTANGULAR BLOCKS	75
APPENDIX II - DESCRIPTION OF MODIFIED THERMAL STRESS COMPUTER PROGRAM, TPA II	124

LIST OF TABLES

<u>Table</u>	<u>Description</u>	<u>Page</u>
I	Summary of Test Specimen Materials	32
II	Summary of Uncooled Throat Runs	33
III	Specifications for Thermal Stress Computer Runs	34
IV	Input Data for Computer Runs 9, 10 and 11	35
V	Input Data for Computer Run 12	36
VI	Input Data for Computer Runs 15 and 16	37
VII	Comparison of Calculated Stresses Resulting From a Linear Temperature Curve and the 40- Second Temperature Curve	38

LIST OF FIGURES

<u>Figure</u>	<u>Description</u>	<u>Page</u>
1	Schematic Sketch of Facility Setup	39
2	Uncooled Throat Test Arrangement	41
3	Photograph of Test Apparatus	43
4	Backpressure Throat Design, Drawing 0528-601	44
5	Test Specimen Holder, Drawing 0528-602	45
6	Retainer Design, Drawing 0528-005	46
7	Uncooled Throat Cooling Water System, Drawing 0528-608	47
8	Pretest Material Specimen Photographs, Phase I	48
9	Pretest Material Specimen Photographs, Phase I	49
10	Pretest Material Specimens, Phase II	50
11	After Run Material Specimen Photographs, Phase I	51
12	After Run Material Specimen Photographs, Phase I	52
13	After Run Material Specimen Photographs, Phase I	53
14	After Run Material Specimen Photographs, Phase II	54
15	After Run Material Specimen Photographs, Phase II	55
16	After Run Material Specimen Photographs, Phase II	56
17	After Run Material Specimen Photographs, Phase II	57
18	Transient Temperatures in Uncooled Throat Ceramic Elements	58
19	Temperature Distribution in Bed and Insulation of a Cylindrical Ceramic Storage Heater	59
20	Subdivisions of a 2 x 2-inch Plan Form to Study Effects of Plan-Form Size and Shape on Thermal Stresses	60
21	Block Geometry and Subdivisions	61
22	Coefficient of Thermal Expansion Versus Temperature	62
23	Modulus of Elasticity Versus Temperature	63
24	Piecewise Constant Temperature Distributions for Studying Effect of Kind of Temperature Curve on Thermal Stress Dis- tribution (Computer Runs 9, 10) (Constant Material Properties)	64

<u>Figure</u>	<u>Description</u>	<u>Page</u>
25	Thermal Stress Versus Curvature of Temperature Profile. Computer Runs 9, 10 and 11	65
26	Thermal Stress Versus Block Thickness. Computer Runs 2, 12 and 6	66
27	Variation of Maximum Stresses with Plan Form Dimension and Thickness	67
28	Thermal Stress Versus Plan Form Size. Computer Runs 4, 2, 5 and 13	68
29	Thermal Stresses Versus Plan Form Shape. Computer Runs 2, 7 and 14	69
30	Thermal Stress Versus Time for Instant Tunnel Start. Computer Runs 1, 2 and 3	70
31	Principle Stresses Near Heated Surface. Computer Run 2	71
32	Principle Stresses 0.3-Inch from Heated Surface. Computer Run 2	72
33	Thermal Stress Versus Material Properties. Computer Runs 3 and 8	73

SECTION I

INTRODUCTION

This program was carried out as part of the development effort for a large hypersonic wind tunnel facility. This facility would provide for large scale hypersonic aerodynamic and propulsion system testing under conditions duplicating actual flight. The necessary high stagnation temperatures would be achieved by heating high pressure air in a regenerative heater, using refractory materials for the matrix.

One of the nozzles for this facility would yield Mach 7 flow and would have an exit diameter of 12 ft. The corresponding flow rate would be 1500 lb/sec at stagnation conditions of 2000 psi and 440°F. The heat flux (cold wall) at the throat would be about 3000 BTU/ft²sec.

The throat section for this nozzle would be one of the more critical components of the facility because of the combination of high thermal loads, high mechanical loads and large size. One design concept would be an all metal structure with backside water cooling and air film cooling. Preliminary design work has indicated that the air film cooling requirement would be equal to about 25% of the mainstream flow. This large film cooling rate could significantly reduce the useful test region size and, therefore, alternate solutions are sought.

One alternative would be to use refractory ceramics and/or metals in a throat section so designed that air film cooling would not be needed. It was the purpose of the work reported herein to examine the feasibility of this uncooled throat concept. Further, the purpose was to establish the feasibility of existing materials, as opposed to the development of new materials.

SECTION II

PRELIMINARY CONSIDERATIONS

2.1 MACH 7 NOZZLE AND VALVE

At the time this work began, a preliminary design of the wind tunnel facility was available. The design incorporated a plug valve with the Mach 7 nozzle. This valve seated on the subsonic contraction and was to open by being retracted into the stilling chamber. The valve would allow a "fast start" of flow through the nozzle by remaining closed until the heater had been pressurized to the desired tunnel stagnation pressure. Alternately, the valve could remain open during heater pressurization. In this case air would flow through the nozzle as soon as pressurization began.

Some pertinent dimensions of the nozzle are: overall length 85 ft, stilling chamber diameter 8 ft, exit diameter 12 ft, throat diameter 10.5-inches. The plug valve would seat 1-1/2 ft upstream of the throat, where the diameter is about 16-inches.

The nozzle was designed in sections. The sections of interest here are the three that formed the subsonic contraction and throat. These were: 1) the contraction section, being the upstream portion of the subsonic contraction; 2) the plug valve seat section, being a continuation of the subsonic contraction; and 3) the throat section. The throat section was 8-1/2 ft long, with an upstream diameter of 14-inches and a downstream diameter of 34-inches.

Cooling provisions were as follows: contraction section backside water cooled; plug valve seat air film cooled with slot located immediately upstream of seat; throat section backside water and air film cooled. Air for film cooling of the plug valve seat would aid in cooling the throat section, and additional air would be introduced through a slot located downstream of the plug valve seat. The film cooling requirements at design condition (2000 psi, 4400°R, 1500 lb/sec) were 9% of the main-stream flow at the upstream slot and 16% at the downstream slot (135 lb/sec and 240 lb/sec, respectively).

The change to an uncooled throat would involve at least the replacement of the 8-1/2 ft long throat section. If the plug valve seat were retained, its film cooling would cause some reduction in heat transfer to the throat. If the seat section were not retained, or if a means of eliminating entirely all air film cooling were found, the heat transfer rates would not be reduced. The maximum rates would occur during a fast start of flow with an initially cold throat. This case was assumed for the theoretical analysis. It was not possible to produce such large rates in the test apparatus.

2.2 UNCOOLED THROAT CONCEPT

The basic concept for the uncooled throat is that of a metal structure lined with a ceramic insulation material. The metal structure would accommodate the mechanical loads from internal pressure and other sources. It would also provide means of attachment to mating nozzle sections and would provide the necessary stiffness in bending.

The ceramic liner could be either a continuous surface or could be composed of separate pieces. The use of separate pieces decreases thermal stress levels and permits accommodation of thermal expansion through many joints. This approach is often used with brittle materials. (One configuration of the Dynasoar nose cap and leading edge thermal protection consisted of many small tiles of zirconia fastened to the backup structure.) It has the disadvantage of requiring some method of holding the insulation blocks in place.

Very few materials are available that can withstand 4000°F in an oxidation atmosphere. Examination of the possibilities resulted in zirconia being selected as the primary candidate. Zirconia has low thermal conductivity and, therefore, a layer one inch thick would provide sufficient insulation. On this basis the size of the insulation elements was selected as nominally a one inch cube.

2.3 HEAT TRANSFER REDUCTION

The thermal shock to the throat could be reduced by a reduction in the heat transfer rate. This could be achieved by the use of film cooling and/or by preheating the insulation layer.

Preheating methods can be divided into two classes: low rate where the heat is applied slowly and high rate where rapid heating is used. Low rate heating will not produce large temperature differences within the ceramics, but will raise the ceramic temperature level. This could be done by electric heaters within or behind the ceramic. Alternatively, heated gases could be passed through the nozzle throat. Still another possibility is to provide flow passages within the ceramic wall and parallel to the nozzle surface which could be used to duct preheat gases from their source to the heater or to a discharge vent.

Whatever the method, low level preheating would require a metal backup structure capable of operating at relatively high temperatures. For example, reduction of the heat transfer rate by a factor of two would require preheating to over 2000°F, which is too high for most metals.

The second approach to preheating would be to heat the throat at a relatively high rate, from the air side. This could be done most conveniently by starting nozzle flow with the hot valve open. That is, flow would pass through the throat during heater pressurization. The disadvantage would be a loss of facility run time.

Air film cooling would reduce the heat transfer rates and would also reduce the maximum temperature reached by the insulation layer. The effect of using the hot valve slot only, with 9% flow, is shown in the table below.

Wall temperatures with film cooling and heat transfer coefficients were calculated by the methods of References 4 and 5, respectively. In the case of heat transfer coefficients, the values predicted in Reference 5 were reduced by a factor of 2/3. This factor has been used to account for typical measured differences between actual rocket nozzles and simple hot air situations. See for example, Reference 6.

Distance Downstream From Throat Feet	Maximum Wall Temperature °F	Initial Heat Flux BTU/ft ² sec	
		with film cool.	without film cool.
0	2500	1900	3200
2	2900	1450	2000
4	3150	750	960
6	3250	380	470
8	3350	200	240

These values are based on stagnation conditions of 2000 psi and 4400°R. The initial heat flux values are based on a wall temperature of 300°F. It is apparent that this level of film cooling would significantly reduce the heat flux and the temperature level within the throat. Without film cooling, maximum wall temperature at the throat would be on the order of 4300°R. The heat flux levels and corresponding thermal shock conditions are still very high, far beyond conditions normally considered for ceramic materials.

2.4 TEST PROGRAM AND ANALYSIS

The thermal stress levels in the insulation layer would exceed the strength of available materials under even the most favorable conditions (small individual blocks with preheating and film cooling). Thus the most important characteristic required of the material is resistance to thermal spalling. Spalling resistance cannot be determined with currently available analytical methods. Most thermal stress resistance analyses are based upon prediction of conditions that will produce stresses equal to the strength, i.e., the initiation of cracks. Thermal spalling, on the other hand, occurs when the stresses exceed the strength, cracks

are initiated, and the amount of damage (spalling) depends upon the crack propagation characteristics of the material. Analytical methods, sufficient for design purposes, are not yet available for prediction of spalling damage. Tests must be used.

A special test setup was designed and fabricated for testing of candidate materials. The test arrangement simulated a small portion of the facility throat wall. The test specimens were small blocks equivalent in size to those that could be used in the fullscale throat. The specimens formed the two parallel sides of a two-dimensional slot throat, and were exposed to high temperature, high pressure air flow. This equipment, the tests, and the results are described in Section III.

Experience and qualitative reasoning indicated that small blocks would have greater spall resistance than large blocks. Information was needed on the influence of size and shape of block. Recognizing that an analysis of spalling itself could not be done, it was felt that a stress analysis would provide valuable insight.

The small blocks that would form the insulation liner would be essentially unrestrained in terms of mechanically applied loads. That is, the thermal stresses would be much higher than the mechanical stresses. Examination of the literature indicated that this case of thermal stress had not been published. Therefore, an analysis was undertaken. The stress analysis and computer programming was performed by the Illinois Institute of Technology Research Institute. This work is described in Section IV, and the report by IITRI is presented in Appendices I and II.

SECTION III

TEST PROGRAM

3.1 FACILITY AND TEST APPARATUS

The material tests were conducted at the Fluidyne Medicine Lake Laboratory. Ceramic specimens were tested by exposure to hot air flow from a zirconia storage heater. The uncooled throat apparatus was connected directly to the discharge outlet of the heater. There was no provision for a fast start of flow over the specimens (no "hot valve" at the heater outlet). Thus, hot air flowed over the specimens during heater pressurization.

A schematic of the heater system is shown in Figure 1. Air is stored at 5000 psi and throttled manually to the desired heater pressure. The air is heated by passing it through a bed of zirconia cored brick. The bed is heated with an air-oxygen-propane burner.

The uncooled throat test apparatus consisted of four major components: a ceramic nozzle entrance ring, a water cooled heater back pressure nozzle, a water cooled test specimen holder, and a water cooled retainer (diffuser section). The assembly of these components is shown in Figures 2 and 3.

The ceramic nozzle entrance ring was utilized to reduce the heater outlet passage to the 2.00-inch heater backpressure (slot) nozzle dimension. This ceramic ring was fabricated from partially stabilized calcia zirconia by the castable process.

The most critical component, from a safety viewpoint, was the watercooled throat (Figure 4). The purpose of this throat was to backpressure the heater. The throat itself is a slot, 1/10-inch wide by 2-inches high, located immediately upstream of the ceramic test specimens. Failure of the throat would allow increased flow through the heater, and possibly flotation of the heater bed.

The water cooled test specimen holder (Figure 5) was designed to hold the test specimens in place and allow minor adjustments to assure proper alignment and centering. Since the shape of the test specimens was changed between the two test phases, the holder internal cavity was modified prior to the second test phase. The hot air slot through the holder is formed by the installed test specimens on two sides and by the backside water cooled zirconium copper holder on the narrow ends of the slot.

The retainer, shown in Figures 2 and 6, is the water cooled diffuser section and provides spray cooling to cool the exhausting hot air. This retainer fastens directly to the large flange containing the

backpressure throat and thereby sandwiches the test specimen holder between the large flange and the retainer. Alignment between the three parts is maintained using dowel pins.

Detailed design of the metal surfaces exposed to hot air flow established a requirement for use of all available high pressure cooling water, 100 gpm at 900 psi. Furthermore, it was necessary to cool different components by passing the water through them in series. The metal surfaces protected by the ceramic test specimens were not cooled. These design compromises introduced an operating limit on stagnation pressure.

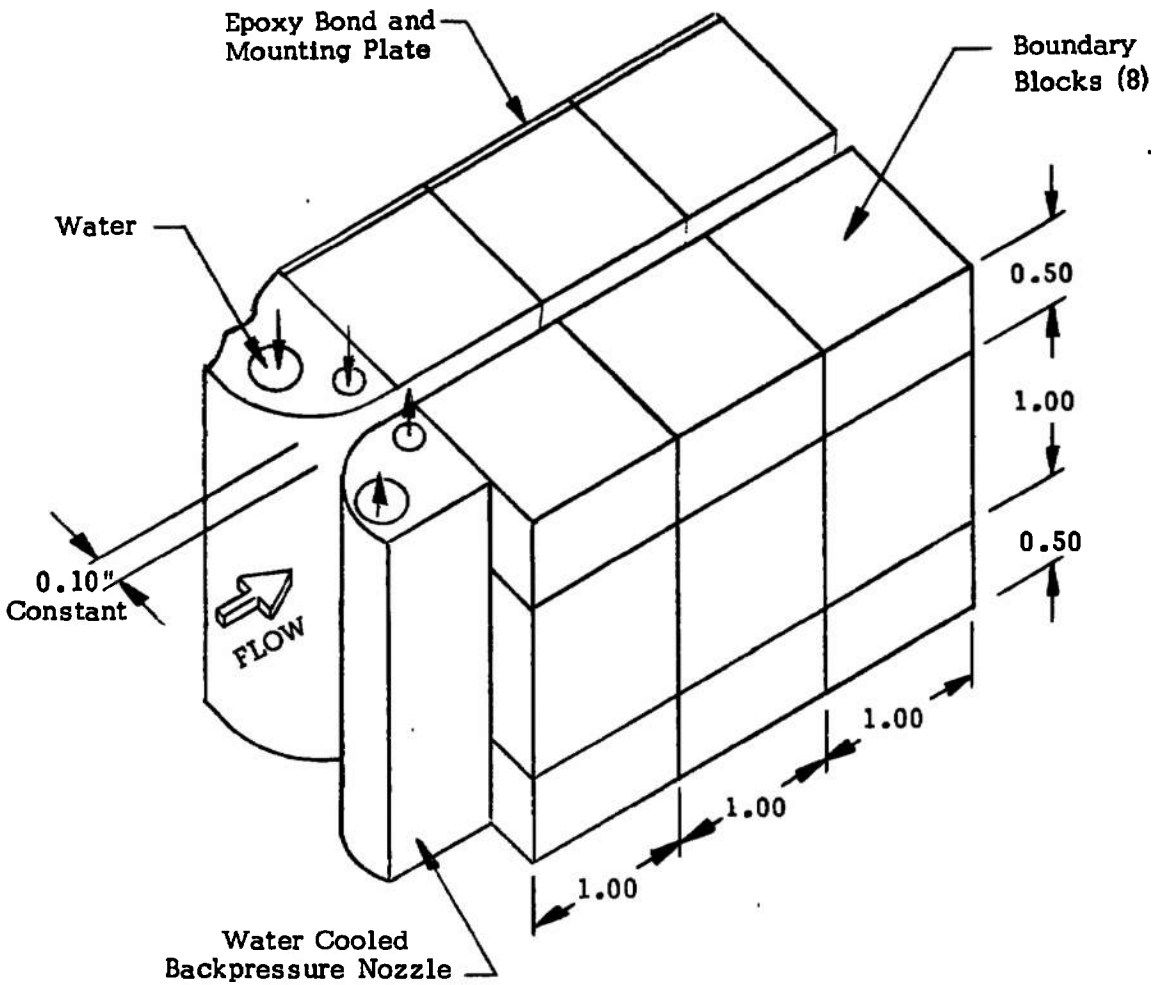
Safety of operation dictated that failure of the ceramic specimens under test not endanger the overall facility. Thus, damage to metal parts downstream of the backpressure throat would be tolerable, but loss of the throat itself would not be tolerable, because throat failure could cause flotation of the heater bed.

The integrity of the backpressure throat could be preserved, even with failure of the test specimens, if the throat cooling water was not affected. However, the throat cooling water and the ceramic specimen holder cooling water are in series. Failure of the ceramic specimens could result in overheating of the specimen holder. More specifically, O-rings that seal the water passages could overheat and leak. At stagnation pressures below about 1000 psi the leakage would be from water to air and therefore not harmful. At air stagnation pressures above 1000 psi the leakage would be air into the water passage. This would tend to restrict the water flow through both the ceramic holder and the backpressure throat.

Thus, 1000 psi was the maximum heater pressure for which a failure of the ceramic specimens could be sustained without a substantial risk to the heater. On this basis an upper test pressure limit of 800 psi was established.

3.2 TEST SPECIMENS

The test program was carried out in two phases, with some difference in the test specimen shapes. The arrangement used for Phase I is shown in the sketch below and in Figure 8. Two assemblies of nine pieces each form the sides of a slot 1/10-inch wide by 2-inches high. The slot was vertical to minimize the possibility of blockage of flow by spalled fragments. Separate pieces were used, with slight spacing, to accommodate thermal expansion and reduce stresses. Spacing was provided by metal shims near the cold side. The assemblies were placed in the specimen holder (Figure 5) and were partially held in place with copper dowels (Figure 8).



A simpler arrangement was used for the Phase II tests. The assemblies were replaced by one piece specimens (see Figure 10) and the dowels were eliminated. The overall shape was changed to trapezoidal. Specimens were held in place by shim plates and set screws acting on the slanting surfaces (see Figure 5).

Only three materials were tested in Phase II, yttria-zirconia and two zirconium diboride alloys. Thermal expansion slots were cut in the zirconia blocks (.010 wide by 1/2-inch deep), but not in the diboride blocks (Figure 10).

The materials tested were available without need for special development. They are not all available on a large scale. This is especially true of the wire reinforced zirconia and the zirconium diboride materials. A brief description of each material is given in Table I.

3.3 TEST PROCEDURES

The basic procedure was to start testing at low pressures and temperatures, examine the specimens after test, and proceed with more severe conditions if warranted. Stagnation pressures and temperature were recorded during the entire test sequence of heater pressurization, steady state run and depressurization.

Stagnation temperature was measured with a bare wire Pt-6RH/Pt-30 Rh thermocouple in the heater air outlet. This outlet is a zirconia insulated passage having a 3-inch internal diameter and is 2-1/2-feet long. The passage was preheated before each run to reduce temperature losses and reduce thermal stresses in the zirconia insulation.

It was not possible to observe the test specimens during the runs. They were located too far upstream in the apparatus. It was possible to observe the air discharge from the test apparatus. However, this viewing was partially obscured by jets of water, which discharged into the airstream for cooling purposes. The combination of the partially obscured viewing and sound was helpful in indicating failure of specimens on several occasions.

Pressurization rates were slower than normal because of the desire to detect some indication of failure during pressurization. Depressurization times varied widely because the heater is partly depressurized by opening a valve in the heater exhaust stack, allowing air to flow out the bottom of the heater. This was not done on a regular schedule, which caused variations.

The test specimen holder, with the specimens, was removed after each run. The specimens were examined without removing them from the holder unless a change was needed for the subsequent test. During this between run period the heater bed was reheated. The specimen holder, with specimens, would be replaced after the desired heater bed temperature was reached.

The heater outlet passage was then preheated by flowing combustion gases. These gases were withdrawn just upstream of the heater backpressure throat, through a side opening in the pipe. During this period the test specimens were cooled by flowing air over them from the open downstream end.

After completion of preheating, the specimen cooling air line was removed and the heater pressurization was started. If unusual sights or sounds were detected during pressurization, the run was terminated. Observation continued during the run on the same basis.

3.4 TEST RESULTS

All the tests reported herein were made at throat heat transfer rates substantially less than that corresponding to the fullscale wind tunnel conditions. The fullscale cold wall heat flux would be about 3000 BTU/ft²sec at stagnation conditions of 2000 psi and 4400°R. The cold wall heat flux values for the test varied from 400 to 1800 BTU/ft²sec.

Cold wall values apply only if flow is established very quickly, and with the wall initially cold, i.e., room temperature. This is possible with a hot valve, as discussed in Section 2.1. Flow through the throat during heater pressurization reduces the heat transfer rates from the calculated cold wall values. In the following discussion, cold wall heat flux values are cited for comparison purposes. However, the actual heat flux rates during the tests were less than these values, and this fact must be considered in examining the results for application to fullscale conditions.

The specimens that were tested are identified in Table I. A summary of the test conditions is given in Table II. Photographs of the test specimens before and after tests are presented in Figures 8 through 17. The damage in some instances is not apparent from the photographs, but is described below.

3.4.1 Phase I Tests

Tungsten-Rhenium Wire Reinforced Zirconia

Specimens 1 and 2. Runs 1, 2, 3. Figures 8 and 11. Cold wall heat flux 400 to 500 BTU/ft²sec.

Oxidation of the wire reinforcement is a basic limitation of this material. It was hoped that specimens of low porosity could be tested, These would have wires exposed only at the surface and, therefore, would provide the least exposure to oxidation.

However, the specimens that were available and tested had large lamination-type pores that exposed wires well below the surface. Under test the specimens swelled and began to flake. Additional testing would have caused spalling and further oxidation.

The zirconia material was a low thermal expansion composition, and was chosen for this reason. Low thermal expansion would reduce thermal stresses and enhance the probability of success. These low expansion compositions are discussed further below.

Medium Grain Size Zirconia

Specimens 3 and 4. Run 4. Figures 8 and 11. Cold wall heat flux 650 BTU/ft²sec.

Specimen 3 was castable calcia-zirconia and Specimen 4 was castable yttria-zirconia with maximum grain size of 60 mesh. Both spalled severely to a depth of 1/8 to 1/4-inch. The yttria-zirconia is at the left side of the photo in Figure 11.

Fine Grain Dense Zirconia

Specimens 5 and 6. Runs 5, 6, 7, 11. Figures 8 and 11. Cold wall heat flux 450 to 1000 BTU/ft²sec.

This material is a very dense (about 5% porosity) partially stabilized zirconia formulated to have a low thermal expansion coefficient. The principal stabilizers are magnesia and calcia. Thus the compositional stability at high temperatures is limited. Whether the life would be adequate for an uncooled throat is still uncertain.

This material is currently used in several commercial applications. It was selected in order to try a dense material, recognizing that cracks could not be avoided. The low thermal expansion characteristics would enhance the probability of success.

The tests produced a mosaic pattern of hairline cracks, spaced about 1/4-inch. There were some open cracks in the side pieces and spalling of one downstream piece. Some of the cracks entered the surface at shallow angles, indicating that more severe tests would cause spalling.

This material may be suitable for small throats, especially if an initial heat shock can be used to precrack the material (Reference 1). In a large throat, it is unlikely that a crack pattern could be produced that would relieve stresses and not allow spalling.

Coarse Grain Calcia-Zirconia

Specimens 7 and 8. Runs 8 and 15. Figures 9, 11, 13. Cold wall heat flux 650 and 1100 BTU/ft²sec.

This material is a partially stabilized castable zirconia. It is used very successfully in wind tunnel air heaters as dense insulation. In this application it has shown excellent resistance to thermal spalling. The large grain size (to 8 mesh) is a disadvantage for the present application. It does not provide a smooth surface, and it is difficult to maintain corners and edges even without severe thermal stress conditions. For this reason a finer grain 60 mesh material was also included in the tests. However, its performance was unsatisfactory, (Specimen 3).

The test of Run 8 produced some spalling of Specimen 7, as shown in Figure 11, but no spalling of Specimen 8. This indicates that the material may not have the uniformity needed for a large throat application. A second test was made with Specimen 8. This test, Run 15, did not produce useful results because of partial melting of the copper dowels (Figure 13).

Coarse Grain Magnesia-Calcia-Zirconia

Specimens 9 and 10. Runs 9, 10, 14. Figures 9 and 12. Cold wall heat flux 650 to 950 BTU/ft²sec.

This material was also a castable, similar to the calcia-zirconia discussed above, but with the magnesia and calcia stabilizers also mentioned earlier. Its behavior was similar to the coarse grain calcia-zirconia. Fine cracks were found on some of the pieces, and there was a slight amount of spalling, about 1/32-inch deep. This can be seen in the center piece in the upper left hand photo in Figure 12.

Medium Grain Magnesia-Calcia-Zirconia

Specimen 11. Runs 11 and 15. Figures 9, 12, 13. Cold wall heat flux 1000 to 1100 BTU/ft²sec.

This material differed from that discussed immediately above only in maximum grain size, having an upper size of 60 mesh. The specimen survived Run 11 with no visible damage. Run 15 did not produce useful results because of melting of the copper dowels.

These results are quite different from those of Run 4, with the 60 mesh castable calcia-zirconia and yttria-zirconia. The difference could be attributed to the lower thermal expansion coefficient of the 1027 type composition. But there is not enough information to determine the reason for the difference in performance.

Pressed Magnesia-Zirconia

Specimens 12 and 13. Runs 12 and 13. Figures 9 and 12.
Cold wall heat flux 850 to 1100 BTU/ft²sec.

This material is another composition having low thermal expansion characteristics. It was fabricated by pressing, as was the fine grain dense zirconia. The tests caused formation of fine cracks, but no spalling occurred. It is uncertain whether the cracks would lead to spalling after repeated thermal stress cycles.

3.4.2 Phase II Tests

Yttria-Zirconia

Specimens 14, 15, 16 and 17, Runs 1 and 5. Figures 10, 14, 16. Cold wall heat flux 1000 BTU/ft²sec.

These specimens were prepared in an attempt to produce a material that would have high resistance to thermal spalling. A combination of fine and coarse grains were used in an effort to impart resistance to crack propagation. The composition was fully stabilized yttria-zirconia.

The results clearly demonstrated that the objective was not achieved. In fact, this material suffered the most complete destruction of any materials tested. The test specimens were completely shattered during Run 1. A repeat run was made, which confirmed this result.

The extent of the damage is evident from the photographs (Figures 14 and 16). An examination of the material, after test, was made to determine if phase inversion had contributed to the failure. The monoclinic content was measured at three locations, hot face, center and cold face. All values were one percent. Hence, the failure was caused by thermal stresses, not by phase inversion.

Zirconium-Diboride

Two zirconium-diboride compositions were tested. These compositions were selected from a family of materials that have been developed by ManLabs under Air Force Contract AF33(615)-3671.

The materials were tested in an effort to determine whether their oxidation resistance would be sufficient for this application. Oxidation protection is provided by a layer of zirconia which forms upon exposure to oxygen, and which provides a barrier to further oxidation. If this coating does not spall under test, thereby exposing parent material to catastrophic oxidation, the material could probably be used in throat construction.

The diborides tested have much higher thermal conductivities than zirconia. Their conductivities lie in the range 35 to 65 BTU/ft.hr^oR, and therefore, are roughly twice as high as that of carbon steel. The high conductivity imparts thermal shock resistance, but does not provide thermal insulation qualities. The question of how this material could be used in an "uncooled" throat was not broached. It was judged of first priority to determine if the material itself was useful.

ManLabs material V, Specimens 18 and 19, were tested in Runs 2, 3 and 9 at cold wall heat fluxes from 850 to 1600 BTU/ft²sec. ManLabs material VIII, Specimens 22 and 23, were tested in Runs 4, 6, 7 and 8, at cold wall heat fluxes from 1000 to 1800 BTU/ft²sec. The specimens after test are shown in Figures 15 and 17.

The high thermal conductivity of the test specimens required that the copper specimen holder be protected by insulation. Layers of zirconia, 1/4-inch thick, were placed between the test pieces and the copper surfaces. In addition, stainless steel metal shim plates were placed outside the zirconia insulators (see Figures 15 and 17). These shim plates acted as bearing plates for set screws that held the assemblies in position.

All four test specimens survived the early test without damage. A layer of grayish zirconia was visible on the wetted flow surface (see Figure 15).

During the last run with each pair of specimens, Runs 8 and 9, the air discharge from the test apparatus became brilliant white, and the test in each case was terminated. In each case the downstream end of one of the specimens had oxidized (Figure 17). These specimens were examined by ManLabs in an effort to understand the cause of the failure. We also examined photographs that were taken after each run.

The cause of the failure was reaction of iron oxide with the protective zirconia layer. Iron oxide and zirconia form a eutectic at 2380°F, which is well below the temperature of the test. Thus the zirconia-iron oxide layer would be sloughed off, exposing the diboride material to the high temperature air stream. Under these conditions of high temperature and high shear, the protective zirconia layer apparently cannot form, allowing continuous oxidation and erosion.

The iron oxide undoubtedly came from the stainless steel shim pieces in the following way. Examination of the after run photographs showed that the 1/4-inch zirconia insulators were eroded near the throat exit. This erosion would allow flow along the sides of the specimens, which would continue erosion of the zirconia insulators. Eventually this bypass flow would reach the steel shim plates. At this point the plates would oxidize, and the iron oxide would be carried into the stream, and into the wake behind the test specimens. There it would combine with the zirconia layer on the diboride specimens.

The flow conditions and time required to produce the failures depended upon the structural integrity of the down stream zirconia insulators. Thus the conditions at which the failures occurred bear no relationship to maximum conditions that the zirconia diboride can tolerate. The failures do emphasize the importance of not contaminating the oxide layer on these materials.

3.5 CONCLUSIONS FROM TEST RESULTS

In examining the results of these tests, it must be remembered that the test conditions were not as severe as those corresponding to the fullscale wind tunnel facility. Hence, the results can be described, but extrapolation to more severe conditions is difficult. The results and conclusions are summarized as follows:

1. The tungsten wire reinforced zirconia that was tested is not suitable for this application because excessive porosity allows oxidation of the wires. Whether a less porous material would be satisfactory is unknown.
2. The behavior of different zirconia materials varied greatly, from only minor cracking to complete fragmentation.
3. A very dense zirconia (about 5 percent porosity) in four tests developed a pattern of tight cracks, but did not spall excessively. Intentional precracking by thermal shock could make this a useful material for small throats. For a larger throat, with a segmented structure, the extensive cracking would probably lead to spalling.
4. Some of the medium and coarse grain zirconias of nominally 25 percent porosity showed little or no spalling and, therefore, show promise. These materials were partially stabilized with calcia and/or magnesia. The magnesia stabilized materials have low thermal expansion characteristics which is highly desirable. On the other hand, these compositions are not stable at high temperatures. Therefore, further information on both spalling resistance and life at high temperatures would be needed to determine their suitability.
5. Zirconium diboride was tested to stagnation conditions of 800 psi and 3550°R without failure. This material has potential for throat construction if a design can be devised that would be compatible with its high thermal conductivity.
6. On the basis of this work and other work with ceramics, it is the authors' opinion that no commercially available material meets the requirements for the most severe conditions of an uncooled throat for hypersonic wind tunnel facilities. Some

reduction in thermal shock would be necessary, most probably by film cooling, especially during the initial flow period when heat transfer rates are high. The cooling rate could be reduced after this initial flow period. Preheating by flowing gases through the throat during heater pressurization would also reduce stresses. This method would cause some reduction in facility run time.

SECTION IV

THERMAL STRESS ANALYSIS

4.1 INTRODUCTION

In parallel with the test program, an analytic study of thermal stresses was performed. This study consisted basically of development of a computer program and then use of the program to obtain numerical solutions for a variety of cases based on the full scale wind tunnel throat.

The computer program was developed under subcontract by the Illinois Institute of Technology Research Institute. Dr. M.A. Salmon of IITRI directed development of the program and running of the initial solutions. IITRI Final Report M6201, Analysis of Thermal Stresses in Rectangular Blocks, summarizes their work. This report is included as Appendix I.

The necessity of undertaking this analytical study stems from a basic scarcity of thermal stress information on unrestrained solids. This class of problems is particularly difficult to analyse (especially so because the stress field is three dimensional); hence almost no information is available in the literature. Developments in finite-element theory have resulted in the ability to analyse thermal stresses in externally unrestrained solid bodies such as the ceramic elements of the present uncooled throat concept.

The model used in the analysis is a right parallelepiped (Figure 21) with a one dimensional (in the direction of one of the major axes) temperature distribution. In the analysis the parallelepiped is subdivided into a larger number of smaller parallelepipeds which are in fact the finite elements. The material properties can be allowed to vary with temperature.

In applying this analysis to high temperature situations, it is essential to keep in mind that the analysis is based strictly on elastic theory. Effects of plastic deformation in reducing stress levels, and in causing residual stresses are ignored.

The underlying purpose in performing the analytical study was to improve the basic understanding of the stress fields within the ceramic elements. Qualitative (and to a useful extent quantitative) information can be gained, for instance on the relationships of stresses to temperature profile, geometry, material properties, etc. Knowledge of these relationships can be used to guide selection of shapes, operating procedure, etc.

4.2 THERMAL STRESS PARAMETERS

As described in other parts of this report, the uncooled throat concept pursued in this program is one of a large number of small ceramic elements as opposed to a monolithic throat structure. Each element is to be held in place with essentially no external restraints to thermal growth of the element. Even though external restraints are assumed not to exist, large thermal stresses can be produced in a solid element such as the parallelepiped configuration employed. Thermal stresses in such a body arise due to nonlinear temperature variations through it. An elastic body with constant properties experiences no thermal stresses if it is subjected to a linear (in cartesian coordinates) temperature variation.* When the temperature distribution is nonlinear, however, thermal stresses arise. Reference 3 contains derivations and proofs of the above relationships.

Broadly speaking, the magnitude of the thermal stresses depends on the amount by which the actual temperature distribution deviates from being linear. Furthermore, the quality of the stress field (distribution of compressive or tensile stresses) will depend on whether the curvature is positive or negative (i.e., the algebraic sign of the second derivative of the temperature distribution).

Again in general terms, the stresses within a block will depend on:

1. Temperature distribution through the block.
2. Overall size and shape of the block.
3. Material properties; modulus of elasticity, Poissons ratio and coefficient of thermal expansion.

4.2.1 Temperature Distributions

Figure 18 shows the time-temperature history for blocks of the facility uncooled throat. The calculation assumes an instantaneous start of flow at 2000 psi and 4400°R. It, therefore, assumes use of

*Another useful property of thermal stress behavior is that superposition of thermal stresses resulting from different temperature profiles applies. Since a linear distribution induces no stresses, any linear temperature distribution can be superimposed on an existing temperature profile without altering the stresses. In this way stress fields can sometimes be more easily visualized.

a hot valve and is the most severe thermal shock conditions that the facility could produce. It was selected for calculation purposes even though the stress levels reach values, in some instances, well above the strength of available materials. Stresses that exceed the material strength do not necessarily cause spalling. Furthermore, the primary purpose of the analysis was to gain an understanding of the stress field.

Note that as the time increases, the hot wall temperature increases, but the value of second derivative of the temperature curve decreases. Therefore, stresses near the heated surface will decrease with time. After a run is completed, the inner surface of the throat will begin to cool, with the result that the temperature curve near this surface will become reversed in curvature. Stresses near the surface will then change from compressive to tensile.

Another example of positive and negative temperature curvature, important to the wind tunnel facility, is shown in Figure 19. This figure shows the radial temperature distribution in the matrix and insulation of a storage heater. Note that this curve has a negative second derivative within the matrix, but a positive second derivative within the insulation.

One result of the analysis was to determine the effect of positive and negative temperature curvature on the stress field in unrestrained blocks. As will be seen, positive curvature causes compressive stresses at the surface, and negative curvature causes tensile stresses at the surface.

4.2.2 Block Shape and Size

Shape and size of an elastic body can significantly affect the magnitude of thermal stress it experiences. In the gross sense, increases in body dimensions will produce larger deviations (from linear) of the temperature profile and also dictate the development of larger internal strain. Both of these factors cause an increase in stress. The shape of a body is important. If one of the dimensions are small compared to the other two, the stress field will tend to be two-dimensional. A change in shape can significantly affect the stress field, depending on the orientation of the change with respect to the direction in which the temperature varies.

For a given one-dimensional temperature distribution and a given plan form of brick, the computer analyses investigated three bricks 1" x 1" in planform, and 1", 1/2", and 1/4" thickness. Consideration of the thickness variable is important because of the following reasons. The best design will result from a compromise of all three considerations.

1. The temperature at the back-side (cold side) must be low enough to be compatible with the adjacent material, and also compatible with the type of bonding or fastening to be used.
2. It is desirable that strains on the backside surface are at a low level to prevent bond failure between the ceramic blocks and the backup material.
3. The thickness variable will have an effect on the maximum thermal stress magnitudes. The thickness should be small enough to reduce maximum tensile and shear stresses (or, more properly, strains) to a tolerable level.

For a given one dimensional temperature distribution and a given thickness of block, the magnitude and distribution of thermal stresses will vary with a change in the planform size and shape of a block. The computer analysis investigated a block 1" thick and 2" x 2" in planform (hot face), then subdivided the block as shown in Figure 20. These results provide information needed to establish a maximum planform size and shape.

4.3 COMPUTER PROGRAM

The program developed obtains thermal stresses created within a rectangular block by the variation of temperature and material properties in one direction. The governing equations are formulated by means of the finite-element method and then solved by the Gauss-Seidel iterative method. A description of the theory and program TPA appears in Appendix I. A revised program TPA II is described in Appendix II.

The method essentially divides the block into a number of elements as shown in Figure 21. Symmetry allows analysis of only one quadrant of the block, permitting greater accuracy for a given number of elements.

The original program, termed TPA was in FORTRAN IV for the IBM 7094 computer. The revised program, TPA II, is also coded in FORTRAN IV but for use on the CDC 6600 computer. TPA II permits a much greater subdivision of the blocks and correspondingly greater accuracy. The CDC 6600 machine has a larger core storage, permitting use of more nodes plus more rapid execution. The program conversion was performed by IITRI.

4.3.1 Assumptions

At least three factors affect the accuracy of the thermal stress calculations.

1. The number of subdivisions of the rectangular block used in calculating the thermal stresses affects the accuracy of the calculations. In general, the capabilities of program TPA II are sufficient to reduce errors to acceptable limits.
2. The analysis is an elastic analysis, which assumes that stress is proportional to strain. The effects of creep and plastic flow are not considered. For the types of ceramics considered in the report, plastic flow occurs only at high temperatures ($> 2000^{\circ}\text{F}$). Also, because of the steep temperature profile, only a small layer of the block is at temperatures greater than 2000°F . Thus the analysis is a reasonable and generally conservative approximation to the true case.
3. Material property data for temperatures in excess of 2000°F are not readily available. The analysis uses estimated and extrapolated values for high temperatures. The property data most in doubt are the modulus of elasticity and Poisson's Ratio. Thus these "estimated" values also contribute to the uncertainty of final calculated results. All computer runs were made for calcia stabilized zirconia with a porosity of 0.05. Coefficient of thermal expansion and modulus of elasticity data are shown in Figures 22 and 23. Due to lack of published data of Poisson's ratio versus temperature, a constant value of 0.29 was used. All of the above property values were based on Reference 2.

4.3.2 Problem Specifications and Input - Output Data

Table III gives a summary of the runs for the block thermal stress analyses. Succeeding graphs and tables show material property data, temperature distributions, and stress data from the computer runs. A total of 16 computer runs were made. Runs 1 through 8 were completed by IITRI on an IBM 7094 computer using TPA. Runs 9 through 16 were run on a CDC 6600 computer by CDC in Minneapolis using TPA II. Description of input data is given Tables IV, V and VI and in Appendixes I and II.

The initial output is an echo of all input data. Following this, the applied nodal forces and starting values for the displacements are printed out, and then whatever intermediate output the user specifies.

The final output consists of the displacements and stresses. The stresses are computed and printed at the centroids of all elements. Program TPA also gives stresses at the centers of all outside element faces. TPA II gives only stresses at the centroids of all elements. IITRI later advised that the stresses at the outside faces should be disregarded in TPA. Better values are obtainable by extrapolating from the interior to the surface.

The output for each given point includes:

1. The three orthogonal normal stresses .
2. The three orthogonal shear stresses .
3. The three principal stresses and their direction cosines .
4. The "effective" stress , defined as

$$s^2 = (\sigma_{xx} - d)^2 + (\sigma_{yy} - d)^2 + (\sigma_{zz} - d)^2 \\ + 2\sigma_{xz}^2 + 2\sigma_{yz}^2 + 2\sigma_{xy}^2 .$$

$$d = \frac{1}{3} (\sigma_{xx} + \sigma_{yy} + \sigma_{zz})$$

The interpretation of the results of the analysis requires some care. The stresses in an element vary linearly in the direction of the coordinate axes. Since the stresses satisfy equilibrium only on the average it is probably most meaningful to consider stresses only at the center of the elements. Estimates of stresses at outside faces can best be made by extrapolating the results obtained at the centers of elements as one proceeds from the interior to the surface.

4.4 CALCULATION RESULTS

This section contains results of the computer analysis. It shows effects of analytically varying the following parameters.

1. Effect of curvature of temperature profile on the internal stress field .
2. Variation of stresses with block thickness .
3. Variation of stresses with plan size and shape of block .
4. Variation of stresses with time from start of run .
5. Principal stresses and maximum shear stresses .
6. Variation of stresses with material properties .

It may be noted here that the calculated stress distributions were examined to assure that they satisfied static equilibrium. That is, forces acting on any plane, and moments about any line in the plane, must be zero. That the results satisfy equilibrium was confirmed by hand calculations of a number of cases.

4.4.1 Effect of Curvature of Temperature Profile

Calculations were made to establish the qualitative effect of temperature profile curvature (i.e., positive and negative second derivatives) on stress distribution. Three temperature curves were used (Figure 24): one with positive curvature, which is the 40-second curve from Figure 18, a reversal of this curve, giving negative curvature, and a linear distribution.

The stress distributions are shown in Figure 25. Consider first the results for the positive curvature temperature profile (at the top of the page). Compressive stresses exist at the surfaces of the block, and tensile stresses exist near the center of the block.


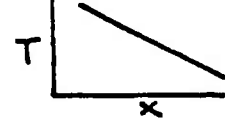

Examination of the stress distributions presented in later figures indicates that this is generally true. In some cases it appears the stresses approach zero at the side of the block, and may even become slightly tensile. But, in general, positive curvature of the temperature distribution produces compressive stresses on the surface and tensile stresses in the interior of a block.

The linear temperature distribution should result in zero stresses (see, for example, Reference 3). The calculated stresses are not zero because of the approximations in the computation method, especially the finiteness of the mesh.

The stress distribution for the negative curvature temperature profile is qualitatively the reverse of that for the positive curvature profile. Tensile stresses exist on and near the surfaces of the block, and compressive stresses exist near the center of the block.

We note also that the maximum stress levels occur in the portion of the block where the second derivative of the temperature distribution is the highest. Comparison of these and other results has also shown that the maximum stress is roughly proportional to the departure of the temperature curve from linearity.

In summary, the following conclusions are made:

Shape of Curve	Surface Stresses	Internal Stresses
	Compressive	Tensile
	Negligible	Negligible
	Tensile	Compressive

1. Stress roughly proportional to ΔT .
2. Maximum stress occurs in region of maximum second derivative of temperature curve.

4.4.2 Effect of Block Size and Shape

A general procedure for sizing a block in the throat insulation layer for acceptable thermal stresses would involve:

1. Select the minimum thickness of block consistent with allowable backside temperature.
2. Using the above thickness, select a reasonable planform size and shape that will result in acceptable thermal stresses.

Thus both thickness and planform are important. (Planform is the surface exposed to the heat transfer.)

The effect of thickness was examined by calculating stresses in 1 x 1-inch planform blocks having thicknesses of 1/4, 1/2 and 1-inch. These results depend strongly on the temperature distribution. In this case the 10-second curve of Figure 18 was used, with temperature dependent properties. For the 1/4 and 1/2-inch thicknesses, only the corresponding portion of the temperature curve, measured from the hot

face, was used. The results are shown in Figure 26. As expected, the stresses decrease as the thickness is decreased. The maximum stresses are plotted in the right hand portion of Figure 27.

The effect of planform size and shape was calculated for various blocks that were all one inch thick, and therefore all had the same temperature distribution. Thus the effect of temperature distribution was eliminated. The 10-second temperature curve of Figure 18 was used, with temperature dependent properties.

The effect of planform size is shown in Figure 28. The effect of planform shape is shown in Figure 29. The maximum stresses in both cases are plotted on the left hand side of Figure 27.

It is clear from these results that a reduction of only one planform dimension (Figure 29) is not very effective in reducing maximum stresses. Both dimensions must be reduced (Figure 28). The shape with the lowest stresses is rod-like, with the temperature varying along the length of the rod. (The $1/4 \times 1/4 \times 1$ -inch block in Figure 28 is equivalent to a rod suddenly heated at one end.)

4.4.3 Variation of Stresses with Time During Run

Figure 30 illustrates how the magnitude and distribution of thermal stresses changed during a wind-tunnel run. Initially, a thin section of the hot surface has very high compressive stresses. As the run progresses, the thermal stress field grows outward away from the hot surface. Maximum tensile stresses increase and maximum stresses (tensile and compressive) shift away from the hot surface. At a later period in time, both tensile and compressive stresses seem to decrease. This is a result of the temperature curve becoming more linear. The lower stresses are, however, offset by reduced strengths of the material at higher temperatures. The curves illustrate the complex nature of the thermal stress history. It is difficult to determine which portion of the run cycle represents a more severe condition for the blocks.

The stress levels are much higher than the strengths of ceramic materials. In an actual run the material would crack and thereby would relieve stresses. The relation between the calculated stress field and spalling is as yet unknown. The early high compressive stresses also indicate high shear stresses at the surface, which would contribute to spalling. The intermediate result shows high tensile stresses in the block interior. And finally, during the cool down cycle, tensile stresses will occur on the outside surfaces of the block. These could also contribute to cracking and spalling.

4.4.4 Principal Stresses and Maximum Shear Stresses

Figures 31 and 32 show the principal stress and maximum shear stresses for a $1 \times 1 \times 1$ -inch block and the 10-second temperature curve.

Information is given for $X = 0.07$ and $X = 0.3$, which are at or near the planes of maximum compressive and tensile stresses.

Comparison of these data with the 1 x 1 x 1-inch block of Figure 26 shows that the principal stresses are almost identical in magnitude with the stresses plotted parallel and perpendicular to the sides of the block. This means that for the cases studied, the principal stress vectors tend to have directions nearly the same as the three principal coordinate axes.

The maximum shear stress is equal to

$$\frac{\text{the maximum principal stress} - \text{the minimum principal stress}}{2}$$

and acts in the plane which bisects the angle between the maximum and minimum principal stresses. The shear stress is important because, in areas where the block is under high compressive thermal stresses, shear may be the mode of failure. Close examination of the direction cosines for the principal stresses, and the corresponding directions of the maximum shearing stresses, suggest that shear failures would occur in a manner to round off, or break corners off, the rectangular block. This is also intuitive, and in fact does often happen.

4.4.5 Variation of Stresses with Material Properties

The purpose of this comparison was to evaluate the effect of reduced modulus of elasticity at high temperatures on the overall thermal stress pattern. Both plots shown on Figure 33 used the 40-second temperature curve and were calculated using nonequal layer divisions.

The stress fields show that utilization of correct material properties is important for the hot surface region. For the case in question, stresses differ by a factor of two in the high compressive regions. However, note that thermal stresses in the remainder of the block are not significantly different.

Also note that the results based on temperature dependent material properties have reduced thermal stresses at the surface. This arises from the fact that modulus of elasticity decreases more than the total strain increases near the surface.

4.4.6 Computer Program Use

As previously indicated, two variations of the program are available for stress calculations: TPA and TPA II. TPA II is the desired program both in terms of capability and overall cost.

For blocks near cubic in shape, and using 5 by 5 nodal points with 10 layers, and an error tolerance of $1.500 \text{ E-}04$, the program converges in about 50 to 70 iterations. Increasing the number of layers to 20 about doubles the number of iterations required (i.e., about 100). When the element shape deviates significantly from a cubic shape, the number of iterations becomes greater, and may take considerably more than 100 to converge. Also, for a given error tolerance, the number of iterations required for convergence will increase as the total temperature difference across the block increases.

Three runs were made with linear distributions to evaluate the calculation accuracy. Table VII shows the results compared with results from the 10-second temperature curve.

This table shows that a 5 by 5 node and 10 layer calculation may give errors of about 5 percent at the center of a block. At the corner of the block the percentage error is much larger, about 30 percent, but the absolute magnitude of the stress error is larger by only a factor of two. Doubling the number of layers reduces the errors by a factor of two.

Also the table indicates that the absolute accuracy of the calculation depends on the slope of the temperature curve. If the temperature gradient is reduced by a factor of two, the magnitude of error is reduced by the same factor.

The approximate cost of running a TPA II problem varies from about \$35 for a 50 iteration calculation to about \$100 for a 150 iteration calculation.

4.5 CONCLUSIONS FROM STRESS ANALYSIS

This portion of the program involved the preparation and utilization of a computer program. The program calculates the three-dimensional thermal stress distribution in an unrestrained rectangular block having a one-dimensional temperature distribution and having temperature dependent properties.

In application to the uncooled throat design problem, the block is considered to be one element of the throat insulation liner. The blocks would be arranged in a mosaic pattern to form a continuous insulation layer.

A number of calculations were made to examine the influence of the shape of the temperature distribution and the size and shape of the block on thermal stress. The results of these calculations are as follows:

1. Temperature distributions having negative second derivatives produce tensile stresses on the surface of the block, and compressive stresses near the center of the block.
2. Temperature distributions having positive second derivatives produce the reverse effect, compressive stresses on the surface and tensile stresses inside of the block.
3. Thermal stresses are roughly proportional to the deviation of the temperature distribution from linearity (a linear distribution produces no stresses if the properties are uniform).
4. Thermal stresses can be reduced significantly by changes in size and/or shape. Reducing overall size is a common approach to reduction of stresses. But if only one or two dimensions can be reduced, the orientation with respect to the temperature distribution is important. The lowest stresses are produced in a block that has a rod-like shape, with the temperature varying along the length of the rod.
5. The calculated stresses were generally much larger than the strength of available high temperature materials. This in itself does not imply failure, but only that the parts will crack. Cracks tend to reduce stresses but also to produce spalling. The relationship between the calculated stress distributions and spalling was not studied.

SECTION V CONCLUSIONS

The basic purpose of the work reported herein was to determine the feasibility of an uncooled throat for a hypersonic wind tunnel facility. Specific results from the test program and from the thermal stress analysis are presented in Section 3.5 and 4.5. The conclusions stated in this section apply to the fullscale throat.

Tests were not made at conditions as severe as would be encountered by a completely uncooled throat in the fullscale nozzle. Furthermore, the results cannot be readily extrapolated to fullscale conditions. Thus, the conclusions that follow necessarily involve engineering judgement.

On the basis of this work, and other experience with ceramics, it is the authors' opinion that a completely uncooled throat for a large wind tunnel is not feasible using currently available commercial materials. However, the results do indicate that materials are available for a ceramic lined throat that could operate at the maximum tunnel flow conditions, but with the thermal shock conditions reduced by the use of film cooling and by preheating through flow of air during heater pressurization.

Film cooling and preheating both reduce the rate of heat transfer and, consequently, the severity of the thermal shock. Film cooling also reduces the maximum temperature reached by the ceramic insulation. The current facility design concept provides for film cooling of the hot valve seat with a flow rate equal to 9 percent of the mainstream flow. This film cooling (in combination with preheating) would probably be adequate for a ceramic lined throat section. In comparison, the film cooling required for the backside cooled throat is 25 percent of the mainstream flow.

The tests indicate that several zirconia and zirconium diboride compositions are available that could withstand the flow conditions with film cooling and preheating. Application of these materials to a fullscale throat poses design problems that have not been solved. The basic concept of a liner composed of many small blocks (nominally one inch cubes) involves attachment of the blocks to a backup structure. This would be the most difficult design problem in applying the zirconia materials.

The tests indicate that several zirconia and zirconium diboride compositions are available that could withstand the flow conditions with film cooling and preheating. Application of these materials to a fullscale throat poses design problems that have not been solved. The basic concept of a liner composed of many small blocks (nominally one inch cubes) involves attachment of the blocks to a backup structure. This would be the most difficult design problem in applying the zirconia materials.

The zirconium diboride materials have sufficient oxidation resistance, if used with film cooling, because of the effect of film cooling in reducing the temperature level. However, these materials have high thermal conductivity, equal to or greater than carbon steel. Since they are not insulators, their use would require a different design concept. It may be possible to use the diboride materials in combination with a zirconia insulation liner.

A computer program was prepared and used for calculation of thermal stresses in blocks that would form the insulation liner. These blocks are characterized by a one-dimensional temperature distribution (normal to nozzle surface) and by having essentially no mechanical restraint.

Calculation results provided a description of the stress distribution and the influence of size and shape of the blocks. Stresses can be reduced most effectively by reducing all dimensions of the surface exposed to the hot flow. That is, cumulative thermal expansion should be as small as possible. Minimum stresses are produced in rod shaped pieces, with the rod axis parallel to the heat flow.

REFERENCES

1. E. Robinson, Limited Testing of Precracked Ceramic Rocket Nozzles, AIAA J. Spacecraft, Vol. 5, No. 12, December 1968.
2. B. Swartz, Thermal Stress Failure of Pure Refractory Oxides, J. Amer. Cer. Soc., Vol. 35, No. 12, December 1952.
3. B. A. Boley and J. H. Weiner, Theory of Thermal Stresses, J. Wiley & Sons, 1960.
4. E.R.G. Eckert, Gas-to-Gas Film Cooling, Heat Transfer and Fluid Mechanics Laboratory, Department of Mechanical Engineering, University of Notre Dame, Tech. Rpt. 68-23, October 1968.
5. D. R. Bartz, A Simple Equation for Rapid Estimation of Rocket Nozzle Convective Heat Transfer Coefficients, J.P.L., Vol. 27, No. 1, January 1957.
6. J. J. Kolozsi, An Investigation of Heat Transfer Through the Turbulent Boundary Layer in an Axially Symmetric Convergent-Divergent Nozzle, Ohio State University, Aerodynamics Laboratory, Tech. Memo No. 8, July 1958.

TABLE I
SUMMARY OF TEST SPECIMEN MATERIALS
TEST PHASE I

<u>Test Specimen</u>	<u>Description</u>
1 and 2	Tungsten-Rhenium wire reinforced, isostatically pressed partially stabilized MgO-CaO zirconia. Density: 350 lbs/ft ³ . Supplier: Thompson Ramo Woolridge, Inc.
3	60D castable, partially stabilized calcia-zirconia. Maximum grain size 60 mesh. Density: 260 lbs/ft ³ . Supplier: Zircoa
4	60D castable, fully stabilized yttria-zirconia. Maximum grain size 60 mesh. Density: 260 lbs/ft ³ . Supplier: Zircoa
5 and 6	Fine grain, dense, pressed partially stabilized magnesia-calcia-zirconia, Zircoa composition 1027. Density: 340 lbs/ft ³ . Supplier: Zircoa
7 and 8	8D castable, partially stabilized calcia-zirconia. Maximum grain size 8 mesh Density: 260 lbs/ft ³ . Supplier: Zircoa
9 and 10	8D castable, partially stabilized magnesia-calcia-zirconia, Zircoa composition 1027. Maximum grain size 8 mesh. Density: 230 lbs/ft ³ . Supplier: Zircoa
11	60D castable, partially stabilized magnesia-calcia-zirconia, Zircoa composition 1027. Maximum grain size 60 mesh. Density: 220 lbs/ft ³ . Supplier: Zircoa
12 and 13	Pressed partially stabilized magnesia zirconia, Zircoa composition 1721. Density: 260 lbs/ft ³ . Supplier: Zircoa

TEST PHASE II

14 and 15	Pressed 10.4% yttria-zirconia, Coors composition ZP-997 grogged. Density: 296 lb/ft ³ . Supplier: Coors Porcelain Co.
16 and 17	Same as 14 and 15
18 and 19	ManLabs Diboride Material V, zirconium diboride with 20 volume percent silicon carbide. Density: 340 lb/ft ³ . Supplier: ManLabs, Inc.
20 and 21	Same as 18 and 19
22 and 23	ManLabs Diboride Material VIII, zirconium diboride with 14 volume percent silicon carbide and 30 volume percent carbon. Density: 330 lb/ft ³ . Supplier: ManLabs, Inc.
24 and 25	Same as 22 and 23

TABLE II.
SUMMARY OF UNCOOLED THROAT RUNS

PHASE I

Run	P _o psia	T _o °R	Press. Time Sec	Run Time sec	Depress. Time sec	Specimens	
						Left	Right
1	345	1800	30	0	130	1	2
2	400	1700	60	19	140	1	2
3	300	2350	23	39	200	1	2
4	415	2200	28	26	280	3	4
5	300	2050	29	3	43	5	6
6	415	1950	36	35	130	5	6
7	405	2050	24	34	152	5	6
8	415	2200	35	32	140	7	8
9	415	2200	54	32	131	9	10
10	415	2800	40	31	140	9	10
11	415	3100	45	36	145	5	11
12	415	2750	31	34	140	12	13
13	415	3300	37	34	220	12	13
14	415	3000	29	39	205	9	10
15	415	3300	33	3	94	8	11

PHASE II

Run	P _o psia	T _o °R	Press. Time Sec	Run Time sec	Depress. Time sec	Specimens	
						Left	Right
1	445	3035	42	31	148	14	15
2	325	3180	40	1	96	18	19
3	400	3160	52	32	141	18	19
4	400	3180	37	21	98	22	23
5	400	3140	48	37	138	16	17
6	600	3160	52	32	141	22	23
7	800	3260	62	31	147	22	23
8	700	3350	48	2	151	22	23
9	600	3550	41	8	139	18	19

TABLE III.
SPECIFICATIONS FOR THERMAL STRESS COMPUTER RUNS

AEDC-TR-70-82

Run	Time (sec)	Dimensions			Variables Studied	Comments
		a	b	Thick-ness		
1	0.1	1.0	1.0	1.0	T	
2	10.0	1.0	1.0	1.0	T, t, s	
3	40.0	1.0	1.0	1.0	T, m	
4	10.0	2.0	2.0	1.0	s	
5	10.0	0.5	0.5	1.0	s	
6	10.0	1.0	1.0	0.25	t	
7	10.0	1.0	0.5	1.0	s	
8	40.0	1.0	1.0	1.0	m	Same thickness division as Run 3
9	40.0	1.0	1.0	1.0	c	Same 't' div. as Runs 10 and 11
10	See Comments	1.0	1.0	1.0	c	Linear temp. curve, 10 layers
11	See Comments	1.0	1.0	1.0	c	Inverted Temp. Curve
12	10.0	1.0	1.0	0.5	t	
13	10.0	0.25	0.25	1.0	s	
14	10.0	1.0	0.25	1.0	s	
15	See Comments	1.0	1.0	1.0	d	Linear temp. curve, 20 layers
16	See Comments	1.0	1.0	1.0	temp.gradient	Linear temp. curve, 10 layers

Legend		
T = Time	s = Plan form size or shape	m = Material properties
t = Thickness	c = Shape of temp. curve	d = Subdivisions of block

TABLE IV.
INPUT DATA FOR COMPUTER RUNS 9, 10 AND 11

Constant Properties Evaluated at Room Temperature

$$E = 26.5 \times 10^6 \quad \alpha = 4.55 \times 10^{-6}$$

$$\text{Poisson's Ratio} = 0.29$$

Layer	RUN 9		Layer	RUN 10		Layer	RUN 11	
	Thickness H	Temp T		Thickness H	Temp T		Thickness H	Temp T
1	0.1	3250	1	0.1	3730	1	0.1	3870
2	0.1	2130	2	0.1	3345	2	0.1	3780
3	0.1	1350	3	0.1	2960	3	0.1	3660
4	0.1	800	4	0.1	2575	4	0.1	3540
5	0.1	460	5	0.1	2190	5	0.1	3370
6	0.1	260	6	0.1	1805	6	0.1	3200
7	0.1	150	7	0.1	1420	7	0.1	2980
8	0.1	110	8	0.1	1035	8	0.1	2720
9	0.1	80	9	0.1	650	9	0.1	2350
10	0.1	70	10	0.1	265	10	0.1	1410

TABLE V.
INPUT DATA FOR COMPUTER RUN 12

Layer No.	Thickness H	Temperature T	Young's Modulus E	Thermal Coefficient α
1	.020	3480	1.8×10^6	7.2×10^{-6}
2	.020	2880	4.0×10^6	7.0×10^{-6}
3	.020	2440	10.0×10^6	6.8×10^{-6}
4	.020	2070	19.3×10^6	6.6×10^{-6}
5	.020	1760	22.0×10^6	6.4×10^{-6}
6	.050	1260	24.5×10^6	6.0×10^{-6}
7	.050	740	25.8×10^6	5.5×10^{-6}
8	.100	300	26.5×10^6	5.0×10^{-6}
9	.100	150	26.5×10^6	4.8×10^{-6}
10	.100	80	26.5×10^6	4.6×10^{-6}

Time = 10 sec.

Thickness = 0.50 in.

Plenform Size = 1" x 1"

TABLE VI.
INPUT DATA FOR COMPUTER RUNS 15 AND 16

Use Room Temperature Properties for All Layers

$$E = 26.5 \times 10^6$$

$$\alpha = 4.5 \times 10^{-6}$$

$$\text{Poisson's Ratio} = 0.29$$

Layer	RUN 15		Layer	RUN 16	
	Thickness H	Temp T		Thickness H	Temp T
1	0.05	3020	1	0.1	1993
2		3627	2		1801
3		3434	3		1609
4		3241	4		1417
5		3048	5		1225
6		2855	6		1033
7		2662	7		841
8		2469	8		649
9		2276	9		457
10		2083	10		265
11		1890			
12		1697			
13		1504			
14		1311			
15		1118			
16		925			
17		732			
18		539			
19		346			
20		153			

TABLE VII.

COMPARISON OF CALCULATED STRESSES RESULTING FROM A LINEAR TEMPERATURE CURVE AND THE 40-SECOND TEMPERATURE CURVE

Temperature Distribution	Nodes and Layers	*Max. Compressive Stresses Center of Hot Surface (KSI)	*Max. Compressive Stresses Corner of Hot Surface (KSI)
40 sec. curve	5 x 5 x 10 layers	105	36
linear-same slope	5 x 5 x 10 layers	6	11
linear-same slope	5 x 5 x 20 layers	3	7
linear-half slope	5 x 5 x 10 layers	3	5

*Stresses parallel to hot surface

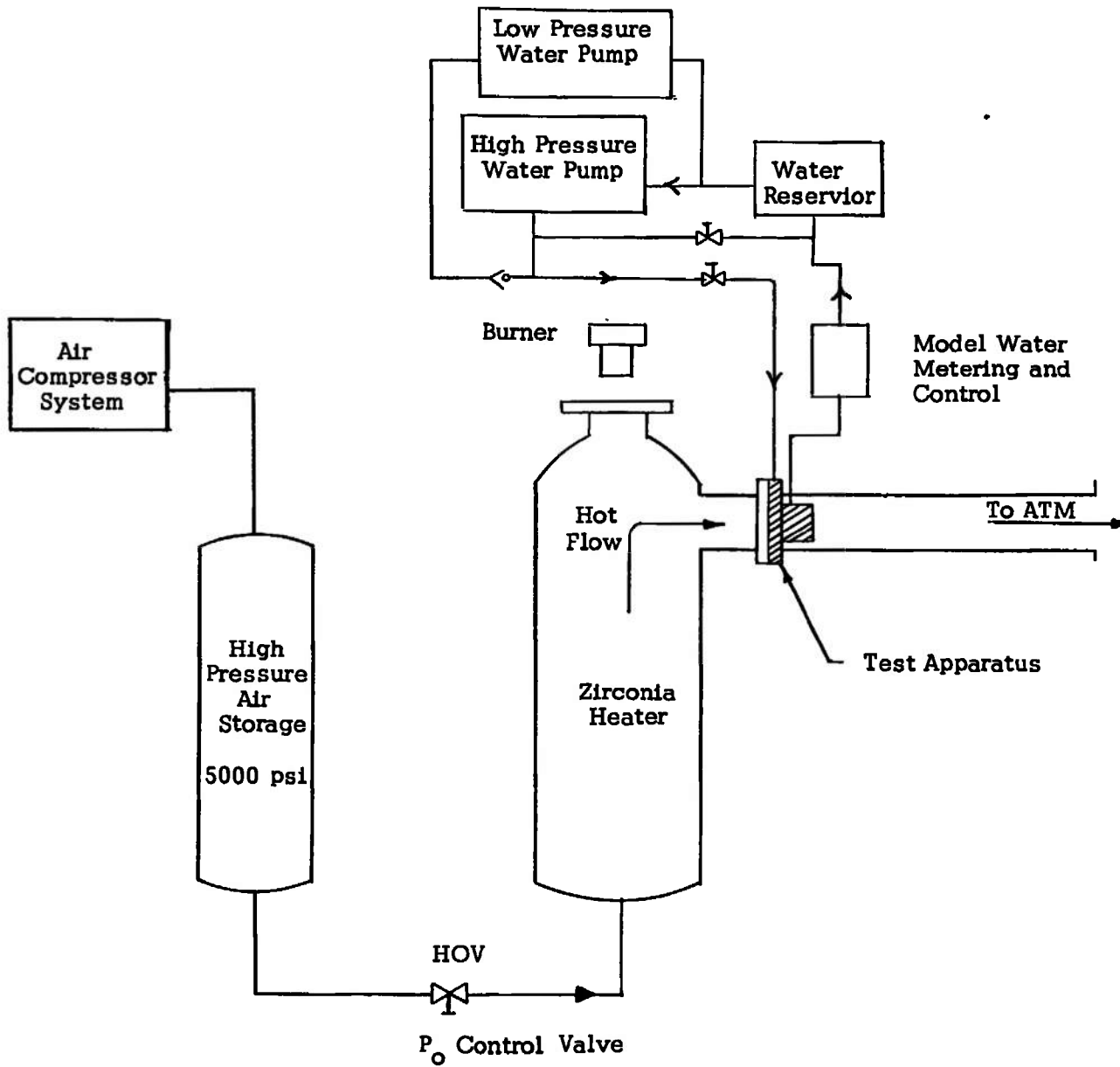


FIGURE 1. FACILITY SETUP FOR UNCOOLED THROAT TESTS

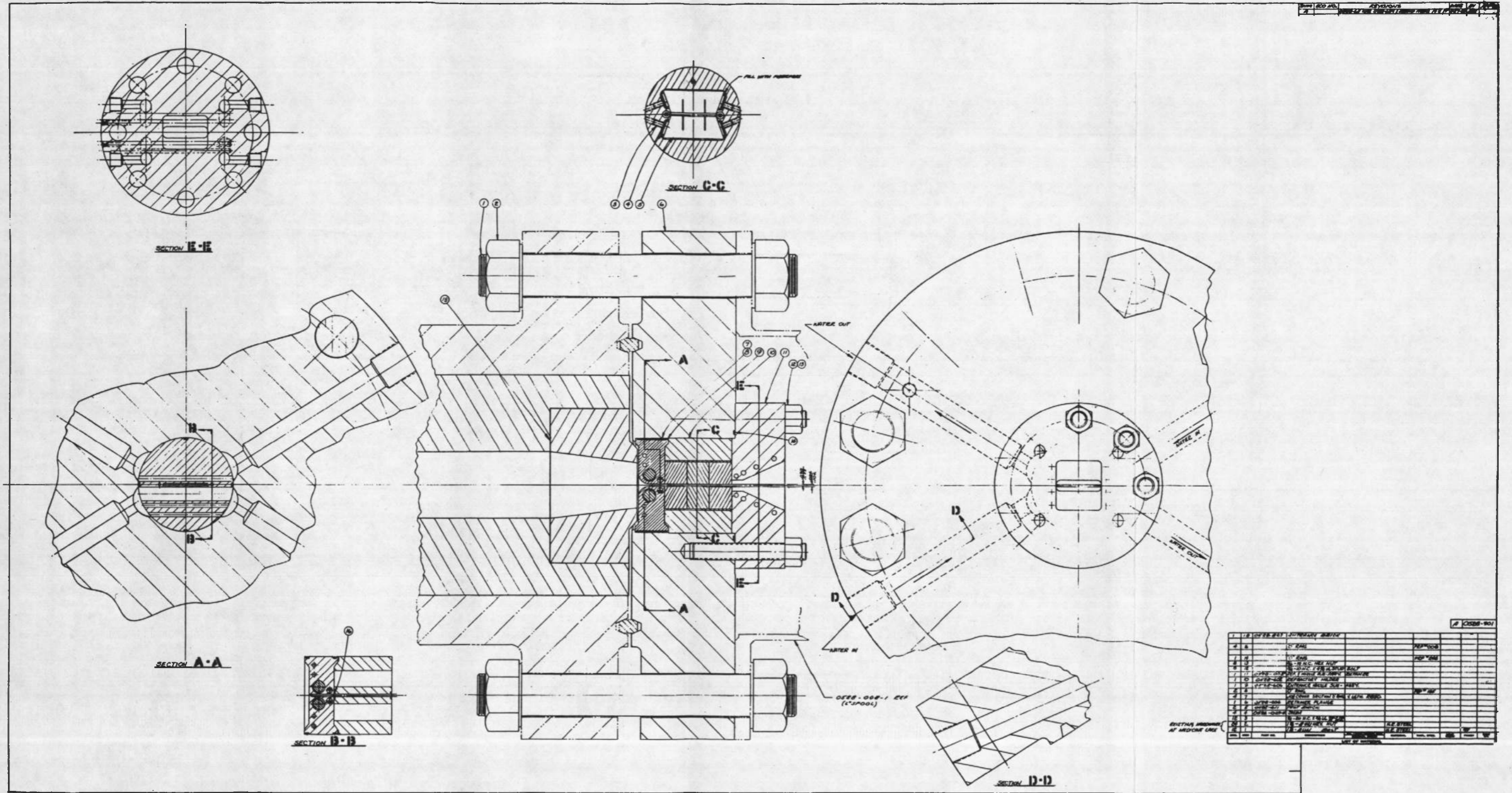


FIGURE 2

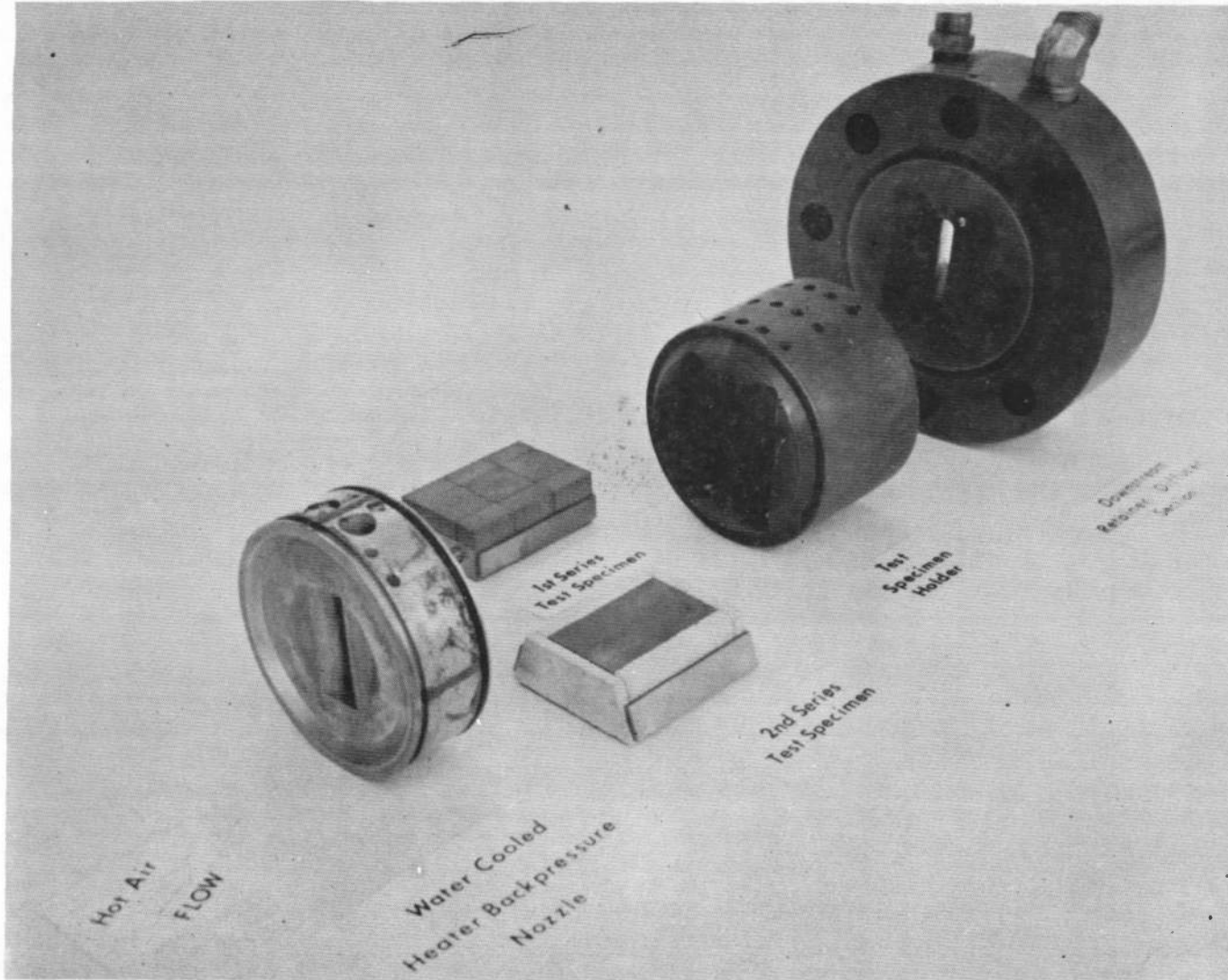


FIGURE 3. TEST APPARATUS COMPONENTS

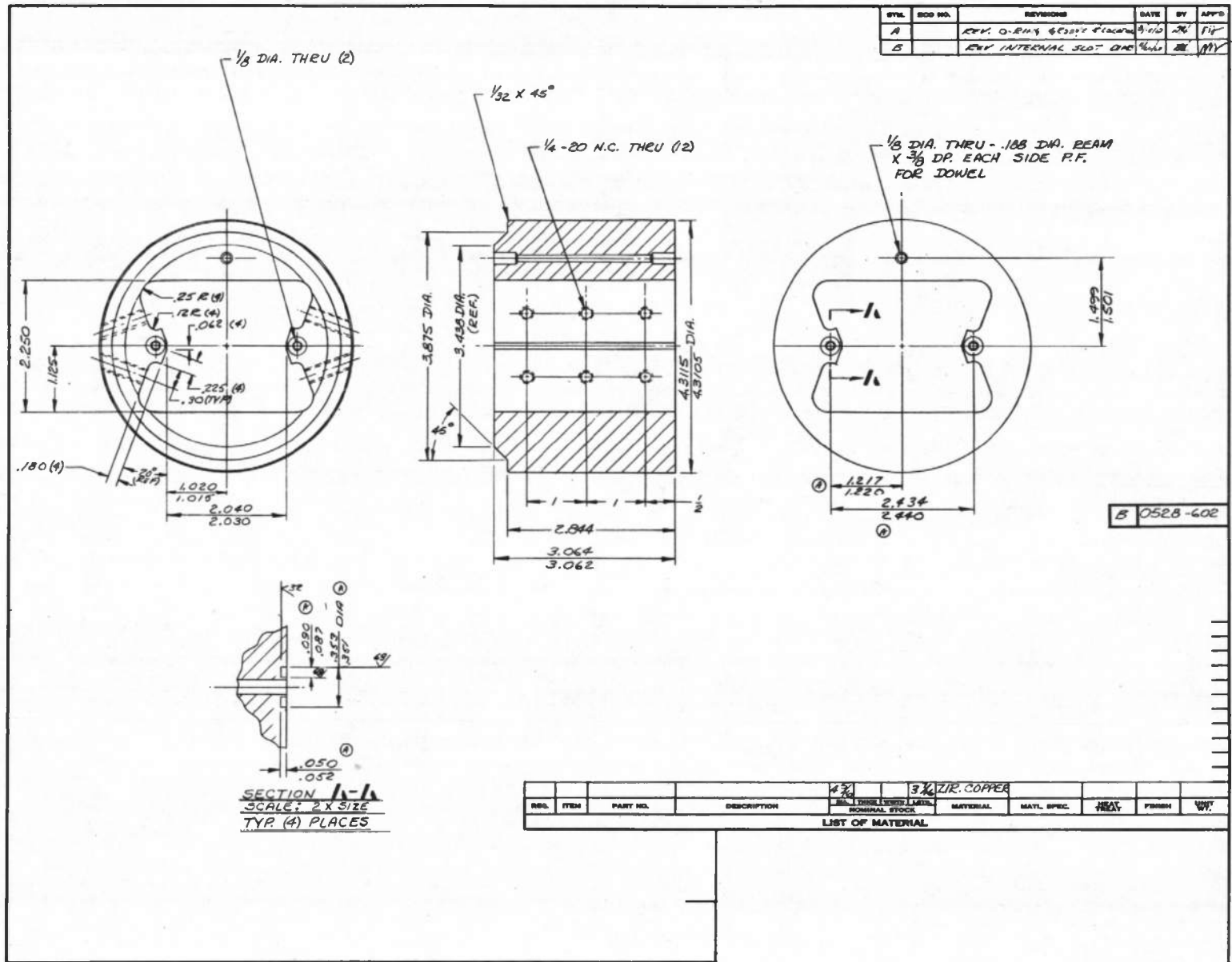


FIGURE 5

REV	REV NO.	REVISION	DATE	BY	CHK
A		REV. 001			
B		REV. 002			
C		REV. 003			
D		REV. 004			

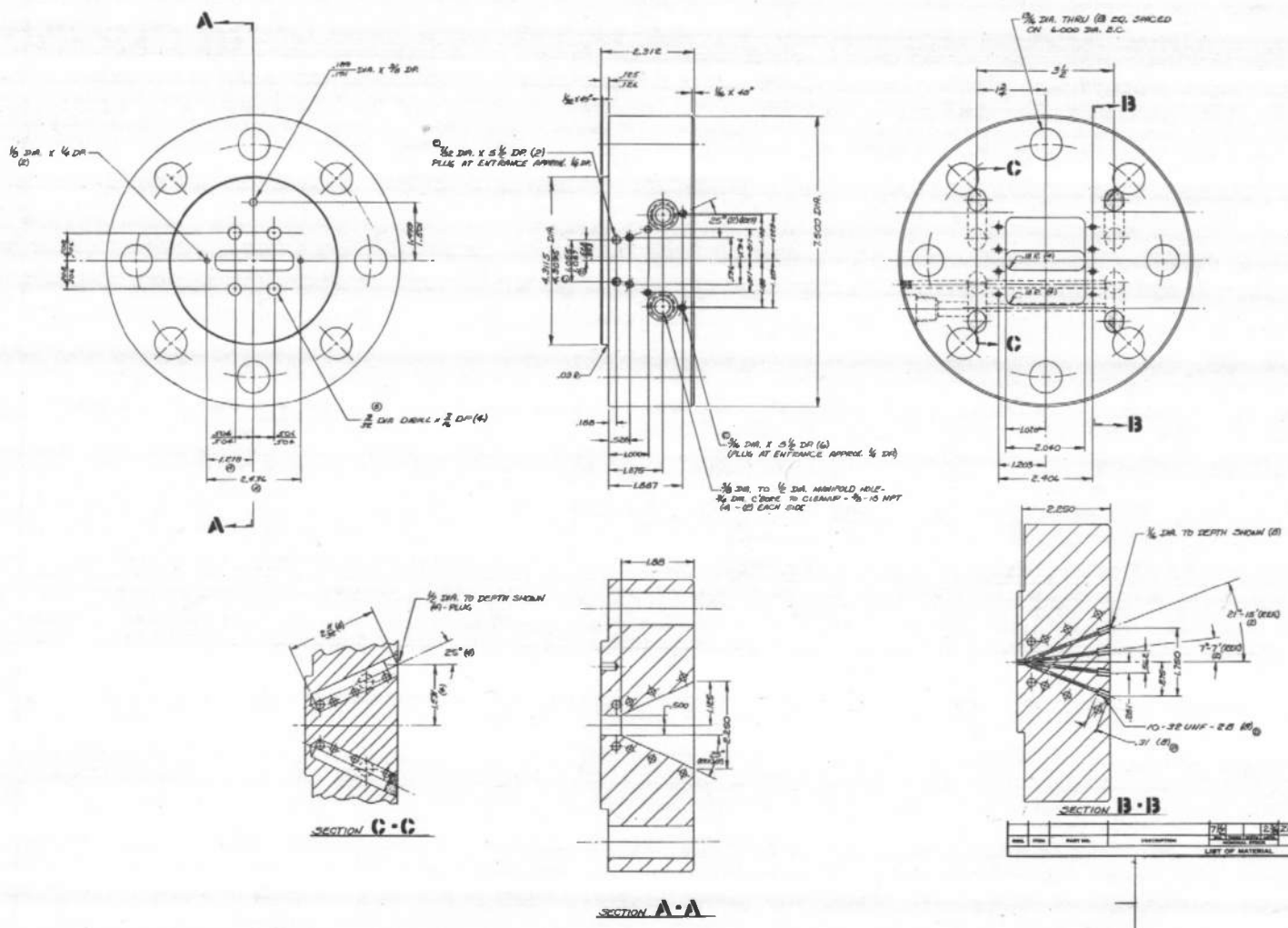


FIGURE 6

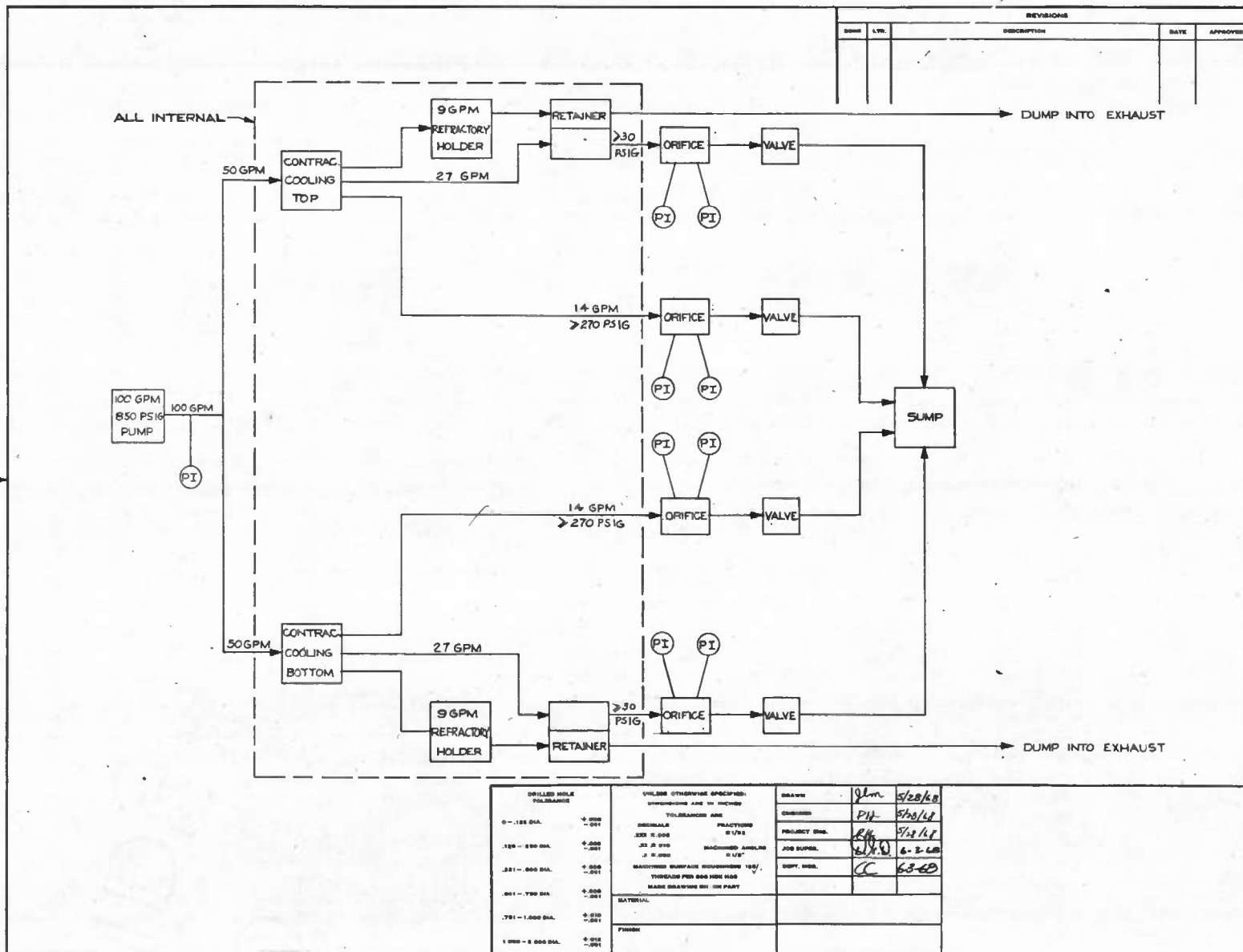
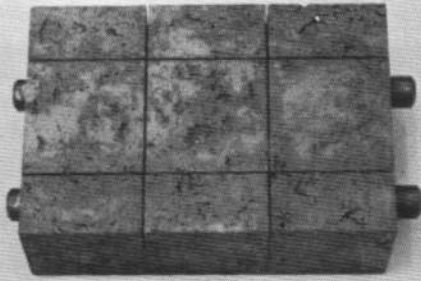
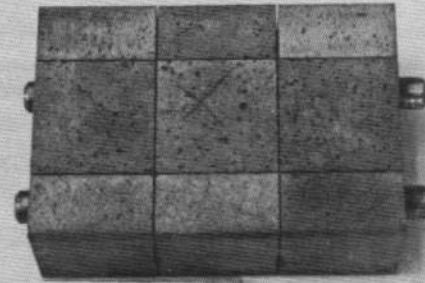


FIGURE 7



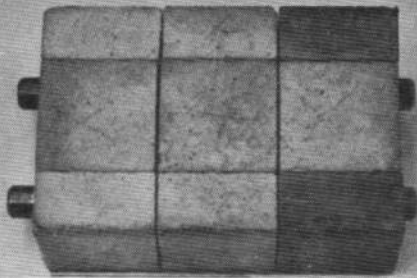
Test Specimen No. 1
and 2 (both identical)

TUNGSTEN REINFORCED ZIRCONIA



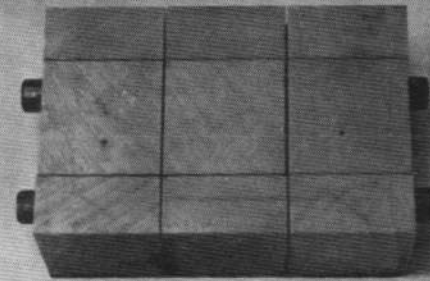
Test Specimen No. 3

60 D CASTABLE ZIRCONIA



Test Specimen No. 4

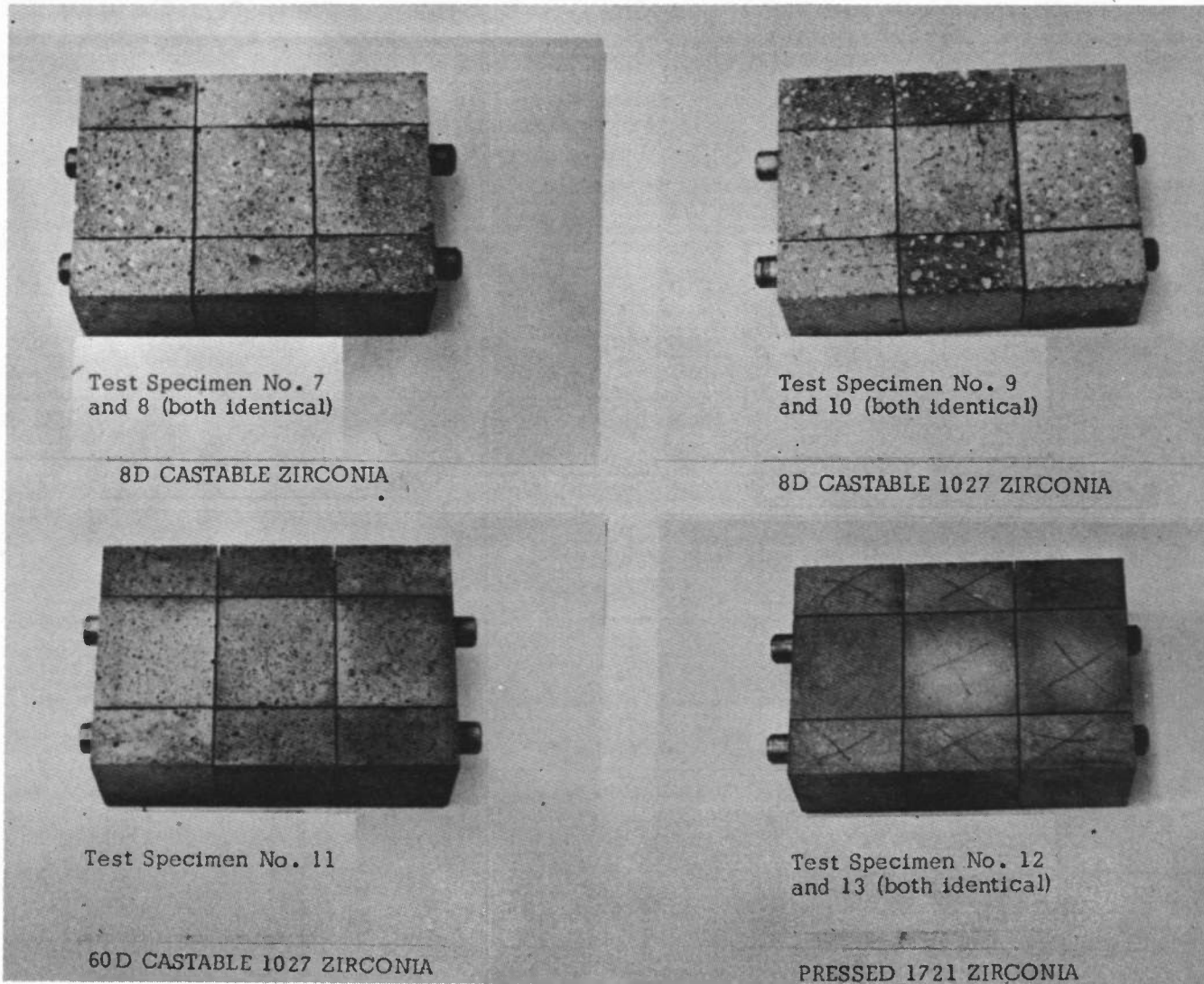
60 D CASTABLE YTTRIA ZIRCONIA



Test Specimen No. 5
and 6 (both identical)

FINE GRAIN DENSE 1027 ZIRCONIA

FIGURE 8. PRETEST MATERIAL SPECIMEN PHOTOGRAPHS



Test Specimen No. 7
and 8 (both identical)

8D CASTABLE ZIRCONIA

Test Specimen No. 9
and 10 (both identical)

8D CASTABLE 1027 ZIRCONIA

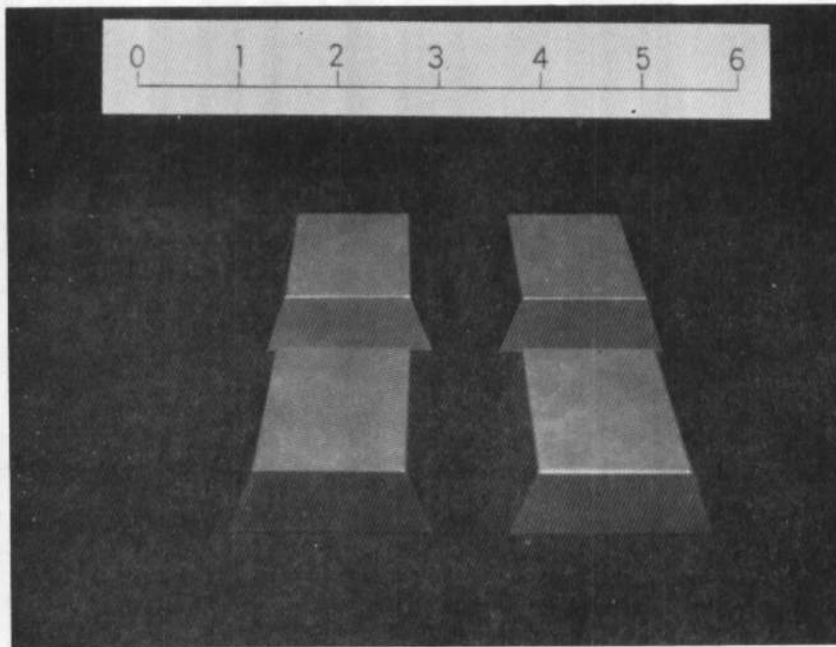
Test Specimen No. 11

60D CASTABLE 1027 ZIRCONIA

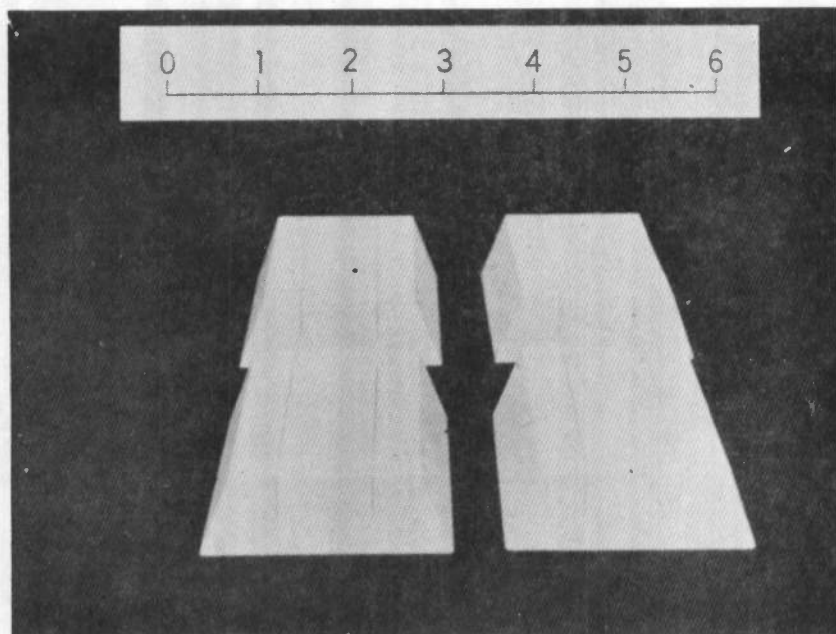
Test Specimen No. 12
and 13 (both identical)

PRESSED 1721 ZIRCONIA

FIGURE 9. PRETEST MATERIAL SPECIMEN PHOTOGRAPHS



Zirconium Diboride Specimens Manufactured by ManLabs



Yttria-Zirconia Specimens Manufactured by Coors

FIGURE 10. PRETEST MATERIAL SPECIMENS, PHASE II

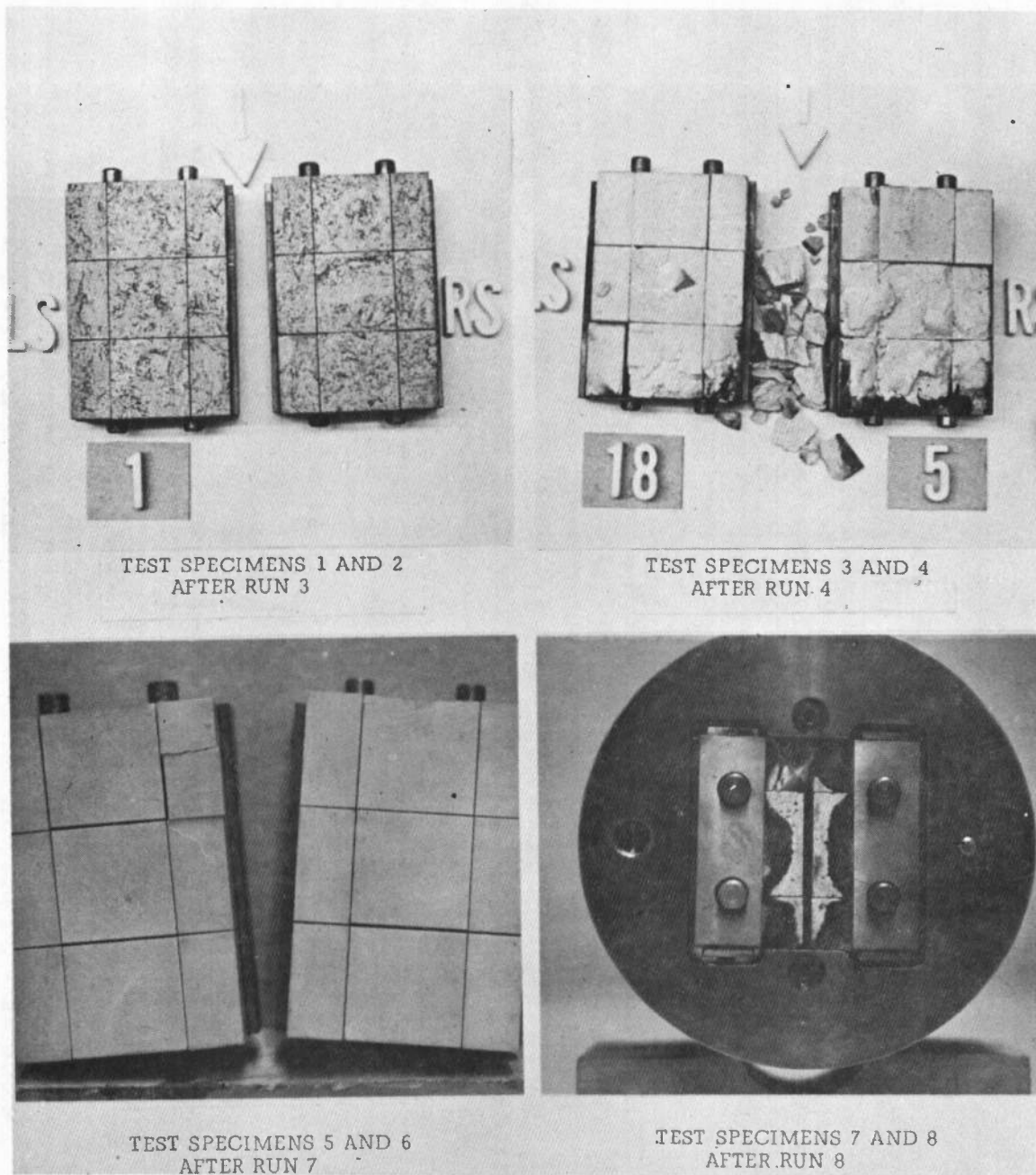


FIGURE 11. AFTER RUN MATERIAL SPECIMEN PHOTOGRAPHS, PHASE I

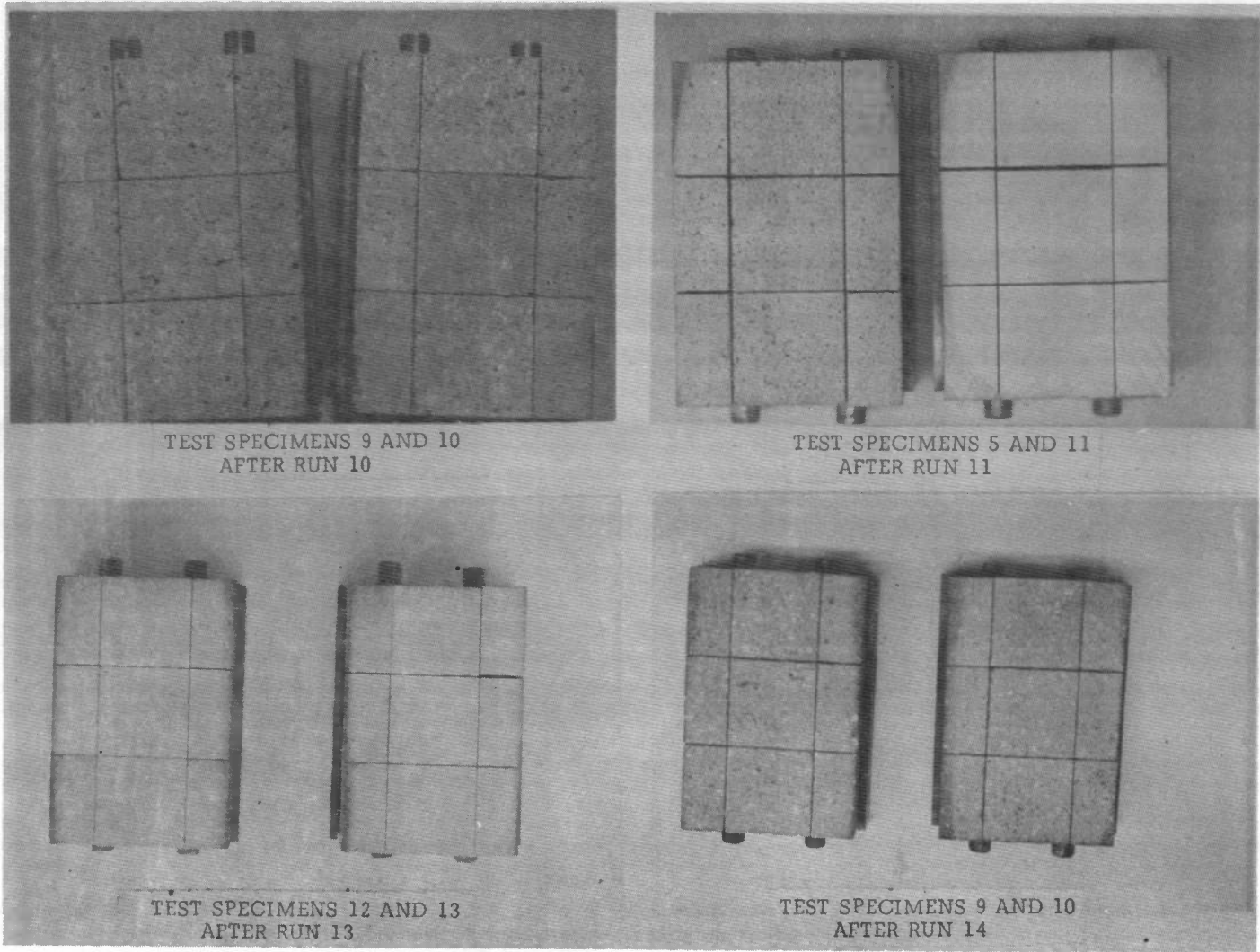


FIGURE 12. AFTER RUN MATERIAL SPECIMEN PHOTOGRAPHS, PHASE I

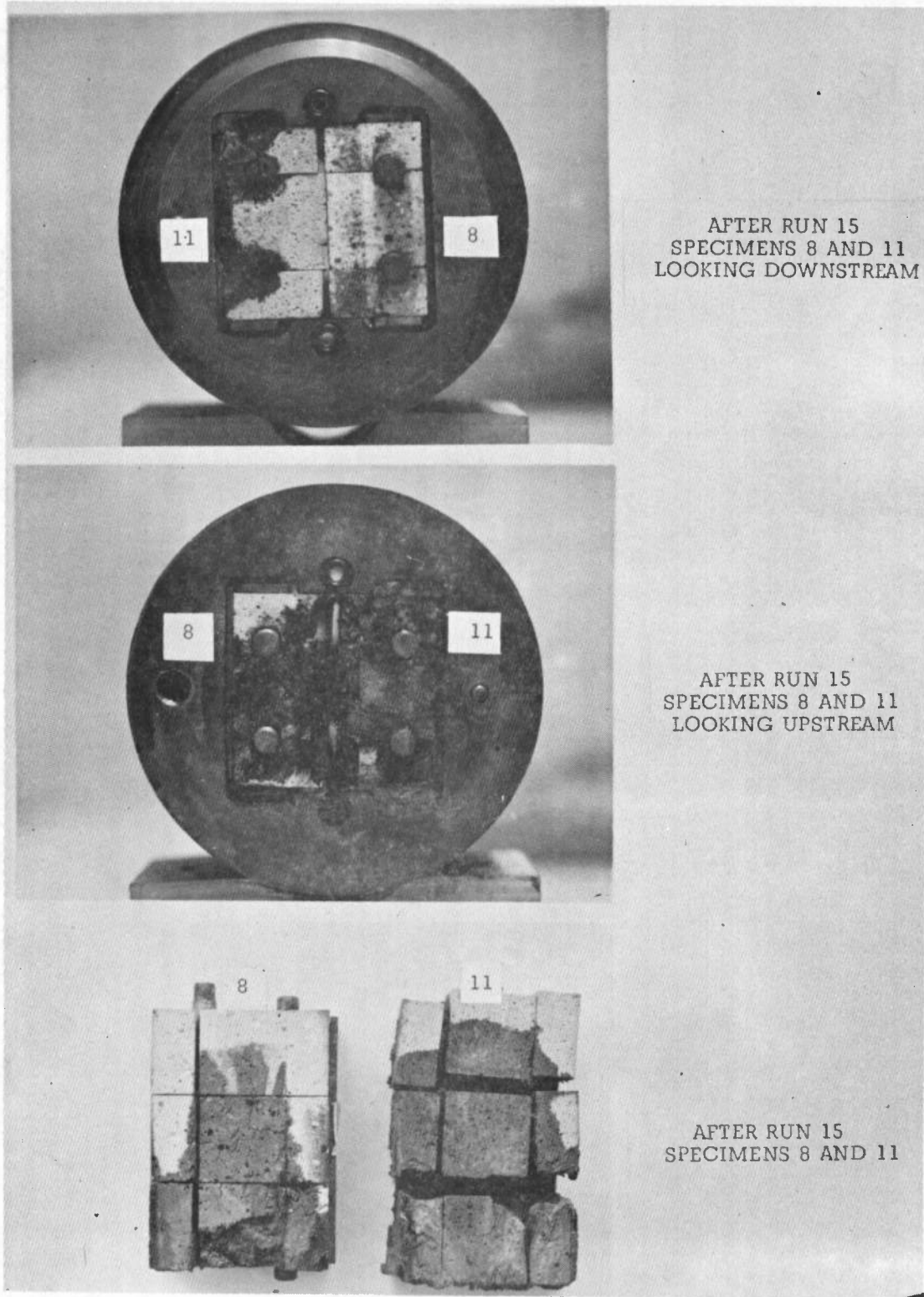
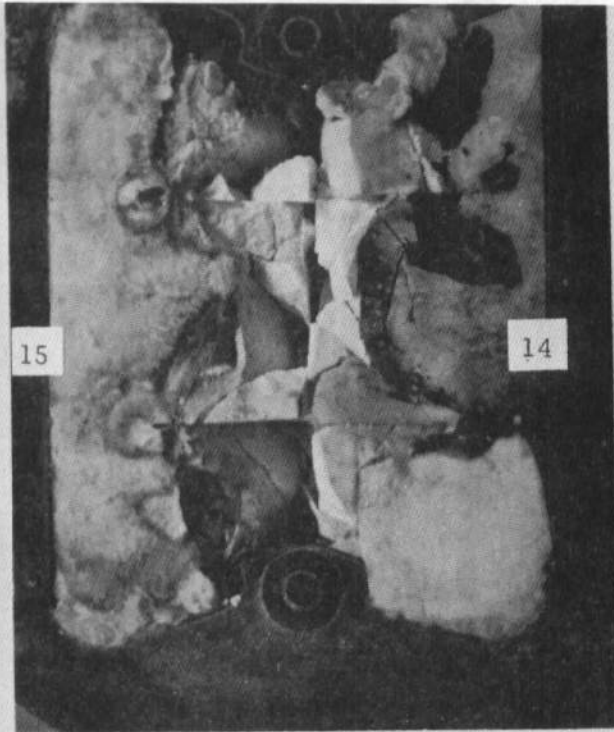


FIGURE 13. AFTER RUN MATERIAL SPECIMEN PHOTOGRAPHS, PHASE I



Test Specimens 14 and 15 in Holder
Looking Upstream After Run 1

← FLOW



Plan View of Test Specimen 14

FIGURE 14. AFTER RUN MATERIAL SPECIMEN PHOTOGRAPHS, PHASE II

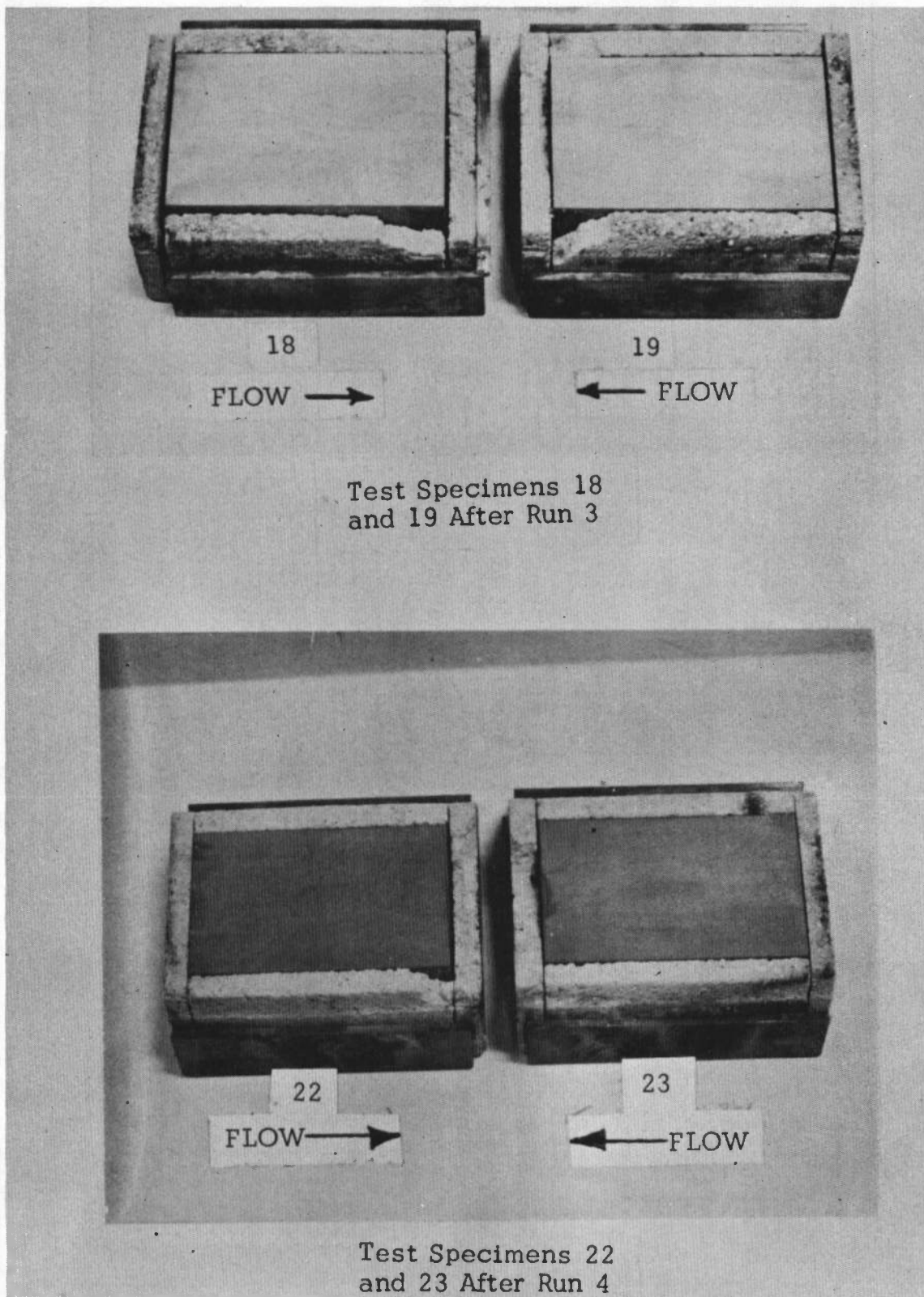


FIGURE 15. AFTER RUN MATERIAL SPECIMEN PHOTOGRAPHS, PHASE II

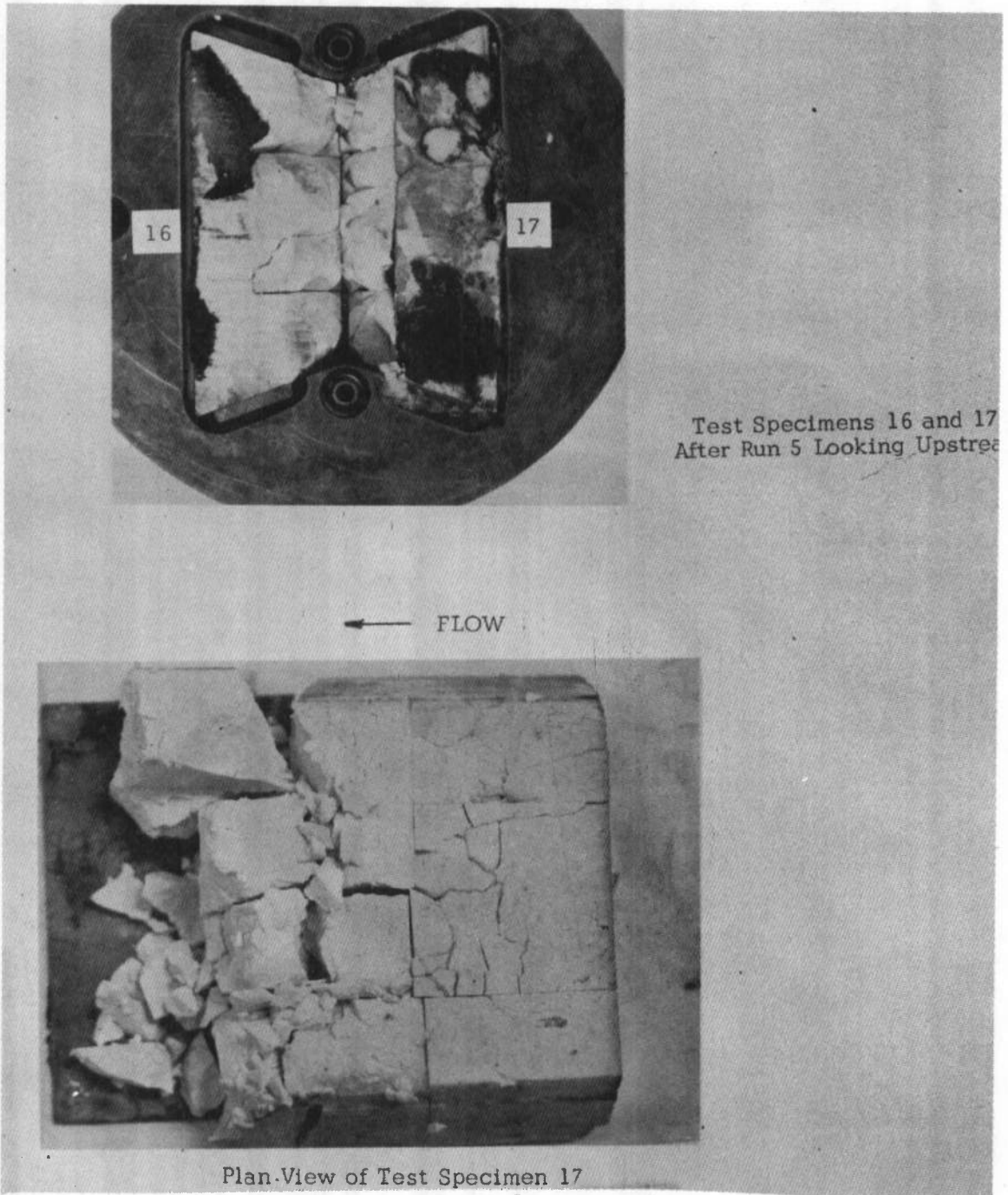
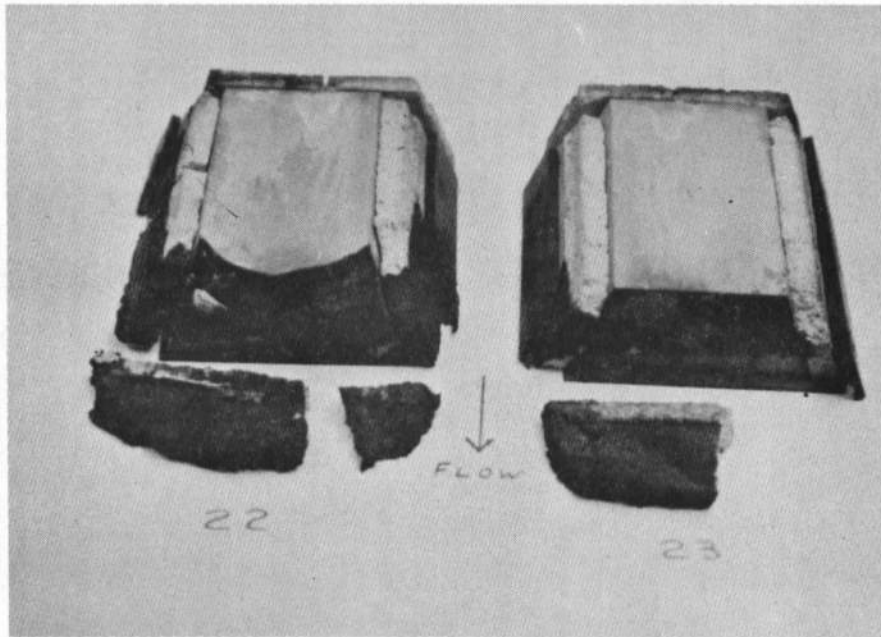
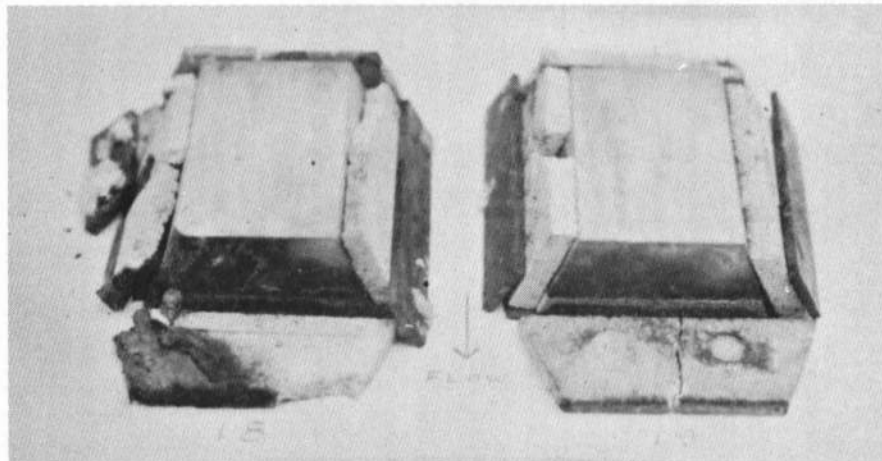


FIGURE 16. AFTER RUN MATERIAL SPECIMEN PHOTOGRAPHS, PHASE II



Test Specimens 22
and 23 After Run 8



Test Specimens 18
and 19 After Run 9

FIGURE 17. AFTER RUN MATERIAL SPECIMEN PHOTOGRAPHS, PHASE II

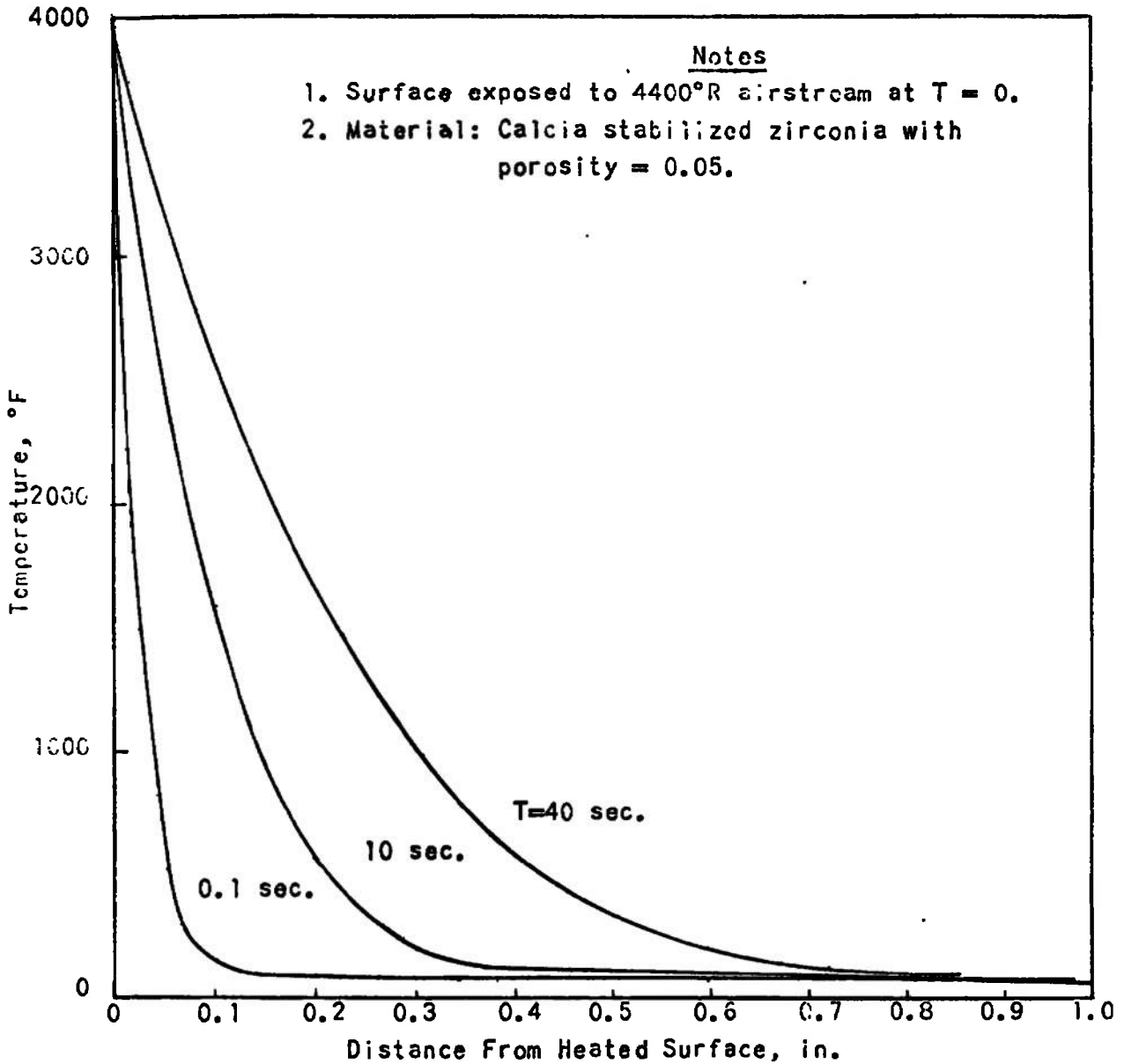


FIGURE 18. TRANSIENT TEMPERATURES IN UNCOOLED THROAT CERAMIC ELEMENTS

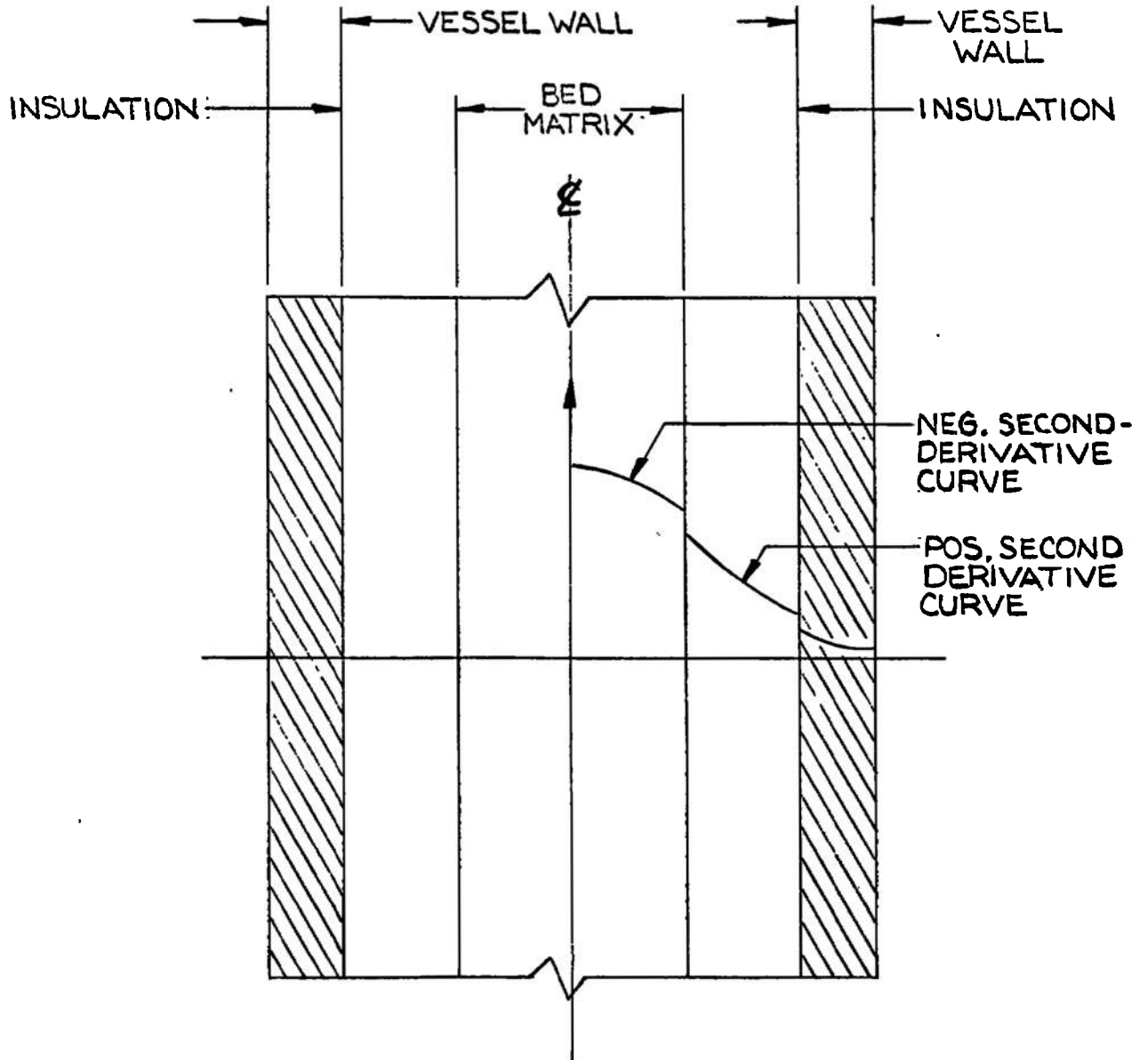


FIGURE 19. TEMPERATURE DISTRIBUTION IN THE BED MATRIX AND INSULATION OF A CYLINDRICAL CERAMIC STORAGE HEATER

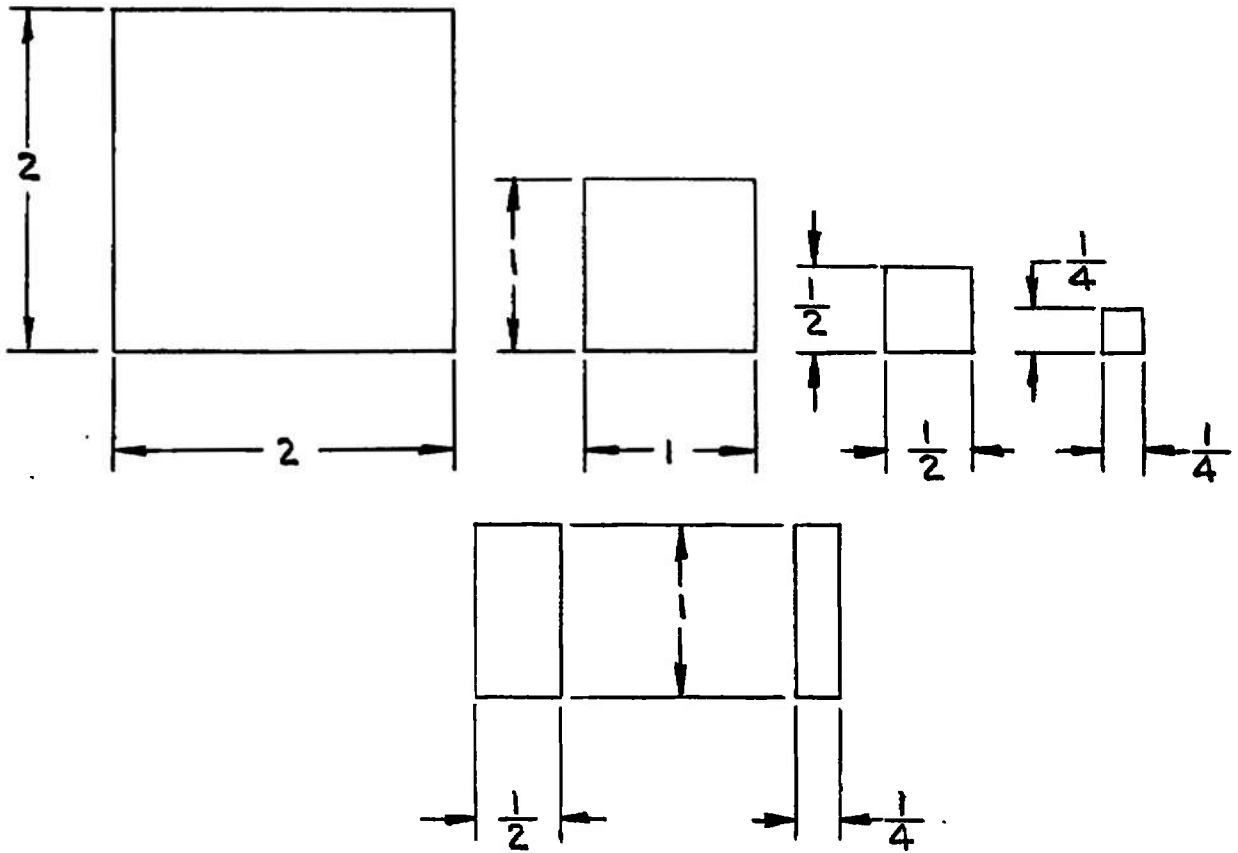
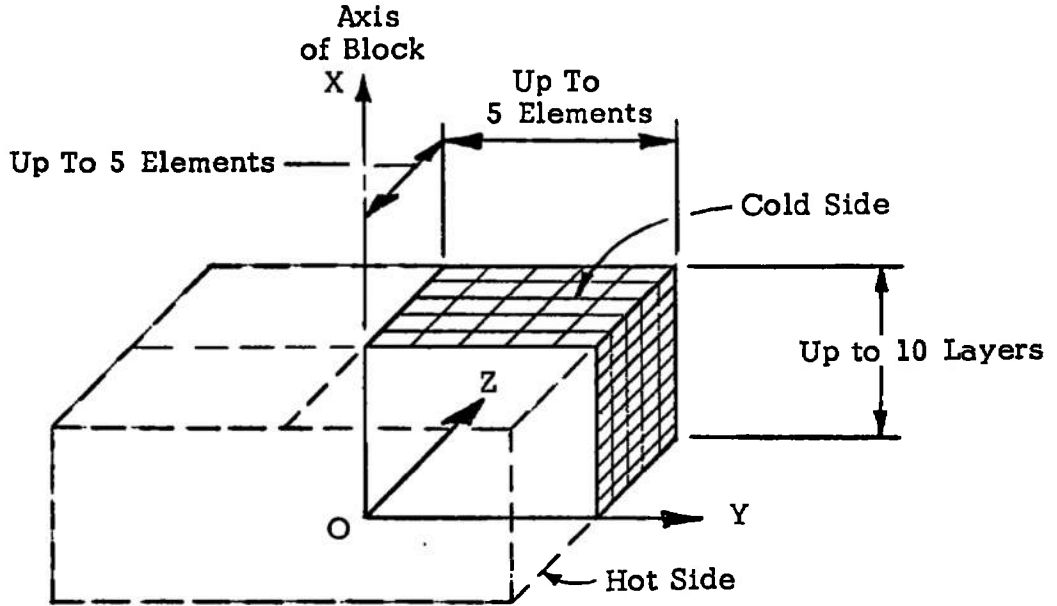
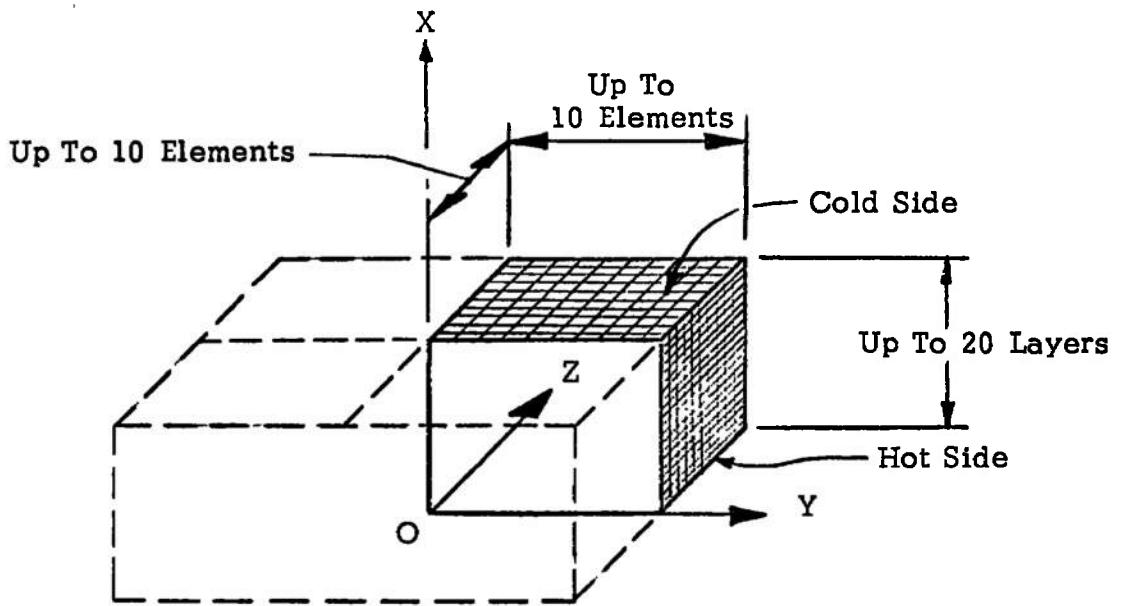


FIGURE 20. SUBDIVISIONS OF A 2" x 2" PLAN FORM INTO SMALLER ELEMENTS TO STUDY THE EFFECT OF PLAN-FORM SIZE AND SHAPE ON THERMAL STRESSES

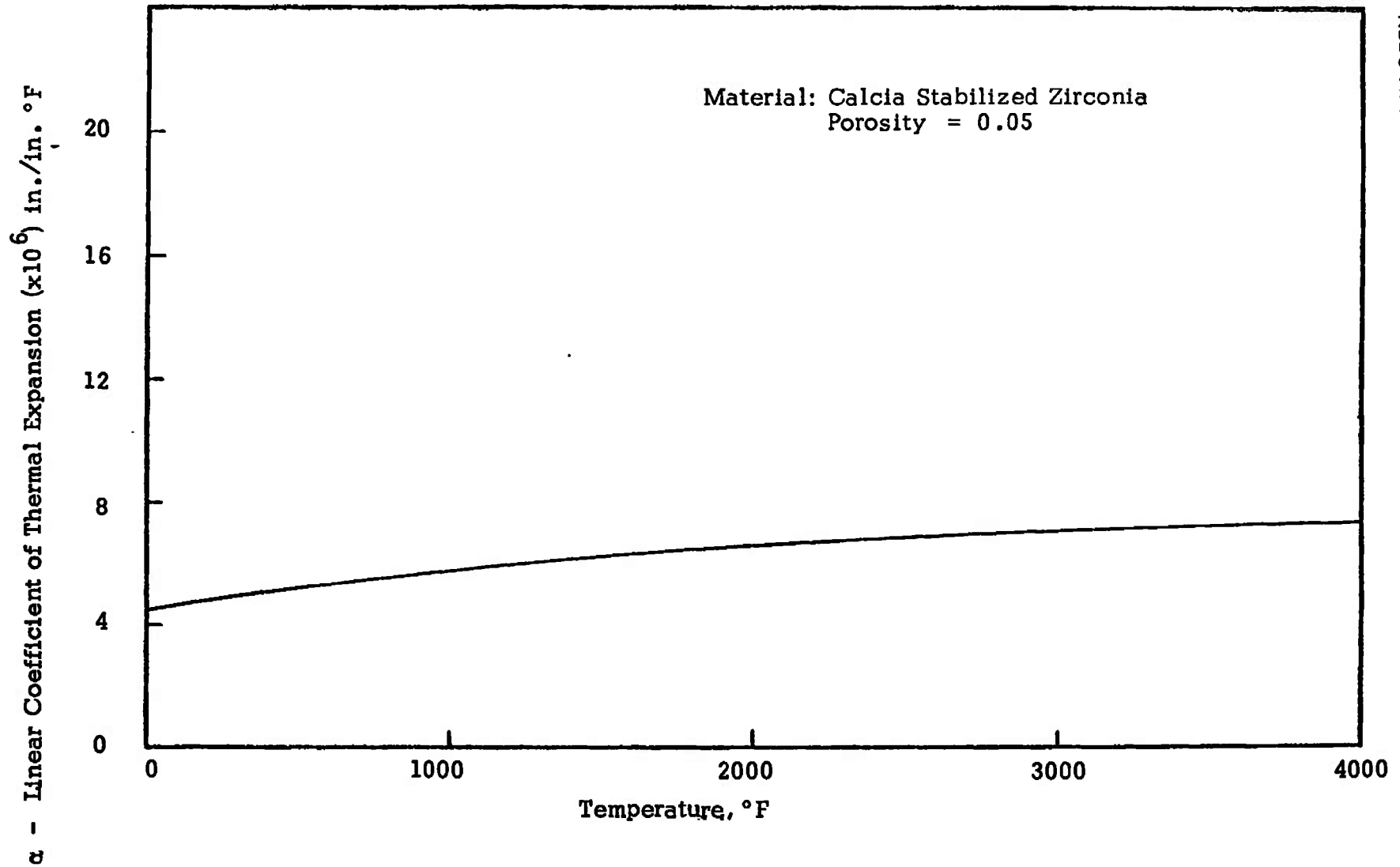


ORIGINAL PROGRAM (TPA)



REVISED PROGRAM (TPA II)

FIGURE 21. BLOCK GEOMETRY AND SUBDIVISIONS

FIGURE 22. COEFFICIENT OF THERMAL EXPANSION, α VS TEMPERATURE T

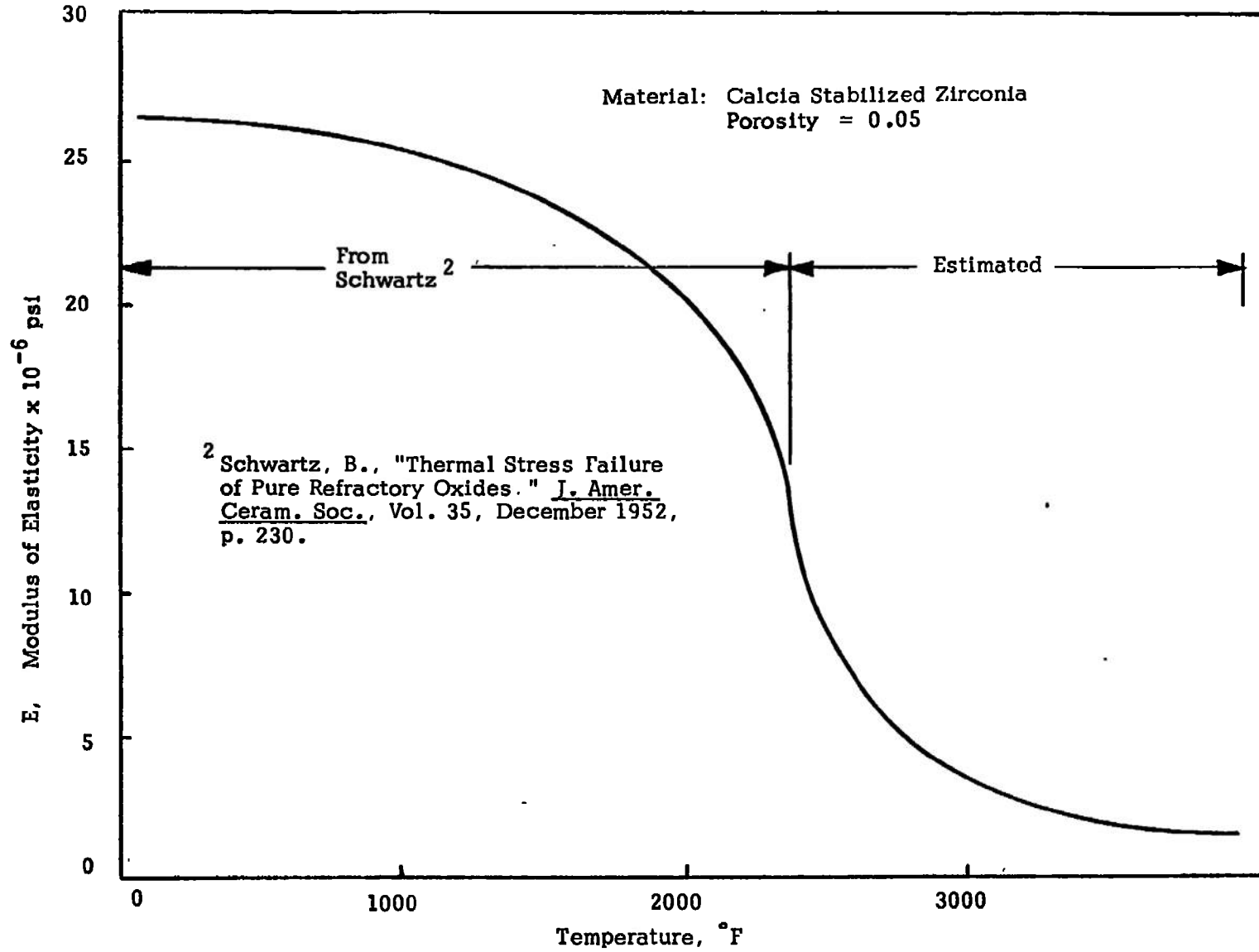


FIGURE 23. MODULUS OF ELASTICITY, E VS TEMPERATURE T

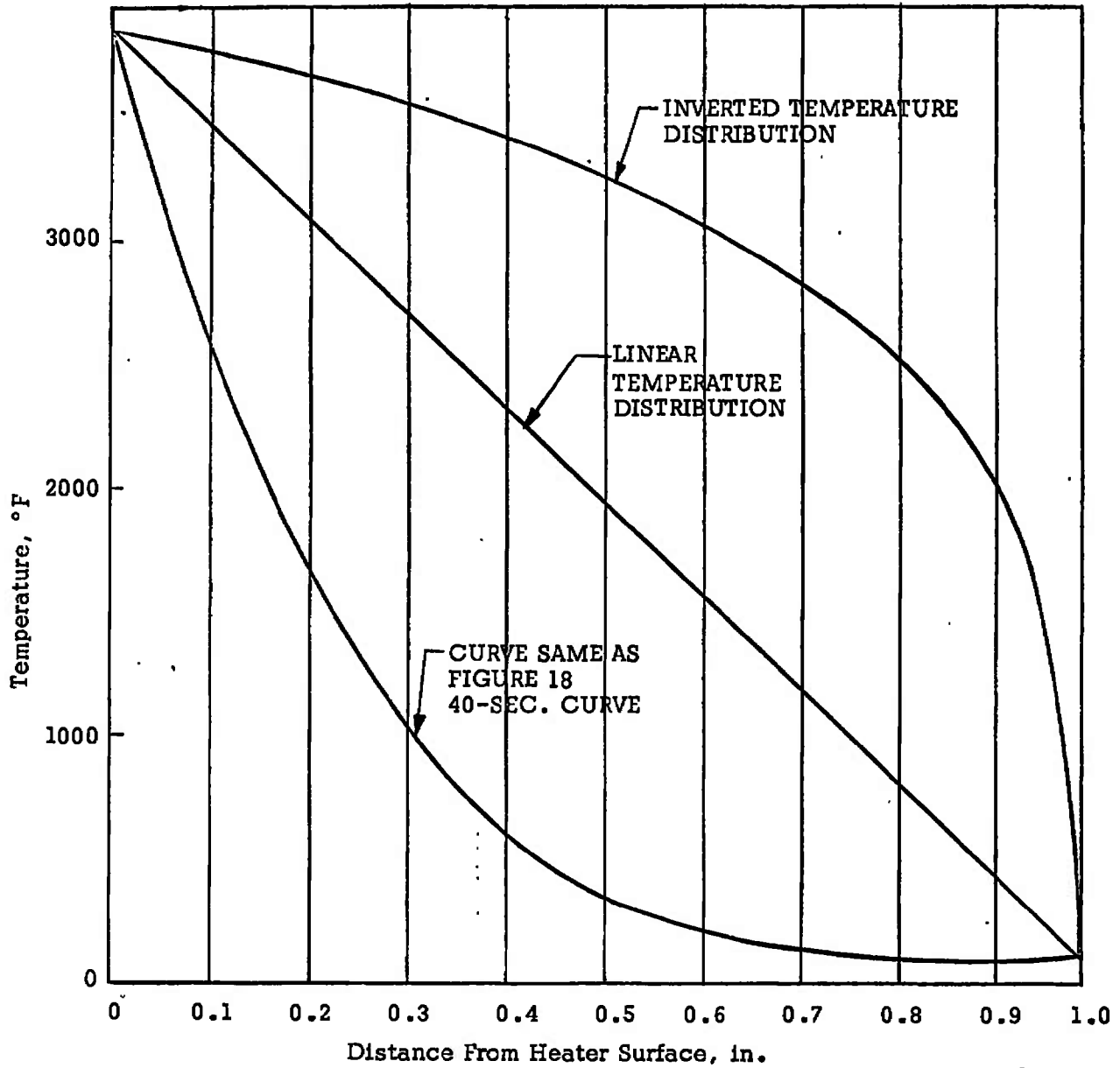


FIGURE 24. PIECEWISE CONSTANT TEMPERATURE DISTRIBUTIONS FOR STUDYING EFFECT OF KIND OF TEMPERATURE CURVE ON THERMAL STRESS DISTRIBUTION (Computer Runs 9 and 10 - CONSTANT MATERIAL PROPERTIES).

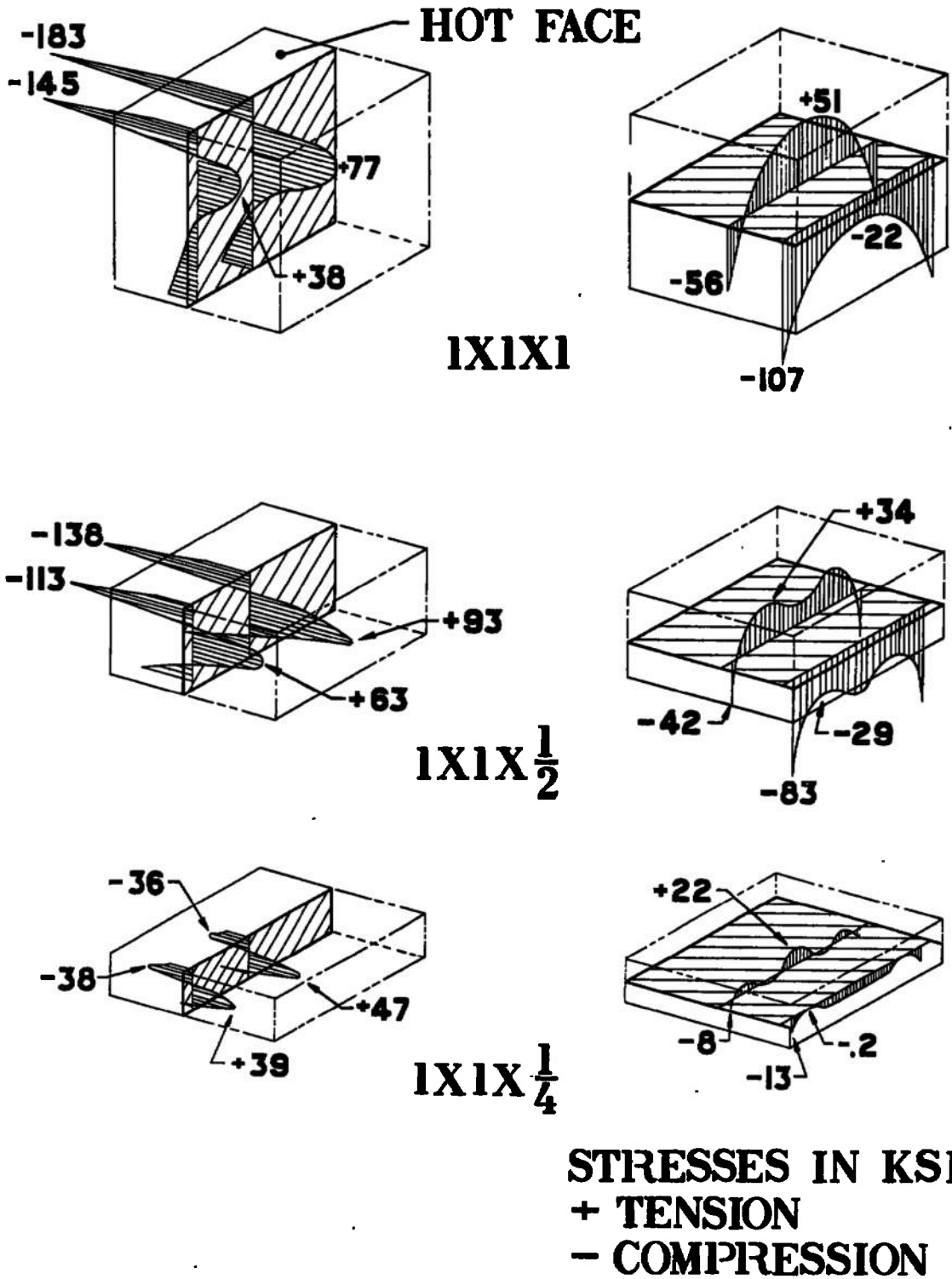


FIGURE 26. THERMAL STRESS VS. BLOCK THICKNESS
 COMPUTER RUNS 2, 12 AND 6

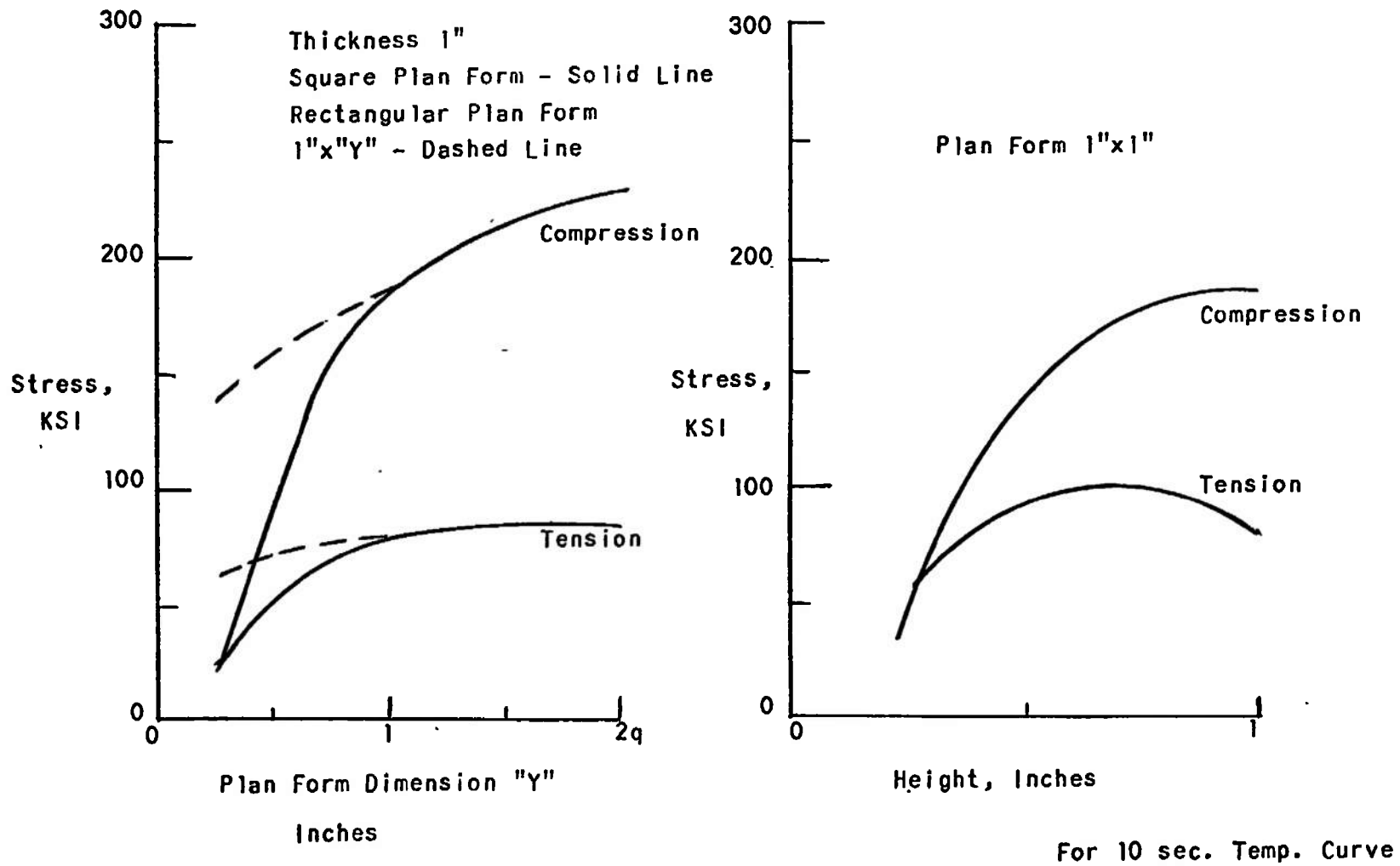


Figure 27 VARIATION OF MAXIMUM STRESSES WITH PLAN FORM DIMENSION & THICKNESS

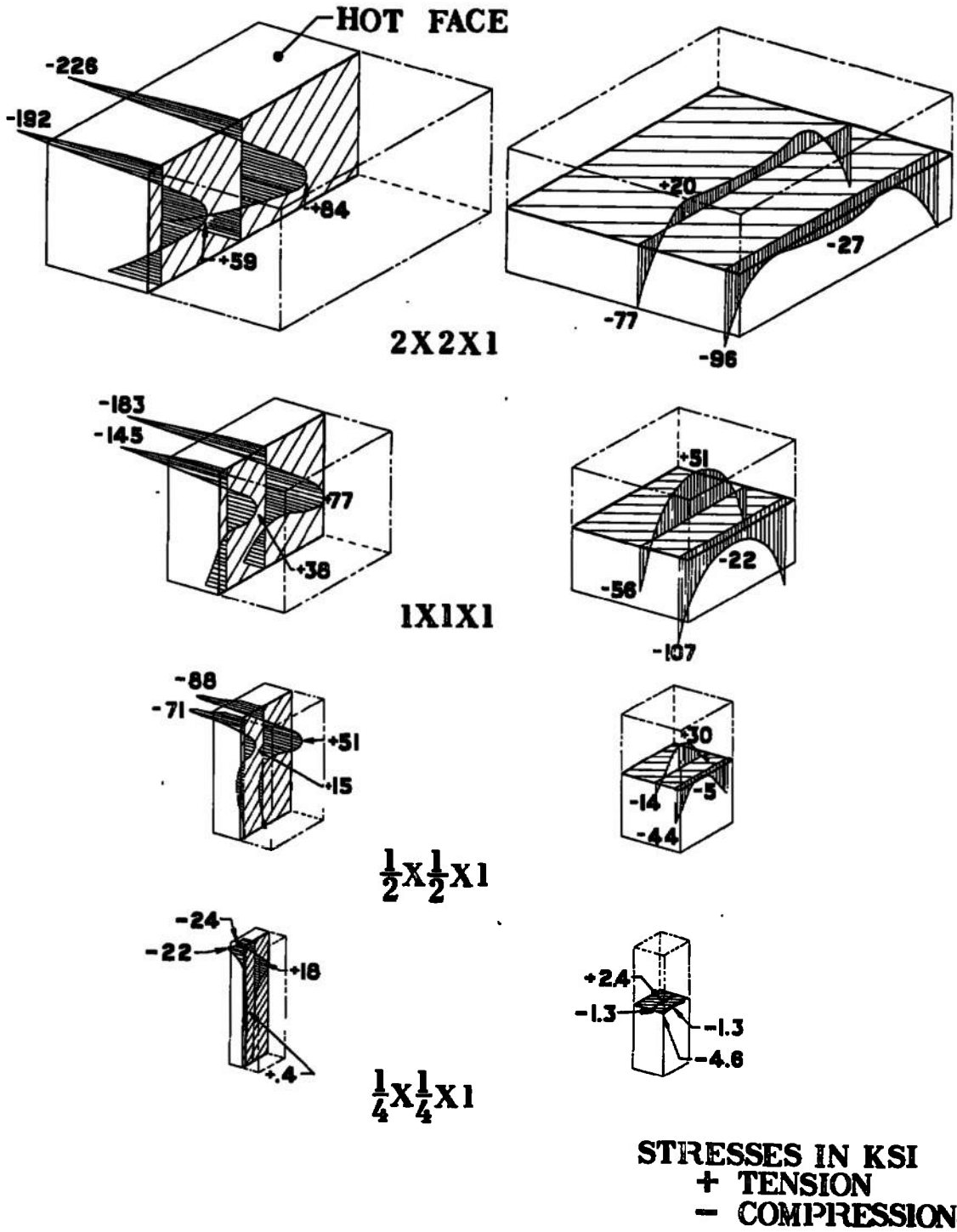


FIGURE 28. THERMAL STRESS VS. PLAN FORM SIZE
 COMPUTER RUNS 4, 2, 5 AND 13

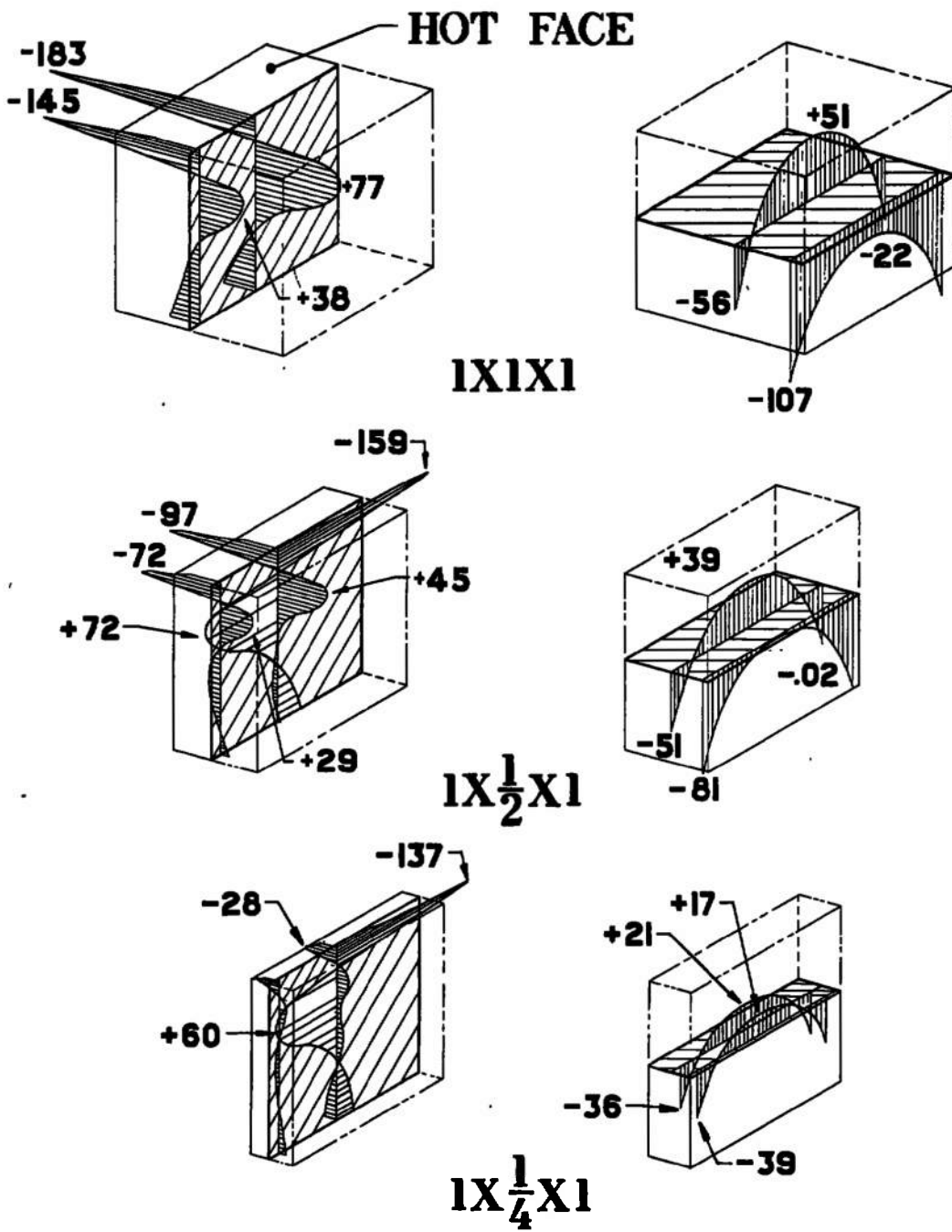


FIGURE 29. THERMAL STRESSES VS. PLAN FORM SHAPE
 COMPUTER RUNS 2, 7 AND 14

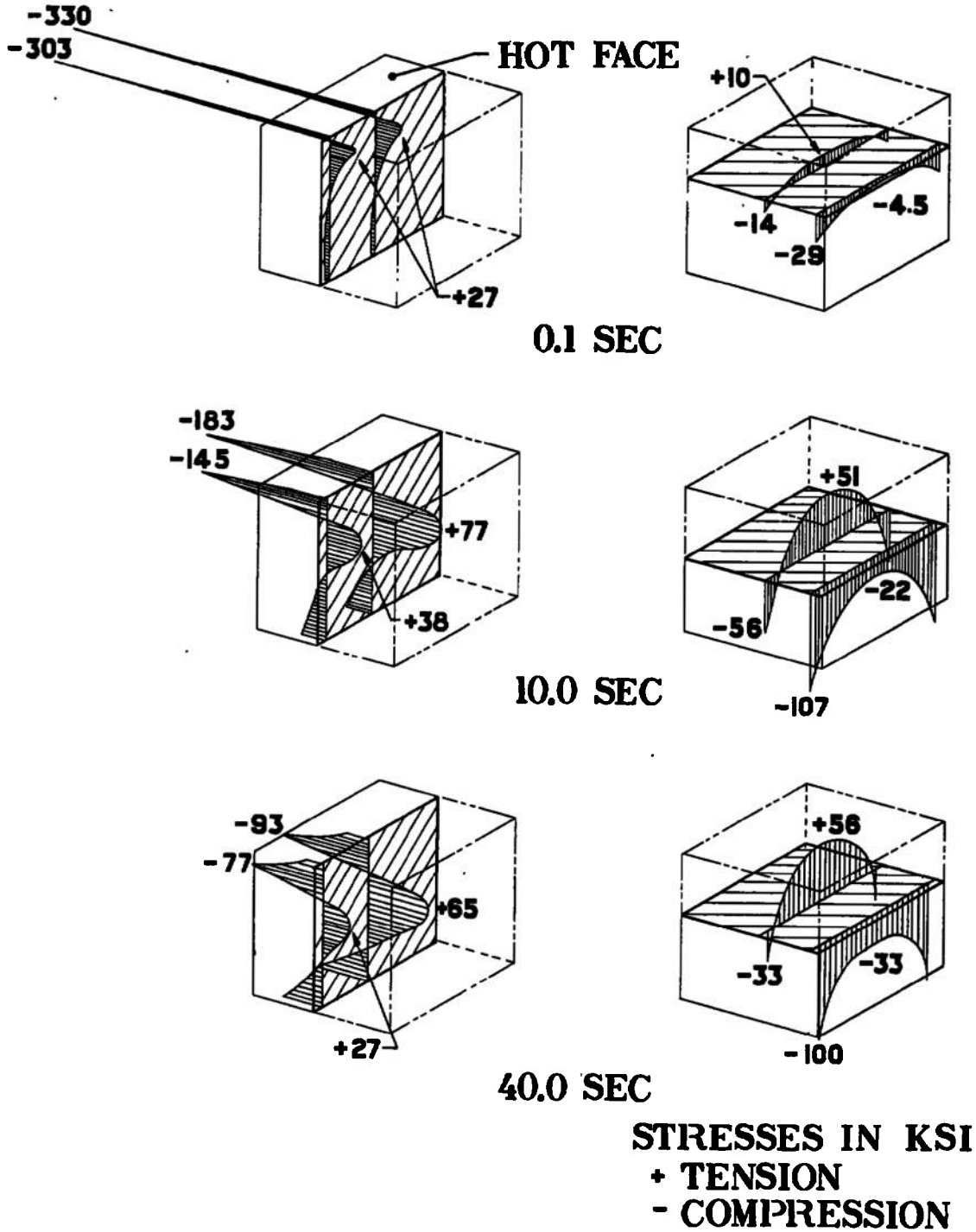
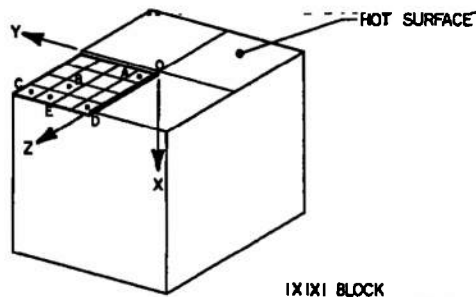


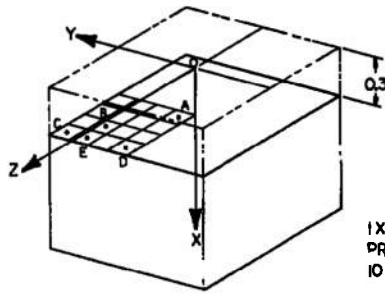
FIGURE 30. THERMAL STRESS VS. TIME FOR INSTANT TUNNEL START
 COMPUTER RUNS 1, 2 AND 3



1X1X1 BLOCK
10 SEC TEMPERATURE CURVE

POINT	X	Y	Z	DIAGRAM PRINCIPAL STRESSES	PRINCIPAL STRESSES				MAX SHEAR KSI
					VALUE KSI	DIRECTION COSINES			
						X-COMP	Y-COMP	Z-COMP	
A	.07	.0625	.0625		-4.2 -183.7 -182.4	+999 +361 +004	-.255 +.714 -.699	-.255 +.699 +.714	90
B	.07	.3125	.3125		+9.8 -112.0 -102.8	+977 +214 +000	-.151 +.692 -.706	-.151 +.689 +.708	61
C	.07	.4375	.4375		-9.9 -54.7 -39.4	+879 +476 +000	-.337 +.622 -.707	-.337 +.622 +.707	32
D	.07	.0625	.4375		+6.1 -145.3 -61.8	+936 +017 +352	-.012 +1000 -.016	-.352 +.011 +.936	76
E	.07	.3125	.4375		+9.4 -95.8 -54.2	+933 +214 +289	-.158 +.966 -.203	-.323 +.143 +.936	53

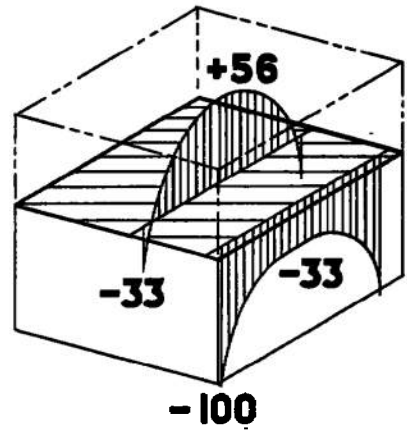
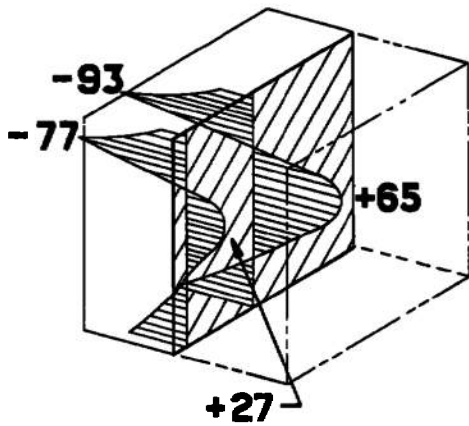
FIGURE 31. PRINCIPLE STRESSES NEAR HEATED SURFACE
COMPUTER RUN 2



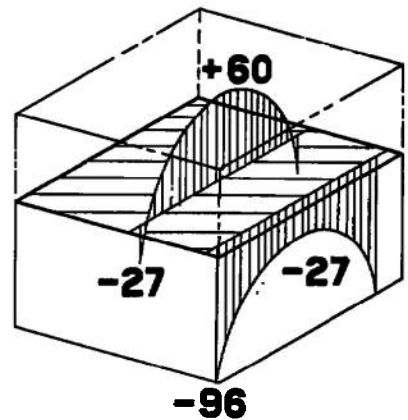
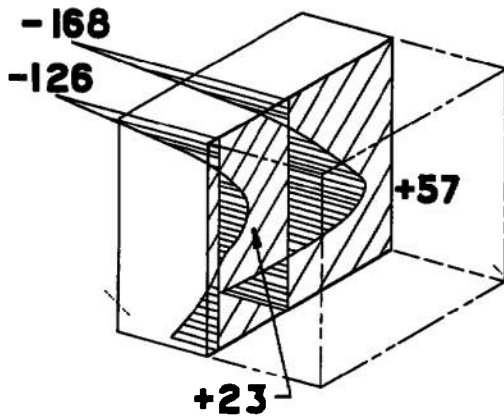
1X1X1 BLOCK
 PRINCIPAL STRESSES AT PLANE WHERE X=0.3
 10 SEC TEMPERATURE CURVE

POINT	X	Y	Z	PICTURE (PLANE X=0.3)	PRINCIPAL STRESSES				MAX SHEAR KSI
					VALUE KSI	DIRECTION COSINES			
						X-COMP	Y-COMP	Z-COMP	
A	.3	.0625	.0625		+ 43.7	+ .972	+ .166	+ .166	18
					+ 78.9	- .234	+ .685	+ .690	
					+ 76.4	+ .001	- .710	+ .704	
B	.3	.3125	.3125		+ 13.5	+ .911	+ .292	+ .292	21
					+ 56.3	- .413	+ .644	+ .644	
					+ 34.6	+ .000	- .707	+ .707	
C	.3	.4375	.4375		- 100.4	+ .999	+ .010	+ .010	58
					- 1.4	- .000	+ .707	- .707	
					+ 15.0	- .014	+ .707	+ .707	
D	.3	.0625	.4375		- 38.5	+ .997	+ .068	+ .024	28
					+ 38.2	- .069	+ .997	+ .355	
					+ 16.6	- .021	- .037	+ .999	
E	.3	.3125	.4375		- 47.2	+ .984	+ .175	- .012	37
					+ 26.5	- .148	+ .865	+ .480	
					+ 13.0	+ .095	- .471	+ .877	

FIGURE 32. PRINCIPLE STRESSES 0.3 INCHES FROM HEATED SURFACE
 COMPUTER RUN 2



**VARYING MAT'L
PROPERTIES**



**CONSTANT MAT'L
PROPERTIES**

**STRESSES IN KSI
+ TENSION
- COMPRESSION**

FIGURE 33. THERMAL STRESS VS. MATERIAL PROPERTIES
COMPUTER RUNS 3 AND 8

APPENDIX I
ANALYSIS OF THERMAL STRESSES
IN RECTANGULAR BLOCKS

Prepared by:
Illinois Institute of Technology Research Institute

December 1967

IIT RESEARCH INSTITUTE
Technology Center
Chicago, Illinois 60616

Final Report M6201

ANALYSIS OF THERMAL STRESSES
IN RECTANGULAR BLOCKS

by

M. A. Salmon
T. Belytschko

for

Fluidyne Engineering Corporation
5900 Olson Memorial Highway
Minneapolis, Minnesota

December 1967

FOREWORD

This study of the thermal stresses in rectangular blocks was performed by M. A. Salmon and T. Belytschko of the Structures Section, Mechanics Research Division of IIT Research Institute (IITRI) for the Fluidyne Engineering Corporation. Mr. P. B. Hasselquist coordinated the work for Fluidyne. The work was performed in the period of June to December 1967.

Respectfully submitted,
IIT RESEARCH INSTITUTE

A handwritten signature in cursive script, appearing to read "M A Salmon".

M. A. Salmon
Senior Scientist

MAS:ms

ANALYSIS OF THERMAL STRESSES
IN RECTANGULAR BLOCKS

ABSTRACT

An analysis of the thermal stresses in a rectangular block by the finite element method is described and a computer program for its implementation is presented. The program is capable of handling a temperature variation in one direction. Temperature dependence of the material properties is taken into account. Up to 10 divisions in the direction of temperature variation can be used; the lengths of these divisions are specified by the user. Up to five equal divisions in the other two directions can be used. Eight problems specified by Fluidyne were solved using the program.

CONTENTS

<u>Section</u>	<u>Page</u>
I INTRODUCTION	1
II ANALYSIS AND COMPUTER PROGRAM	1
APPENDIX A - COMPUTER PROGRAM	9
A. Introduction	9
B. Input Data	99
C. Description of Output	10
APPENDIX B - SPECIFICATION OF PROBLEMS SOLVED	45

ILLUSTRATIONS

<u>Figure</u>		<u>Page</u>
1	Prism Geometry	2
2	Subdivision of Quadrant of Block into Prismatic Elements	7
3	Coefficient of Thermal Expansion, α Vs Temperature T	46
4	Modulus of Elasticity, E Vs Temperature T	47
5	Piecewise Constant Temperature Approximation for Time = 0.1 sec (Run 1)	48
6	Piecewise Constant Temperature Approximation for Time = 10 sec, Thickness t = 1 in. (Runs 2,4,5 and 7)	49
7	Piecewise Constant Temperature Approximation for Time = 10 sec, Thickness t = 0.25 in. (Run 6)	50
8	Piecewise Constant Temperature Approximation for Time = 40 sec, (Runs 3 and 8)	51

TABLES

<u>Table</u>		<u>Page</u>
1	Input Data Format	11
2	Problem Specifications for Runs 1 to 8	52
3	Data for Run 1	53
4	Data for Runs 2, 4, 5, and 7	54
5	Data for Run 3	55
6	Data for Run 6	56

I. INTRODUCTION

This report describes a computer program for the thermal stress analysis of rectangular blocks by the finite element method. This computer program has been developed by IITRI for the Fluidyne Corporation and applied to the solution of eight specific problems. The computer printout for these problems has been delivered to Fluidyne.

The method of analysis and the computer program used to implement it are described in the following report. Instructions for the use of the computer program and the program listing are given in Appendix A. Appendix B contains the data specified by Fluidyne for the eight problems and the input data prepared from these specifications by IITRI.

II. ANALYSIS AND COMPUTER PROGRAM

An element stiffness matrix for a rectangular prism given by Melosh¹ is used in the analysis. The prism geometry is shown in Fig. 1. The following expression is used to relate the components of displacement to the nodal displacements

$$u = \Phi X \tag{1}$$

where

$$u^t(x,y,z) = [u_x, u_y, u_z]$$

$$X^t = [u_x^{(1)} \dots u_x^{(8)}, u_y^{(1)} \dots u_y^{(8)}, u_z^{(1)} \dots u_z^{(8)}]$$

and

$$\Phi = \begin{bmatrix} \phi & & \\ & \phi & \\ & & \phi \end{bmatrix}$$

¹Melosh, R. J., Structural Analysis of Solids Proc. ASCE, Vol. 9, No. ST4, August 1963.

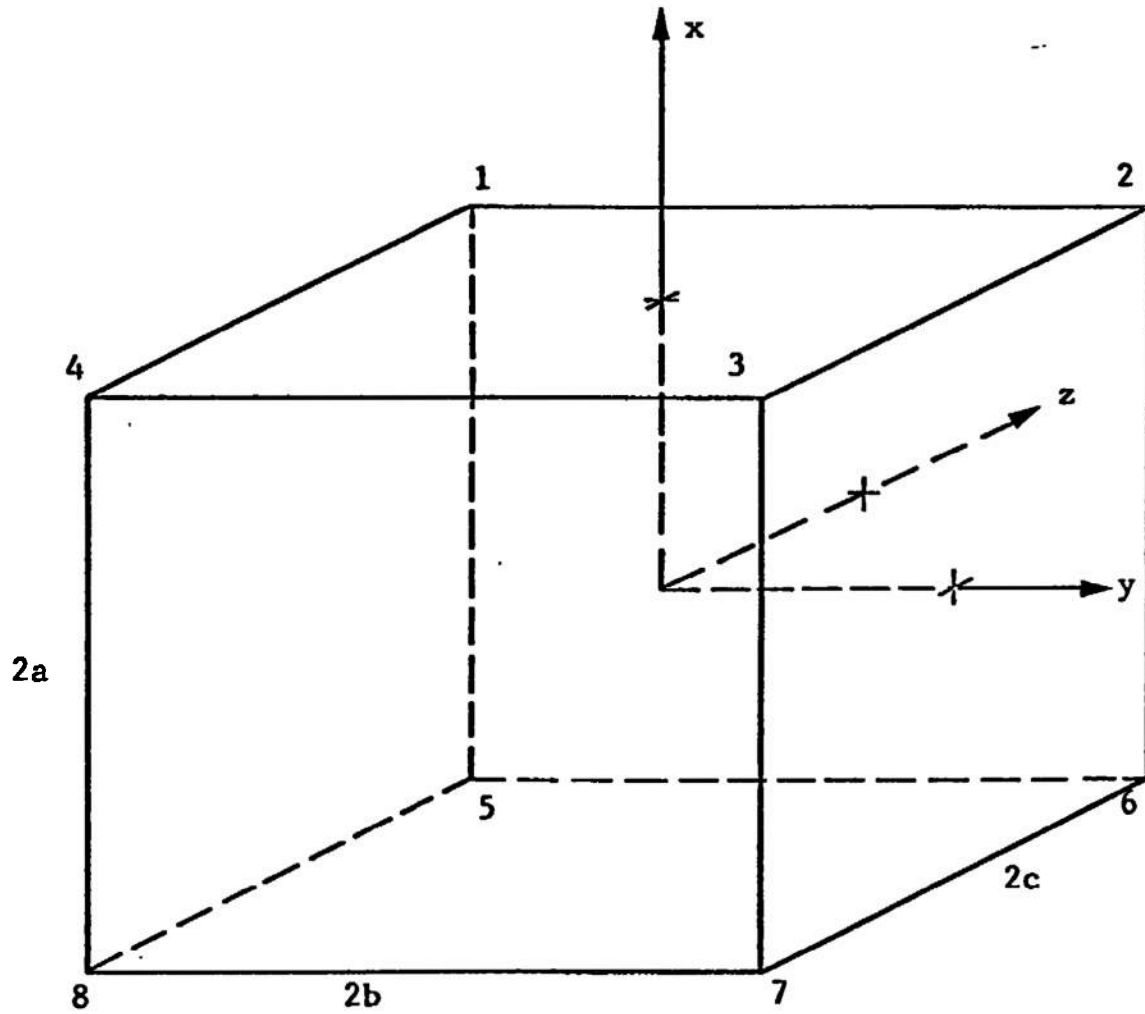


Fig.I-1 PRISM GEOMETRY

in which

$$\frac{\delta \phi}{abc} = \left[\begin{array}{l} -(\xi+1)(\eta-1)(\zeta+1), (\xi+1)(\eta+1)(\zeta+1), \\ -(\xi+1)(\eta+1)(\zeta-1), (\xi+1)(\eta-1)(\zeta-1), \\ (\xi-1)(\eta-1)(\zeta+1), -(\xi-1)(\eta+1)(\zeta+1), \\ (\xi-1)(\eta+1)(\zeta-1), -(\xi-1)(\eta-1)(\zeta-1) \end{array} \right]$$

where

$$\xi = x/a, \quad \eta = y/b, \quad \zeta = z/c .$$

The displacement field given by Eq. (1) satisfies the requirements that displacements of contiguous elements be compatible, that rigid body displacements produce no strain, and that states of uniform strain can be represented. Thus convergence of the solutions to the exact one as the fineness of the mesh is increased is assured.

The strain-displacement relations are

$$\epsilon = D u \quad (2)$$

where

$$\epsilon^t = \left[\epsilon_{xx}, \epsilon_{yy}, \epsilon_{zz}, \gamma_{xy}, \gamma_{xz}, \gamma_{yz} \right]$$

and

$$D^t = \left[\begin{array}{cccccc} \partial/\partial x & 0 & 0 & \partial/\partial y & \partial/\partial z & 0 \\ 0 & \partial/\partial y & 0 & \partial/\partial x & 0 & \partial/\partial z \\ 0 & 0 & \partial/\partial z & 0 & \partial/\partial x & \partial/\partial y \end{array} \right]$$

The stress strain law for an isotropic elastic material is

$$\sigma = C \epsilon_e \quad (3)$$

where the elastic strains are expressed in terms of the total strains and the thermal strains by

$$\varepsilon = \varepsilon_e + \varepsilon_t \quad (4)$$

and where

$$C = \begin{bmatrix} C_1 & C_2 & C_2 & & & \\ C_2 & C_1 & C_2 & & & \\ C_2 & C_2 & C_1 & & & \\ & & & C_3 & & \\ & & & & C_3 & \\ & & & & & C_3 \end{bmatrix}$$

in which

$$C_1 = \frac{E(1-\nu)}{(1+\nu)(1-2\nu)}$$

$$C_2 = \frac{E\nu}{(1+\nu)(1-2\nu)}$$

$$C_3 = \frac{E}{2(1+\nu)} \cdot$$

The stresses derived from the assumed displacement field of Eq. (1) do not satisfy the equations of equilibrium in the element. The finite element method consists in the selection of a nodal force vector F whose components correspond to the elements of the nodal displacement vector X by the application of the principle of virtual work. That is, the requirement is enforced that

$$\bar{X}^t F = \int_V \bar{\varepsilon}^t \sigma \quad (5)$$

where \bar{X} and ϵ are the virtual nodal displacement vector and the corresponding strains, respectively. Substitution of the expressions for stress and strain as functions of nodal displacement in Eq. (5) gives the result,

$$F = \int_V \phi^t D^t \{ C D \phi X - C \epsilon_t \} \quad (6)$$

where use has been made of the fact that the elements of \bar{X} may be chosen in an arbitrary manner.

Equation (6) may be written in the form

$$K X = F + F_p \quad (7)$$

where

$$K = \int_V \phi^t D^t C D \phi \quad (8)$$

and

$$F_p = \int_V \phi^t D^t C \epsilon_t \quad (9)$$

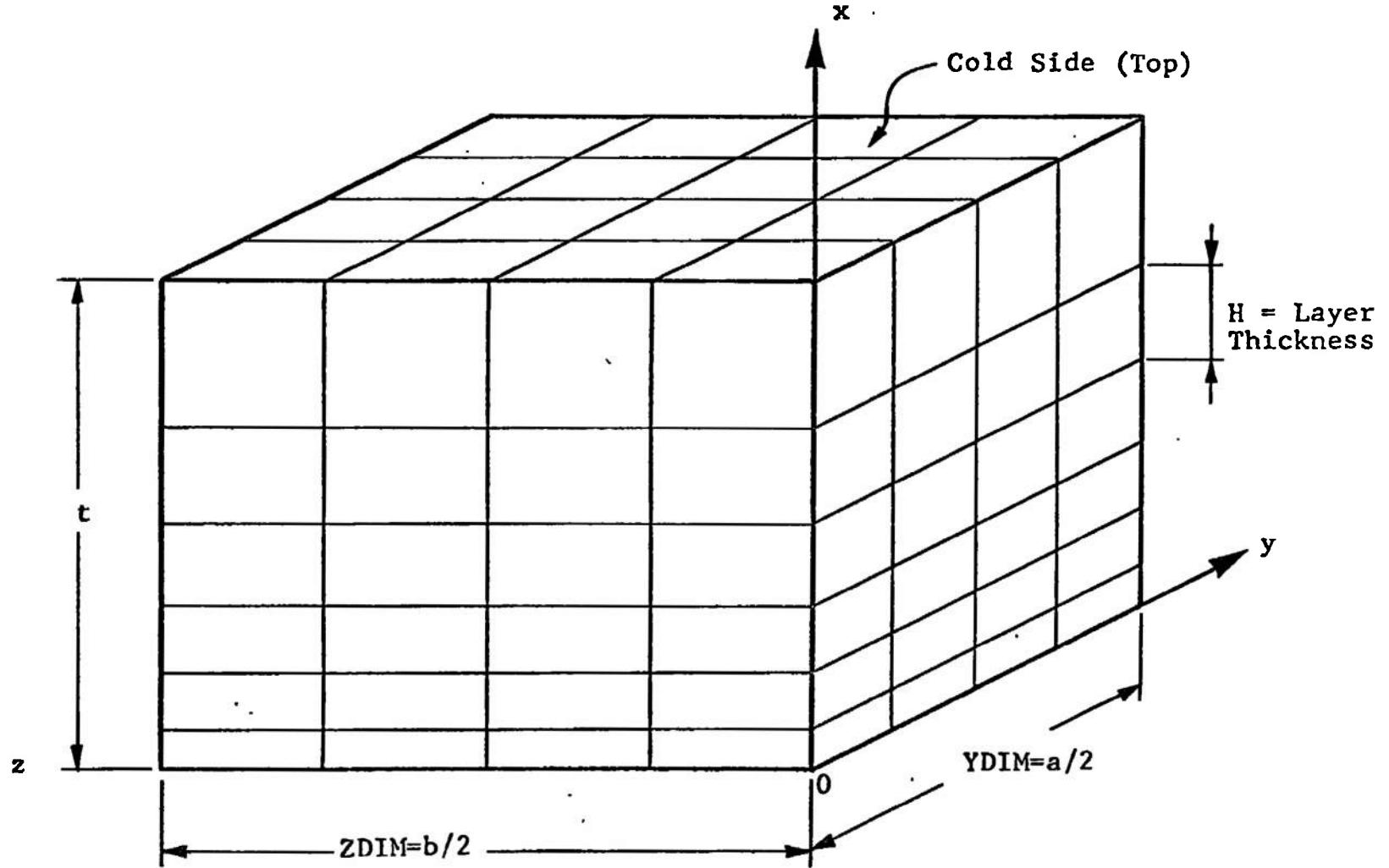
are the element stiffness matrix and the thermal force vector, respectively.

The thermal strains are simply

$$\epsilon_t^t = \alpha T [1, 1, 1, 0, 0, 0]$$

where α is the coefficient of expansion and T is the temperature rise.

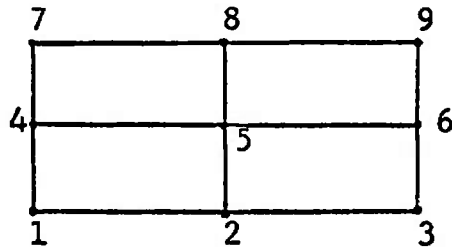
The formation of the element stiffness matrix in the computer program is accomplished by the evaluation of Eq. (7) (the exact expression for the integrals involved are used). The equilibrium equations for the assembly of prismatic



Block Dimensions: $a \times b \times c$

Fig. I-2 SUBDIVISION OF QUADRANT OF BLOCK INTO PRISMATIC ELEMENTS

where the A and B are square matrices of order $3m$. The elements of the A matrices are the forces on the nodes in that layer due to displacements of those nodes, while the elements of the B matrices are forces due to displacements of nodes in the layer above. Due to the fact that the elements in a layer are identical, any node in a layer can be identified with one of the nine nodes shown in the sketch.



The A and B matrices for this arrangement are of order 27, thus 1458 storage locations are required for each layer.

The interpretation of the results of the analysis requires some care. The stresses in an element vary linearly in the direction of the coordinate axes. Since the stresses satisfy equilibrium only on the average it is probably not meaningful to consider stresses anywhere but at the center of the element. Estimates of stresses at outside faces can best be made by extrapolating the results obtained at the centers of elements as one proceeds from the interior to the surface. The computer program does give stresses calculated at the centers of the outside faces of elements. However, examination of the results shows that these values are not as good as those given by extrapolation of values at the centers of elements. Hindsight shows that it was not a good idea to printout stresses at the outside faces and these results should be ignored.

APPENDIX A
COMPUTER PROGRAM

A. INTRODUCTION

TPA is a FORTRAN IV program for obtaining the thermal stresses created within a rectangular prism by the variation of temperature and material properties in one direction. The governing equations are formulated by means of the finite element method and then solved by the Gauss-Seidel method. The program's capacity limits problems to 10 layers of elements in the direction of the thermal gradient and up to five elements in each of the other two directions.

B. INPUT DATA

Let the direction of the thermal gradient be denoted by x and let the remaining two orthogonal directions be denoted by y and z respectively. The x -direction must correspond to an axis of the prism. Since the prism is symmetric with respect to the x - y and x - z planes, only a quadrant of the prism is considered. The geometry of this quadrant is specified by giving its y and z dimensions and the number of nodes desired in x , y , and z directions. The nodes in the y and z directions will be equally spaced. The spacing between the nodes in the x -direction which corresponds to the thicknesses of the element layers, are specified by the user in the layer cards.

For each layer of elements the user must provide a "layer" card which gives its thickness and the temperature, Young's modulus E , Poisson's ratio ν , and the thermal expansion coefficient α .

The only other required input is composed of two control numbers NUREAD and NUPRNT and the following parameters for the Gauss-Seidel method: the maximum number of iterations NIT, the error printout cycle NPERR, displacement and modified force printout cycle NPOTPT, the tolerance TOL and initial relaxation factor XFAC. The initial relaxation factor should be about 1.5.

After the iterative method is started if a given iteration does not reduce the error, the relaxation factor is reduced. The Gauss-Seidel method terminates after the error fails to decrease when the number of iterations exceeds NIT, or if the error meets the tolerance TOL. During the iterations the error and displacements are printed out according to the value of NPERR and NPOTPT, respectively. It is recommended that the displacements not be printed out more than once or twice during the solution, for it is very time-consuming.

The control number NUREAD determines whether the starting values of the displacements are to be read off a tape or to be computed. The second control number, NUPRNT gives the user the option of saving the displacements on tape or interpolating to a lattice with a larger number of elements. These options allow the user to run the problem to a certain point, save the displacements on a tape and continue later from the same point by using these displacements as starting values.

The interpolation routine inserts the displacement values for a lattice with n_1 elements in the z-direction, n_2 elements in the y-direction, and m elements in the x-direction to obtain the starting values for $2n_1$ by $2n_2$ by m lattice. When this option is used the second problem is then automatically run with the interpolated displacements as starting values. A detailed description of the input data required is given in Table 1.

C. DESCRIPTION OF OUTPUT

The initial output is an echo of all data. Following this, the applied nodal forces and starting values for the displacements are printed out, and then whatever intermediate output the user specifies.

The final output consists of the displacements and stresses. The stresses are computed and printed at the centroids of all elements and at the centers of all outside faces.

TABLE I-1
INPUT DATA FORMAT

Card 1	TITLE CARD (12A6)	
Column		
1 - 72	Any alphanumeric information	
Card 2	PARAMETER CARD (6I5, 4F10.0)	
Column		
1 - 5	NX	- Number of nodes in x-direction
6 - 10	NY	- Number of nodes in y-direction
11 - 15	NZ	- Number of nodes in z-direction
16 - 20	NIT	- Maximum number of iterations
21 - 25	NPERR	- Error printout cycle
26 - 30	NPOTPT	- Displacement and modified force printout cycle
31 - 40	DIMY	- y-dimension of prism quadrant
41 - 50	DIMZ	- z-dimension of prism quadrant
51 - 60	TOL	- Error tolerance for Gauss-Seidel
61 - 70	XFAC	- Initial relaxation factor
Card 3	LAYER PROPERTY CARDS (I5, 5E10.0)	
Column		
1 - 5	Layer number	
6 - 15	H	- Thickness of layer
16 - 25	T	- Temperature of layer
26 - 35	E	- Young's modulus for layer
36 - 45	PR	- Poisson's ratio for layer
46 - 55	ALFA	- Thermal expansion coefficient for layer
Card 4	CONTROL CARD	
Column		
1 - 5	NUREAD	- Determines how initial displacements are obtained - 0 calculated - 1 read from card reader - 2 read from tape 8 - 3 read from tape 10
6 - 10	NUPRNT	- Gives the following options - 0 none of the options used - 1 displacements are saved on tape 10 - 2 displacements are used to interpolate to a larger lattice - 3 interpolation and displacements from larger problem saved on tape 10
Card 5	INTERPOLATION CARD (OPTIONAL), (3I5, 2E10.0)	
Column		
1 - 5	NIT	- Maximum number of iterations for second problem
6 - 10	NPERR	- Error printout cycle for second problem
11 - 15	NPOTPT	- Displacement printout cycle for second problem
16 - 25	TOL	- Error tolerance for second problem
26 - 35	XFAC	- Initial relaxation factor for second problem

The stresses are printed out in the following manner. For each point there are five lines. The first line gives the x, y and z coordinates of the point. The second line gives the xx, yy, zz, xy, xz and yz components of the stresses and the effective stress σ_e . The effective stress σ_e is computed by the formula

$$\sigma_e^2 = (\sigma_{xx} - S)^2 + (\sigma_{yy} - S)^2 + (\sigma_{zz} - S)^2 + 2(\sigma_{xy} + \sigma_{yz} + \sigma_{xz})$$

where

$$S = 1/3 (\sigma_{xx} + \sigma_{yy} + \sigma_{zz}) .$$

The remaining three lines give the three principal stresses and the corresponding principal directions. If the solutions to additional problems are desired, the data sets are repeated. Any number of problems can be solved in sequence.

```

C*****TPA00020
C  THERMAL STRESS ANALYSIS OF RECTANGULAR PRISM TPA00030
C
C      TAPE 8 IS USED TO INPUT DISPLACEMENTS IF
C      NUREAD = 2 OPTION IS USED
C
C      TAPE 10 IS USED TO SAVE DISPLACEMENTS IF
C      NPRINT = 2 OPTION IS USED
C
C*****TPA00040
COMMON A(18,9,189)
COMMON/SOL/F(21,10,30),U(21,10,30),IMAX,JMAX,KMAX,SUM,XFAC,TEMP(20
1),ALFA(20),H(20),E(20),PR(20),BDIM,CDIM
COMMON>IDEN/MIDEN(10),NIDEN(10),NITER
DIMENSION FTEMP(6300),FTEMP1(6300),TITLE(12)
DOUBLE PRECISION F,FTEMP
EQUIVALENCE(F(1,1,1),FTEMP(1)),(FTEMP1(1),TITLE(1))
C
C ***** READ AND PRINT DATA ***** TPA00110
C
C      1 READ(5,100) TITLE,IMAX,JMAX,KMAX,NIT,NPERR,NPOTPT,DIMJ,DIMK,TOL, TPA00120
C      IXFAC,DELERR TPA00130
C      IF (IMAX.EQ.0) STOP TPA00140
C      100 FORMAT (12A6/6I5,3F10.0,2F5.0) TPA00150
C      NLayer=IMAX-1 TPA00160
C      READ(5,101)(K,H(K),TEMP(K),E(K),PR(K),ALFA(K),J=1,NLayer) TPA00180
C      101 FORMAT(I5,5F10.0) TPA00190
C      DIMI=0. TPA00200
C      DO 2 I=1,NLayer TPA00210
C      2 DIMI=DIMI&H(I) TPA00220
C      WRITE(6,200) TITLE,IMAX,DIMI,JMAX,DIMJ,KMAX,DIMK,NIT,NPERR,NPOTPT TPA00230
C      1,TOL,XFAC,DELERR TPA00240
C      200 FORMAT(1H1 12A6/ TPA00250
C      1 14H0 -X-DIRECTION,I4,3X5HNODES5X7HLENGTH=F8.4/ TPA00260
C      2 14H0 Z-DIRECTION,I4,3X5HNODES5X7HLENGTH=F8.4/ TPA00270
C      3 14H0 Y-DIRECTION,I4,3X5HNODES5X7HLENGTH=F8.4/ TPA00280
C      4 30H0 MAXIMUM NO. OF ITERATIONS---I3/ TPA00290
C      5 30H0 ERROR PRINT CYCLE---I3/ TPA00300
C      6 30H0 OUTPUT PRINT CYCLE---I3/ TPA00310
C      7 30H0 ERROR TOLERANCE---E12.4/ TPA00320
C      8 30H0 OVER RELAXATION FACTOR---F7.3/ TPA00330
C      9 30H0 DELERR ---F7.3) TPA00340
C      WRITE(6,201) TPA00360
C      201 FORMAT (1H040X18H LAYER PROPERTIES/11H0 LAYER NO.11X9HTHICKNESS9XT TPA00370
C      11HTEMPERATURE13X7HMODULUS5X15HPOISSON S RATIO4X16HEXPANSION COEFF TPA00380

```

AEDC-TR-70-92

2.)		TPA00390
	WRITE (6,203)(K,H(K),TEMP(K),E(K),PR(K),ALFA(K),K=1,NLAYER)	TPA00400
203	FORMAT (I8,3X,5E20.5)	TPA00410
300	READ (5,204) NUREAD,NUPRNT	TPA00420
204	FORMAT (10I5)	TPA00430
	WRITE (6,205) NUREAD,NUPRNT	TPA00440
205	FORMAT (1H0,5X,8HNUREAD =,I2,5X,8HNUPRNT =,I2)	TPA00450
C		TPA00460
C	**** FORM EQUATIONS ****	TPA00470
C		TPA00480
	XNJ= JMAX-1	TPA00490
	XNK= KMAX-1	TPA00500
	BDIM=DIMK/XNK	TPA00510
	CDIM=DIMJ/XNJ	TPA00520
	CALL FSEQ	TPA00530
	NITER=0	TPA00540
	NUREAD=NUREAD&1	TPA00550
	GO TO (60,60,80,80),NUREAD	
C		TPA00570
C	**** MAKE INITIAL ESTIMATE OF DISPLACEMENTS ****	TPA00580
C		TPA00590
	60 CALL DISPL(H,TEMP,ALFA,DIMJ,DIMK,IMAX,JMAX,KMAX,U,DIMI)	TPA00600
	GO TO 91	TPA00650
	80 READ (8) ((U(I,J,K),K=1,30),J=1,10),I=1,IMAX)	
	91 CONTINUE	TPA00690
C		TPA00700
C	**** ITERATION ON NODAL DISPLACEMENTS ****	TPA00710
C		TPA00720
	SF=0.	TPA00730
	DO 250 J=1,6300	
	FTEMP1(J)=FTEMP(J)	
250	SF = SF & DABS(FTEMP(J))	TPA00750
	SUMP=1.E&35	TPA00760
	DELFAC= (XFAC-0.8)/10.0	TPA00770
	KOUNT=0	TPA00780
	IF (NIT.EQ.0) GO TO 401	TPA00810
C		TPA00830
C	SET UP ROW AND COLUMN IDENTIFIERS	TPA00840
C		TPA00850
	MIDEN(1)=1	TPA00860
	DO 20 M=2,JMAX	TPA00870
20	MIDEN(M)=2	TPA00880
	MIDEN(JMAX)=3	TPA00890
	NIDEN(1)=1	TPA00900
	DO 21 N=2,KMAX	TPA00910

21	NIDEN(N)=2	TPA00920
	NIDEN(KMAX)=3	TPA00930
10	SUM=0.0	TPA00960
	NITER=NITER&1	TPA00970
	DO 11 L1=1,IMAX	TPA00980
	DO 11 M1=1,JMAX	TPA00990
	DO 11 N1=1,KMAX	TPA01000
	I3=1&(L1-1)*9	
	CALL SOLVE(A(1,1,I3),L1,M1,N1)	
11	CONTINUE	TPA01020
	IMID=IMAX/2	
	UMID=U(IMID,1,1)	
	DO 1101 L1=1,IMAX	
	DO 1101 M1=1,JMAX	
	DO 1101 N1=1,KMAX	
1101	U(L1,M1,N1)=U(L1,M1,N1)-UMID	
	DO 601 J=1,6300	
601	FTEMP(J)=FTEMP1(J)	TPA 103
C		TPA01040
C	**** CYCLE COUNT AND PRINT CHECK ****	TPA01050
C		TPA01060
	SUM=SUM/SF	TPA01070
C	CHECK WHETHER RELAXATION FACTOR IS TO BE MODIFIED	TPA01080
C		TPA01090
	IF (ABS(SUM).LT.1.E-10) GO TO 12	TPA01100
	IF (((SUMP-SUM)/SUM).LT.DELERR) GO TO 55	TPA01110
	KOUNT=KOUNT&1	TPA01120
	IF (KOUNT.GE.10) GO TO 52	TPA01130
	XFAC=XFAC-DELFAC	TPA01140
	GO TO 55	TPA01150
52	IF (SUM.GT.SUMP) GO TO 12	TPA01160
55	SUMP=SUM	TPA01170
	IF(MOD(NITER,NPERR).EQ.0) WRITE(6,202) NITER,SUM	TPA01180
202	FORMAT(20HO NO. OF ITERATIONS=I4,5X,6HERROR=E15.7)	TPA01190
	IF(MOD(NITER,NPOTPT).EQ.0) CALL OUTDIS(U,H,IMAX,JMAX,KMAX,BDIM,	TPA01200
	1 CDIM,1)	TPA01210
C	CHECK IF ERROR MEETS TOLERANCE	TPA01220
	IF (SUM-TOL) 12,12,13	TPA01230
13	IF(NITER.LT.NIT) GO TO 10	TPA01240
12	WRITE(6,202) NITER,SUM	TPA01250
	NUPRNT=NUPRNT&1	TPA01260
	GO TO (401,890,900),NUPRNT	TPA01280
890	WRITE (10) (((U(I,J,K),K=1,30),J=1,10),I=1,IMAX)	TPA01290
	WRITE (6,891)	
891	FORMAT (1HO,5X,30HDISPLACEMENTS SAVED ON TAPE 10)	TPA01310
		TPA01320

GO TO 401	TPA01330
900 READ (5,902) I,IMAX,JMAX,KMAX,NIT,NPERR,NPOTPT,TOL,XFAC	TPA01340
902 FORMAT (7I5,2E10.3)	TPA01350
IF (I.NE.(-619)) GO TO 401	TPA01360
CALL INTERP	TPA01370
GO TO 300	TPA01410
C	TPA01420
C CALCULATE AND OUTPUT STRESSES	TPA01430
401 CALL PART2	TPA01440
GO TO 1	TPA01450
END	TPA01460
SUBROUTINE DISPL(H,T,ALFA,DIMJ,DIMK,IM,JM,KM,U,D)	TPA01510
C*****	TPA01480
C INITIAL ESTIMATE OF DISPLACEMENTS	TPA01490
C*****	TPA01500
DIMENSION H(20),T(20),ALFA(20),U(21,10,30),XI(21),ZJ(21),YK(21),Y(
110),Z(10)	
NL=IM-1	TPA01540
DO 1 I=1,NL	TPA01550
ZJ(I)=T(I)*ALFA(I)*DIMJ	TPA01560
1 YK(I)=T(I)*ALFA(I)*DIMK	TPA01570
XI(I)=0	TPA01580
DO 2 I=2,IM	TPA01590
XI(I)=XI(I-1)&H(I-1)*ALFA(I-1)*T(I-1)	TPA01600
ZJ(I)=(ZJ(I-1)&ZJ(I))/2.	TPA01610
2 YK(I)=(YK(I-1)&YK(I))/2.	TPA01620
YK(IM)=T(NL)*ALFA(NL)*DIMK	TPA01630
ZJ(IM)=T(NL)*ALFA(NL)*DIMJ	TPA01640
Y(1)=0.	TPA01650
Z(1)=0.	TPA01660
DO 3 I=2,JM	TPA01670
3 Z(I)=FLOAT(I-1)/FLOAT(JM-1)	TPA01680
DO 4 I=2,KM	TPA01690
4 Y(I)=FLOAT(I-1)/FLOAT(KM-1)	TPA01700
DO 5 I=1,IM	TPA01710
DO 5 J=1,JM	TPA01720
DO 5 K=1,KM	TPA01730
U(I,J,K)=XI(I)	
U(I,J,K&10)=YK(I)*Y(K)	TPA 175
5 U(I,J,K&20)=ZJ(I)*Z(J)	
S=0.	TPA01770
DO 6 I=1,IM	TPA01780
DK=U(I,JM,KM&10)/2.0	
IF (I-1) 61,61,62	TPA01800
61 DS=H(I)*DK	TPA01810

GO TO 6	TPA01820
62 DS=(H(I)&H(I-1))*DK	TPA01830
IF(I.EQ.IM)DS=H(I-1)*DK	TPA01840
6 S=S&DS	TPA01850
DEL=(S/D-U(IM,JM,KM&10))/D*DIMK	TPA 186
DO 8 J=1,JM	TPA01870
Z=FLOAT(J-1)/FLOAT(JM-1)*DIMJ	TPA01880
DO 8 K=1,KM	TPA01890
Y=FLOAT(K-1)/FLOAT(KM-1)*DIMK	TPA01900
R=(Z*Z&Y*Y)/DIMK**2*DEL	TPA01910
DO 8 I=1,IM	TPA01920
8 U(I,J,K)=U(I,J,K)&R	
IMID=IM/2	TPA01940
UMID=U(IMID,1,1)	
DO 9 I=1,IM	TPA01960
DO 9 J=1,JM	TPA01970
DO 9 K=1,KM	TPA01980
9 U(I,J,K)=U(I,J,K)-UMID	
RETURN	TPA02000
END	TPA02010
SUBROUTINE SOLVE(A,L,M,N)	TPA02060
C*****	TPA02030
C GAUSS SEIDEL ITERATION	TPA02040
C*****	TPA02050
DIMENSION A(18,9,9),FR(3),UR(3),D(3),DU(3)	
COMMON/SOL/F(21,10,30),U(21,10,30),IMAX,JMAX,KMAX,SUM,XFAC,TEMP(20	
I),ALFA(20),H(20),E(20),PR(20),8DIM,CDIM	
COMMON>IDEN/MIDEN(10),NIDEN(10),NITER	
DOUBLE PRECISION F	
DOUBLE PRECISION FR	TPA02110
IK=3*MIDEN(M)-3&NIDEN(N)	TPA02140
DO 1 I=1,3	TPA02150
I3=N&(I-1)*10	TPA 216
I4=I&(I-1)*3	
UR(I)=U(L,M,I3)	
FR(I)=F(L,M,I3)	
1 D(I)=A(IK,IK,I4)	
MML=M-1	TPA02190
MMU=M&1	TPA02200
NNL=N-1	TPA02210
NNU=N&1	TPA02220
IF (MIDEN(M)-2) 5,7,6	TPA02230
5 MML=1	TPA02240
GO TO 7	TPA02250
6 MMU=JMAX	TPA02260


```

7 IF (NIDEN(N)-2) 8,10,9
8>NNL=1
9>NNL=1
10>NNL=N
11>NNL=N
12>NNL=N
13>NNL=N
14>NNL=N
15>NNL=N
16>NNL=N
17>NNL=N
18>NNL=N
19>NNL=N
20>NNL=N
21>NNL=N
22>NNL=N
23>NNL=N
24>NNL=N
25>NNL=N
26>NNL=N
27>NNL=N
28>NNL=N
29>NNL=N
30>NNL=N
31>NNL=N
32>NNL=N
33>NNL=N
34>NNL=N
35>NNL=N
36>NNL=N
37>NNL=N
38>NNL=N
39>NNL=N
40>NNL=N
41>NNL=N
42>NNL=N
43>NNL=N
44>NNL=N
45>NNL=N
46>NNL=N
47>NNL=N
48>NNL=N
49>NNL=N
50>NNL=N
51>NNL=N
52>NNL=N
53>NNL=N
54>NNL=N
55>NNL=N
56>NNL=N
57>NNL=N
58>NNL=N
59>NNL=N
60>NNL=N
61>NNL=N
62>NNL=N
63>NNL=N
64>NNL=N
65>NNL=N
66>NNL=N
67>NNL=N
68>NNL=N
69>NNL=N
70>NNL=N
71>NNL=N
72>NNL=N
73>NNL=N
74>NNL=N
75>NNL=N
76>NNL=N
77>NNL=N
78>NNL=N
79>NNL=N
80>NNL=N
81>NNL=N
82>NNL=N
83>NNL=N
84>NNL=N
85>NNL=N
86>NNL=N
87>NNL=N
88>NNL=N
89>NNL=N
90>NNL=N
91>NNL=N
92>NNL=N
93>NNL=N
94>NNL=N
95>NNL=N
96>NNL=N
97>NNL=N
98>NNL=N
99>NNL=N
100>NNL=N

```

```

TPA02270
TPA02280
TPA02290
TPA02300
TPA02310
TPA02320
TPA02330
TPA02340
TPA02350
TPA02360
TPA02370
TPA02380
TPA 240
TPA02400
TPA02410
TPA02420
TPA02430
TPA02440
TPA02450
TPA02460
TPA02470
TPA02480
TPA02490
TPA02500
TPA02510
TPA02520
TPA02530
TPA02540
TPA02550
TPA02560
TPA 257
TPA02580
TPA02590
TPA02600
TPA02610
TPA 262
TPA02630
TPA02640
TPA02650
TPA02660
TPA02670

```

	NNLTMP=NNL	TPA02680
	MMLTMP=M&1	TPA02690
	IF (MMLTMP.GT.MMU) GO TO 31	TPA02700
29	DO 30 MM=MMLTMP,MMU	TPA02710
	DO 26 NN=NNLTMP,NNU	TPA02720
	IJ = 3*(MIDEN(M)&MM-M)&NIDEN(N)&NN-N-3	TPA02730
25	DO 26 IX=1,3	TPA02740
	DO 26 JX=1,3	TPA02750
	I4=JX&(IX-1)*3	
	I3=NN&(IX-1)*10	
26	F(LL,MM,I3)=F(LL,MM,I3)-A(IK,IJ,I4)*DU(JX)	TPA 277
30	NNLTMP=NNL	TPA02770
	IF (IK.GT.9) GO TO 35	TPA02780
31	IF (L.EQ.IMAX) GO TO 35	TPA02790
	LL=LL&1	TPA02800
	IK=IK&9	TPA02810
	MMLTMP=MML	TPA02820
	GO TO 29	TPA02830
35	CONTINUE	TPA02840
900	RETURN	TPA02850
	END	TPA02860
	SUBROUTINE OUTDIS (U,H,IMAX,JMAX,KMAX,BDIM,CDIM,NT1)	TPA03050
		TPA03060
		TPA03070
C	PRINTS OUT DISPLACEMENTS AND COORDINATES OF NODES	
C	DIMENSION XC(3),U(21,10,30),H(20)	
	KOUNT=3	TPA03090
	GO TO (10,20),NT1	TPA03100
10	WRITE(6,900)	TPA03110
900	FORMAT(1H1,35X,29HD I S P L A C E M E N T S U//10X,1HX,11X,1HY,	TPA03120
	1 11X,1HZ,16X,3HU-X,14X,3HU-Y,14X,3HU-Z)	TPA03130
	GO TO 30	TPA03140
20	WRITE (6,899)	TPA03150
899	FORMAT(1H1,35X,16HF O R C E S F //10X,1HX,11X,1HY,	TPA03160
	1 11X,1HZ,16X,3HF-X,14X,3HF-Y,14X,3HF-Z)	TPA03170
30	XC(1)=0.	TPA03180
	DO 101 L=1,IMAX	TPA03190
	WRITE(6,901)	TPA03200
	KOUNT=KOUNT&1	TPA03210
	DO 100 K=1,KMAX	TPA03220
	XC(2)=FLOAT(K-1)*BDIM	TPA03230
	DO 100 J=1,JMAX	TPA03240
	XC(3)=FLOAT(J-1)*CDIM	TPA03250
	WRITE(6,902) XC,U(L,J,K),U(L,J,K&10),U(L,J,K&20)	TPA 402
	KOUNT=KOUNT&1	TPA03270
	IF(KOUNT.LT.51) GO TO 100	TPA03280

```

          KOUNT=0
          GO TO (110,120),NT1
110 WRITE(6,900)
          GO TO 100
120 WRITE (6,899)
100 CONTINUE
101 XC(1)=XC(1)&H(L)
          RETURN
901 FORMAT(1H0)
902 FORMAT(1X,3F12.6,5X,3(1PE17.5))
          END
          SUBROUTINE ASSEM(A,AT,BLK)
C*****
C ASSEMBLE STIFFNESS MATRIX BY LAYERS
C*****
          DIMENSION A(18,9,9),AT(18,9,9),LOC(4,4),BLK(3,3,64)
          DIMENSION ILOC(16)
          EQUIVALENCE (ILOC(1),LOC(1,1))
          DATA (ILOC(J),J=1,16)/4,5,7,8,5,6,8,9,2,3,5,6,1,2,4,5/
          DO 1 I=1,4
          DO 1 J=1,4
          JB=LOC(I,J)
          JT=JB&9
          JJ=J&4
          DO 1 K=1,4
          J5=JJ&(K-1)*8
          J4=J&(K-1)*8
          KB=LOC(I,K)
          KK=K&4
          J3=JJ&(KK-1)*8
          DO 1 L=1,3
          DO 1 M=1,3
          I3=L&(M-1)*3
          A(JB,KB,I3)=A(JB,KB,I3)&BLK(L,M,J3)
          A(JT,KB,I3)=A(JT,KB,I3)&BLK(L,M,J5)
1 AT(JB,KB,I3)=AT(JB,KB,I3)&BLK(L,M,J4)
          RETURN
          END
          SUBROUTINE FSEQ
C*****
C FORM SYSTEM OF EQUATIONS
C*****
          COMMON AB(18,9,189)
          COMMON/SOL/F(21,10,30),U(21,10,30),IMAX,JMAX,KMAX,SUM,XFAC,TEMP(20
1),ALFA(20),H(20),E(20),PR(20),BDIM,CDIM

```

TPA03290
 TPA03300
 TPA03310
 TPA03320
 TPA03330
 TPA03340
 TPA03350
 TPA03360
 TPA03370
 TPA03380
 TPA03390
 TPA03700
 TPA03670
 TPA03680
 TPA03690
 TPA03730
 TPA03740
 TPA03750
 TPA03760
 TPA03770
 TPA03780
 TPA03790
 TPA03800
 TPA03810
 TPA03820
 TPA03860
 TPA03870
 TPA03920
 TPA03890
 TPA03900
 TPA03910

```

DOUBLE PRECISION F
DIMENSION BLK(3,3,64),BLKT(3,3,64),AT(18,9,9)
EQUIVALENCE (U(1,1,1),BLK(1,1,1)),(U(1,1,10),BLKT(1,1,1))
DO 1 I=1,21
DO 1 J=1,10
DO 1 K=1,10
DO 1 L=1,3
I3=K&(L-1)*10
F(I,J,I3)=0.
1 U(I,J,I3)=0.
DO 2 I=1,18
DO 2 J=1,9
DO 2 K=1,3
DO 2 L=1,3
I3=K&(L-1)*3
AT(I,J,I3)=0.
DO 2 M=1,IMAX
I4=K&(L-1)*3&(M-1)*9
2 AB(I,J,I4)=0.
LMAX=IMAX-1
DO 3 L=1,LMAX
L1=L&1
ALFAT=TEMP(L)*ALFA(L)
CALL BSTIF(H(L),BDIM,CDIM,E(L),PR(L),BLK,BLKT)
CALL ASSEM(AB(1,1,9*L-8),AT,BLK)
CALL LOAD(H(L),BDIM,CDIM,E(L),PR(L),ALFAT,JMAX,KMAX,L,F)
DO 4 I=1,18
DO 4 J=1,9
DO 4 K=1,3
DO 4 LK=1,3
I3=K&(LK-1)*3&(L1-1)*9
I4=K&(LK-1)*3
AB(I,J,I3)=AB(I,J,I3)+AT(I,J,I4)
4 AT(I,J,I4)=0.
3 CONTINUE
RETURN
END
SUBROUTINE BFORCE(A,B,C,E,PR,ALFAT,FB)
C*****TPA04290
C COMPUTE THERMAL NODE FORCES ON BLOCK
C*****TPA04310
DIMENSION FB(3,B),BDIM(3),IPHI(8,4),IPHITE(32)
EQUIVALENCE (IPHITE(1),IPHI(1,1))
DATA (IPHITE(J),J=1,32)/ &1,&1,&1,&1,-1,-1,-1,-1,
1 -1,&1,&1,-1,-1,&1,&1,-1,

```

```

2          &1,&1,-1,-1,&1,&1,-1,-1,
3          -1,&1,-1,&1,&1,-1,&1,-1 /
  C1=E/(1.-2.*PR)
  BDIM(1)=A
  BDIM(2)=B
  BDIM(3)=C
  V=A*B*C
  DO 1 I=1,3
  CI=V/4./BDIM(I)
  DO 1 J=1,8
  IS=1
  DO 2 M=1,4
  IF(M.EQ.I) GO TO 2
  IS=IS+IPHI(J,M)
2 CONTINUE
  S=IS
1 FB(I,J)=C1*CI*ALFAT*S
  RETURN
  END
  SUBROUTINE LOAD(A,B,C,E,PR,ALFAT,      JMAX,KMAX,L,F)
C*****
C ADD THERMAL FORCES TO NODES IN LAYER
C*****
  DIMENSION F(21,10,30),FB(3,8),LOC(8)
  DOUBLE PRECISION F
  DATA(LOC(I),I=1,8)/8,7,5,6,4,3,1,2/
  JU=JMAX-1
  KU=KMAX-1
  LL=L
  LU=L&1
  CALL BFORCE(A,B,C,E,PR,ALFAT,FB)
  DO 1 J=1,JU
  DO 1 K=1,KU
  KK=0
  DO 1 IL=LL,LU
  DO 1 M=1,2
  DO 1 N=1,2
  KK=KK&1
  JF=LOC(KK)
  JM=J&M-1
  KN=K&N-1
  DO 1 IN=1,3
  I3=KN&(IN-1)*10
1 F(IL,JM,I3)=F(IL,JM,I3)&FB(IN,JF)
  RETURN

```

```

TPA04360
TPA04370
TPA04380
TPA04390
TPA04400
TPA04410
TPA04420
TPA04430
TPA04440
TPA04450
TPA04460
TPA04470
TPA04480
TPA04490
TPA04500
TPA04510
TPA04520
TPA04570
TPA04540
TPA04550
TPA04560
TPA04590
TPA04600
TPA04610
TPA04620
TPA04630
TPA04640
TPA04650
TPA04660
TPA04670
TPA04680
TPA04690
TPA04700
TPA04710
TPA04720
TPA04730
TPA04740
TPA04750
TPA 476
TPA04770

```

```

END TPA04780
SUBROUTINE INTERP TPA05350
C INTERPOLATES DISPLACEMENTS U TO A GRID OF DOUBLE SIZE TPA05360
C RESULT IS INSERTED INTO F TPA05370
COMMON/SOL/F(21,10,30),U(21,10,30),IMAX,JMAX,KMAX,SUM,XFAC,TEMP(20
1),ALFA(20),H(20),E(20),PR(20),BDIM,CDIM
DOUBLE PRECISION F
DO 10 L=1,IMAX TPA05400
DO 10 J=1,JMAX TPA05410
J1=(J&1)/2 TPA05420
J2=1 TPA05430
IF ( (MOD (J,2)).EQ.0 ) J2=2 TPA05440
J3=J1&J2-1 TPA05450
DO 10 K=1,KMAX TPA05460
K1=(K&1)/2 TPA05470
K2=1 TPA05480
IF ( (MOD(K,2)).EQ.0 ) K2=2 TPA05490
K3=K1&K2-1 TPA05500
DO 6 I=1,3 TPA05510
S=0. TPA05520
DO 5 JZ=J1,J3 TPA05530
DO 5 KZ=K1,K3 TPA05540
I3=KZ&(I-1)*10
I4=K&(I-1)*10
5 S=S&U(L,JZ,I3)
6 F(L,J,I4)=S/FLOAT(K2*J2)
IF(K.EQ.1) F(L,J,K&10)=0.
IF (J.EQ.1) F(L,J,K&20)=0.
10 CONTINUE TPA05590
RETURN TPA05600
END TPA05610
SUBROUTINE PART2 TPA05640
C*****TPA05650
C THERMAL STRESS ANALYSIS OF RECTANGULAR PRISM TPA05660
C PART II STRESS OUTPUT TPA05670
C*****TPA05680
COMMON/STR/ XC1,KOUNT,J,K TPA05690
COMMON/SOL/F(21,10,30),U(21,10,30),IMAX,JMAX,KMAX,SUM,XFAC,TEMP(20
1),ALFA(20),H(20),E(20),PR(20),BDIM,CDIM
DOUBLE PRECISION F
COMMON>IDEN/MIDEN(10),NIDEN(10),NITER
DIMENSION UT(8,3) TPA05730
C TPA05750
C PRINTOUT DISPLACEMENTS TPA05760
C TPA05770

```

```

CALL OUTDIS (U,H,IMAX,JMAX,KMAX,BDIM,CDIM,1)
C
C PRINTOUT STRESSES AT CENTROID OF EACH ELEMENT
C
WRITE(6,1000)
1000 FORMAT(1H1,30X,65HS T R E S S E S   A T   C E N T R O I D S   O F
1  E L E M E N T S//)
KOUNT=3
IM=IMAX-1
JM=JMAX-1
KM=KMAX-1
XC1=H(1)/2.
DO 155 L=1,IM
ALFAT=ALFA(L)*TEMP(L)
DO 150 K=1,KM
DO 150 J=1,JM
CALL SETUT(UT,L,J,K)
150 CALL STRES(H(L),8DIM,CDIM,0.,0.,0.,UT,E(L),PR(L),ALFAT)
155 XC1=XC1&(H(L&1)&H(L))/2.0
900 RETURN
END
SUBROUTINE STRES (A,B,C,PSI,ETA,ZETA,U,E,PR,ALFAT)
C
C SUPPLY U(8,3)-DISPLACEMENTS AT 8 NODES OF ELEMENT
C A,B,C - DIMENSIONS OF ELEMENT E,PR- ELAST CONSTANTS
C PSI,ETA,ZETA - LOCAL COORD. WHERE STRESS IS TO BE CALCD.
C
C S(7) AND EPSI(7) WILL GIVE STRESSES AND STRAINS RESP.
C (XX,YY,ZZ,XY,XZ,YZ, AND EFFECTIVE)
C S AND PRINCIPAL STRESSES AND DIRECTIONS WILL BE PRINTED OUT
C KOUNT IS LINE COUNT ON PAGE BEING PRINTED
C XC1 IS X-COORDINATE OF CENTROID OF LAYER
C
COMMON/STR/ XC1,KOUNT,JZ,KZ
DIMENSION XC(3),W1(6),W2(3,3),W3(3)
DIMENSION FEE(8,4),D(3),XLOC(3),U(8,3),EPSI(7),S(7),FEE1D(32)
EQUIVALENCE (FEE1D(1),FEE(1,1))
DATA(FEE1D(J),J=1,32)/&1.,&1.,&1.,&1.,-1.,-1.,-1.,-1.,
1 &1.,&1.,-1.,-1.,&1.,&1.,-1.,-1.,
2 -1.,&1.,&1.,-1.,-1.,&1.,&1.,-1.,
3 -1.,&1.,-1.,&1.,&1.,-1.,&1.,-1./
D(1)=1./A
D(2)=1./B
D(3)=1./C
XLOC(1)=PSI
TPA05780
TPA05790
TPA05800
TPA05810
TPA05820
TPA05830
TPA05840
TPA05850
TPA05860
TPA05870
TPA05880
TPA05890
TPA05900
TPA05910
TPA05920
TPA05930
TPA05940
TPA05950
TPA05960
TPA06210
TPA06220
TPA06240
TPA06250
TPA06260
TPA06270
TPA06280
TPA06290
TPA06300
TPA06310
TPA06320
TPA06330
TPA06340
TPA06350
TPA06360
TPA06420
TPA06430
TPA06440
TPA06450

```

```

XLOC(2)=ETA
XLOC(3)=ZETA
C
ISTRAN=1
DO 21 I1=1,3
DO 21 I2=1,I1
SUM1=0.
SUM2=0.
DO 20 J=1,8
PROD1=FEE(J,4)
PROD2=FEE(J,4)
DO 12 K=1,3
IF (K.EQ.I2) GO TO 11
PROD1=PROD1*(XLOC(K)&FEE(J,K))
11 IF (K.EQ.I1) GO TO 12
PROD2=PROD2*(XLOC(K)&FEE(J,K))
12 CONTINUE
SUM1=SUM1&PROD1*U(J,I1)*D(I2)
SUM2=SUM2&PROD2*U(J,I2)*D(I1)
20 CONTINUE
S (ISTRAN)=(SUM1&SUM2)/8.0
21 ISTRAN=ISTRAN&1
EPSI(1)=S(1)
EPSI(2)=S(3)
EPSI(3)=S(6)
EPSI(4)=S(2)
EPSI(5)=S(4)
EPSI(6)=S(5)
DO 25 I=1,3
25 EPSI(I)=EPSI(I)-ALFAT
DIL=EPSI(1)&EPSI(2)&EPSI(3)
C1=E*PR/(1.&PR)/(1.-2.*PR)
C2=E/(1.&PR)
SUM2=0.
DO 30 J=1,3
S(J)=C1*DIL&C2*EPSI(J)
30 SUM2=SUM2&S(J)
DO 31 J=4,6
31 S(J)=C2*EPSI(J)
C
CALCULATE EFFECTIVE STRESS AND STRAIN
SUM1=0.
DO 40 J=1,3
40 SUM1=SUM1&(S(J)-SUM2/3.)*2
DO 41 J=4,6
41 SUM1=SUM1&2.*S(J)*2

```

```

TPA06460
TPA06470
TPA06480
TPA06490
TPA06500
TPA06510
TPA06520
TPA06530
TPA06540
TPA06550
TPA06560
TPA06570
TPA06580
TPA06590
TPA06600
TPA06610
TPA06620
TPA06630
TPA06640
TPA06650
TPA06660
TPA06670
TPA06680
TPA06690
TPA06700
TPA06710
TPA06720
TPA06730
TPA06740
TPA06750
TPA06760
TPA06770
TPA06780
TPA06790
TPA06800
TPA06810
TPA06820
TPA06830
TPA06840
TPA06850
TPA06860
TPA06870
TPA06880
TPA06890
TPA06900

```



```

S(7)=SQRT(SUM1)
C
C      OBTAIN PRINCIPAL STRESSES AND DIRECTIONS
W1(1)=S(1)
W1(2)=S(4)
W1(3)=S(2)
W1(4)=S(5)
W1(5)=S(6)
W1(6)=S(3)
CALL JACOBI(W1,W2,W3,3)
IF (KOUNT.GT.5) GO TO 60
WRITE(6,101)
101 FORMAT(25X,74HPOSITION / STRESS COMPONENTS / PRINCIPAL STRESSES ANTPA07100
1D DIRECTIONS (3 LINES)/14X,1HX,13X,1HY,13X,1HZ/12X,2HXX,15X,2HYY, TPA07110
215X,2HZZ,15X,2HXY,15X,2HXZ,15X,2HYZ,9X,10HEFF.STRESS/25X, TPA07120
2 12HPRINC.STRESS,11X, 6HX-COMTPA07130
3P,11X,6HY-COMP,11X,6HZ-COMP,3X,13HOF PRINC.DIR.) TPA07140
KOUNT=KOUNT&3 TPA07150
60 XC(1)=XC1&PSI*A/2. TPA07160
XC(2)=FLOAT(KZ-1)*B&(ETA&1.0)*B/2. TPA07170
XC(3)=FLOAT(JZ-1)*C&(ZETA&1.0)*C/2.0 TPA07180
WRITE(6,102) XC,S,(I,W3(I) ,(W2(J,I),J=1,3),I=1,3) TPA07190
102 FORMAT(1H0,3X,3F14.6/1X,7(1PE17.5)/(15X,16,1PE17.5,3F17.5)) TPA07200
KOUNT=KOUNT&6 TPA07210
IF(KOUNT.LT.53) GO TO 70 TPA07220
KOUNT=0 TPA07230
WRITE(6,103) TPA07240
103 FORMAT (1H1) TPA07250
70 CONTINUE TPA07260
RETURN TPA07270
END TPA07280
SUBROUTINE SETUT(UT,L,J,K) TPA07300
C TPA07310
C      OBTAINS DISPLACEMENTS UT FOR A PARTICULAR ELEMENT TPA07320
C TPA07330
COMMON/SOL/F(21,10,30),U(21,10,30),IMAX,JMAX,KMAX,SUM,XFAC,TEMP(20
1),ALFA(20),H(20),E(20),PR(20),BDIM,CDIM
DOUBLE PRECISION F
DIMENSION UT(8,3) TPA07360
L2=L&1 TPA07370
L3=1 TPA07380
DO 40 L1=1,2 TPA07390
DO 30 I=1,3 TPA07400
I3=K&(I-1)*10
UT(L3,I)=U(L2,J,I3&1)

```



```

C
C LOWER THRESHHOLD BY 2**1/2 TIMES N WHEN NO OFF-DIAGONAL
C ELEMENTS EXCEED CURRENT VALUE
C
35 XNORM=XNORM/SIGMA
C
C NEW SWEEP THROUGH MATRIX
C
40 IND=0
   IJ=0
45 DO 100 J=2,N
   IJ=IJ&1
   JM1=J-1
   DO 100 I=1,JM1
   IJ=IJ&1
   IF(ABS(A(IJ))-XNORM) 100,100,50
C
C ELEMENT EXCEEDS THRESHHOLD - NEW SWEEP NECESSARY
C
50 IND=1
C
C PIVOTAL SET FOR THIS ROTATION
C
   II=(I*(I&1))/2
   JJ=(J*(J&1))/2
   TEMP=A(IJ)
   DII=A(II)
   DJJ=A(JJ)
   XLAM=-TEMP
   XMU=0.5*(DII-DJJ)
   XMEGA= XLAM/SQRT(XLAM*XLAM&XMU*XMU)
   IF(XMU) 55,60,60
55 XMEGA=-XMEGA
C
C CALCULATE SINE AND COSINE OF ANGLE OF ROTATION
C
60 SINE= XMEGA/(SQRT(2.0*(1.0&SQRT(1.0-XMEGA*XMEGA))))
   COSIN= SQRT(1.0-(SINE**2))
C
C TRANSFORM MATRIX AND VECTORS
C
   KJ=(J*(J-1))/2
   KI=(I*(I-1))/2
   DO 95 K=1,N
   IF(K-I) 85,62,65

```

```

62 KI=II
   KJ=KJ&1
   GO TO 92
65 IF(K-J) 70,67,80
67 KJ=JJ
   KI=KI&K-1
   GO TO 92
70 KJ=KJ&1
75 KI=KI&K-1
   GO TO 90
80 KJ=KJ&K-1
   GO TO 75
85 KJ=KJ&1
   KI=KI&1
90 AKJ=A(KJ)
   A(KJ)= A(KI)*SINE&AKJ*COSIN
   A(KI)= A(KI)*COSIN-AKJ*SINE
92 BKI= B(K,I)
   B(K,I)= BKI*COSIN-B(K,J)*SINE
   B(K,J)= BKI*SINE&B(K,J)*COSIN
95 CONTINUE
   A(IJ)= (DII-DJJ)*(COSIN*SINE)&TEMP*((COSIN**2)-(SINE**2))
   A(II)= DII*(COSIN**2)&DJJ*(SINE**2)-(2.0*TEMP*(COSIN*SINE))
   A(JJ)= DII*(SINE**2)&DJJ*(COSIN**2)&(2.0*TEMP*(COSIN*SINE))
100 CONTINUE
    IF(IND) 40,110,40
110 IF(XNORM-ZNORM) 120,35,35
C
C   SORT VALUES AND VECTORS
C
120 DO 140 I=1,N
    II=(I*(I&1))/2
    TEMP=A(II)
    DO 130 J=I,N
        JJ=(J*(J&1))/2
        IF(TEMP-A(JJ)) 130,125,125
125 IT=J
    ITJ=JJ
    TEMP=A(JJ)
130 CONTINUE
    C(I)=A(ITJ)
    A(ITJ)=A(II)
    DO 140 K=1,N
        A(II)=B(K,I)
        B(K,I)=B(K,IT)

```

```
140 B(K,IT)=A(II)
C
C   NORMALIZE VECTORS
C
   DO 175 J=1,N
   XNORM=0.0
   DO 155 I=1,N
155 XNORM=XNORM&B(I,J)*B(I,J)
   XNORM= SQRT(XNORM)
   DO 160 I=1,N
160 B(I,J)=B(I,J)/XNORM
175 CONTINUE
180 RETURN
   END
```

APPENDIX B

SPECIFICATION OF PROBLEMS SOLVED

Eight problems were specified by Fluidyne for solution as part of the work on this project. The computer output for these eight runs has been delivered to Fluidyne. The problem specifications for these runs are given in this appendix. In all solutions four divisions of the block in the y and z directions were used. Ten division in the direction of the temperature gradient (the x direction) were used in each case. A value of Poisson's ratio = 0.29 was used in each case.

Figures 3 and 4 give respectively the variation of the expansion coefficient α and the modulus E with temperature. The variation of temperature with distance from the heated face for the four conditions considered is shown in Fig. 5 through 8. The piecewise linear approximations used in the analyses are also shown in these figure . The layer thicknesses and properties used in the runs are given in Table 3 through 6.

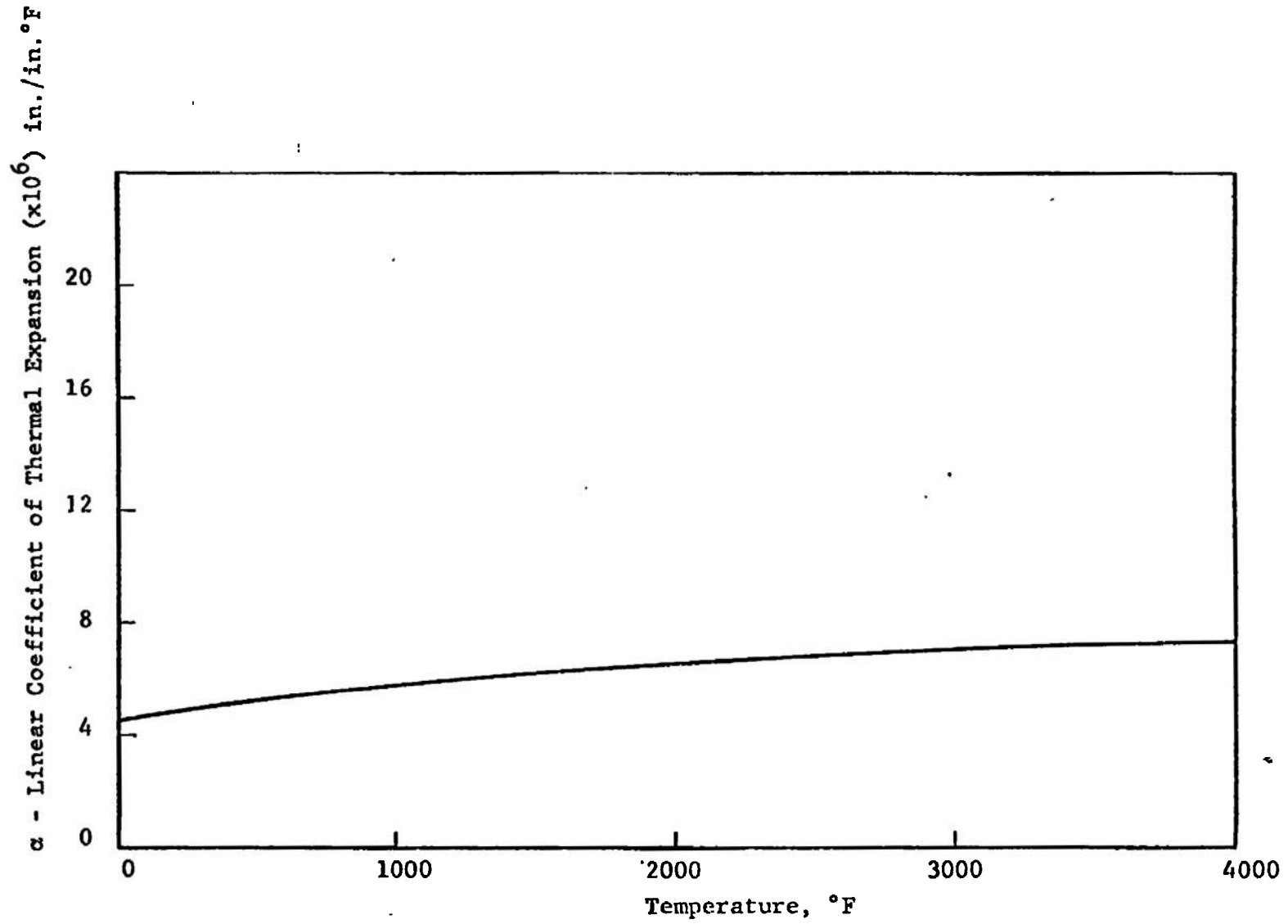


Fig. I-3 COEFFICIENT OF THERMAL EXPANSION, α VS TEMPERATURE T

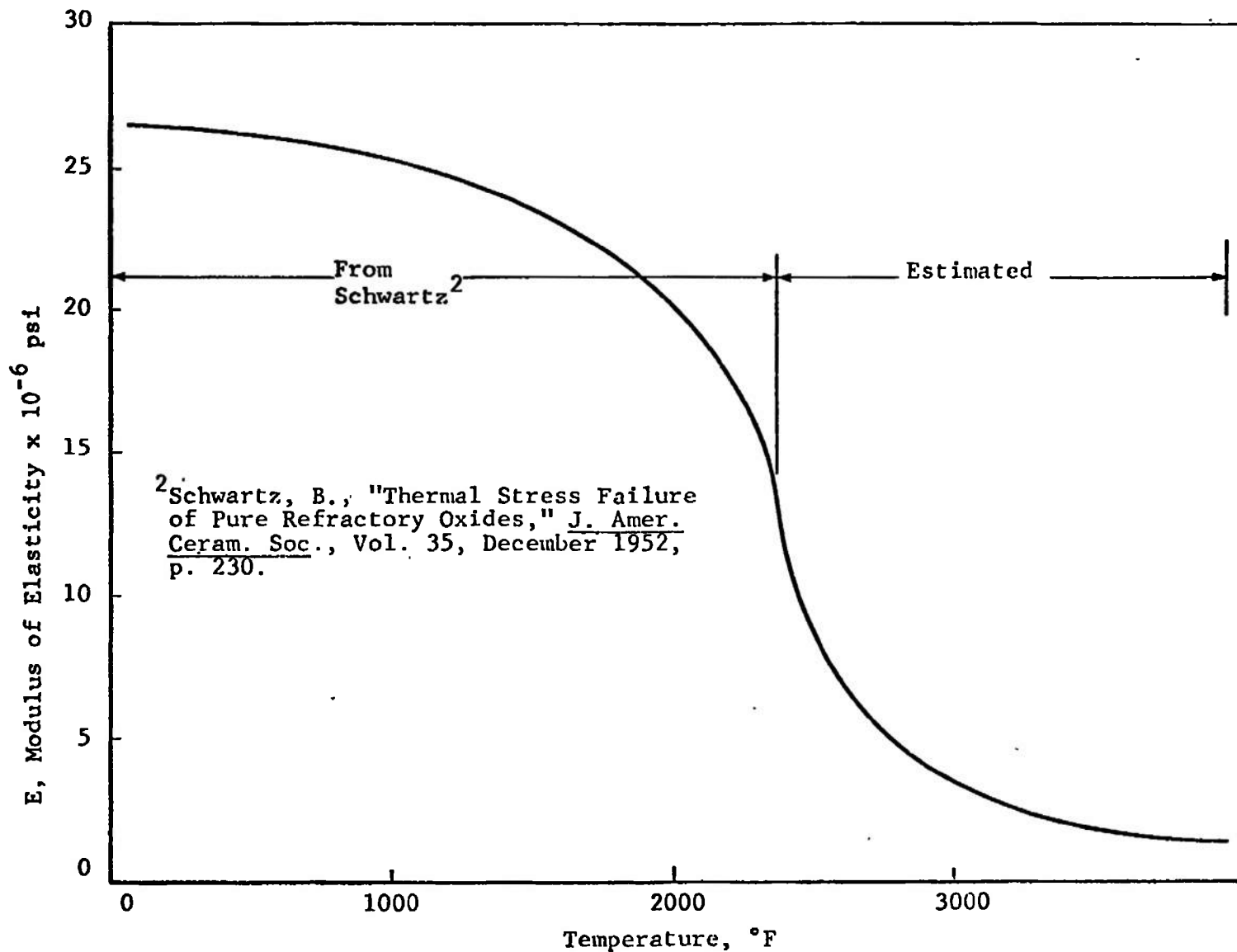


Fig. I-4 MODULUS OF ELASTICITY, E VS TEMPERATURE T

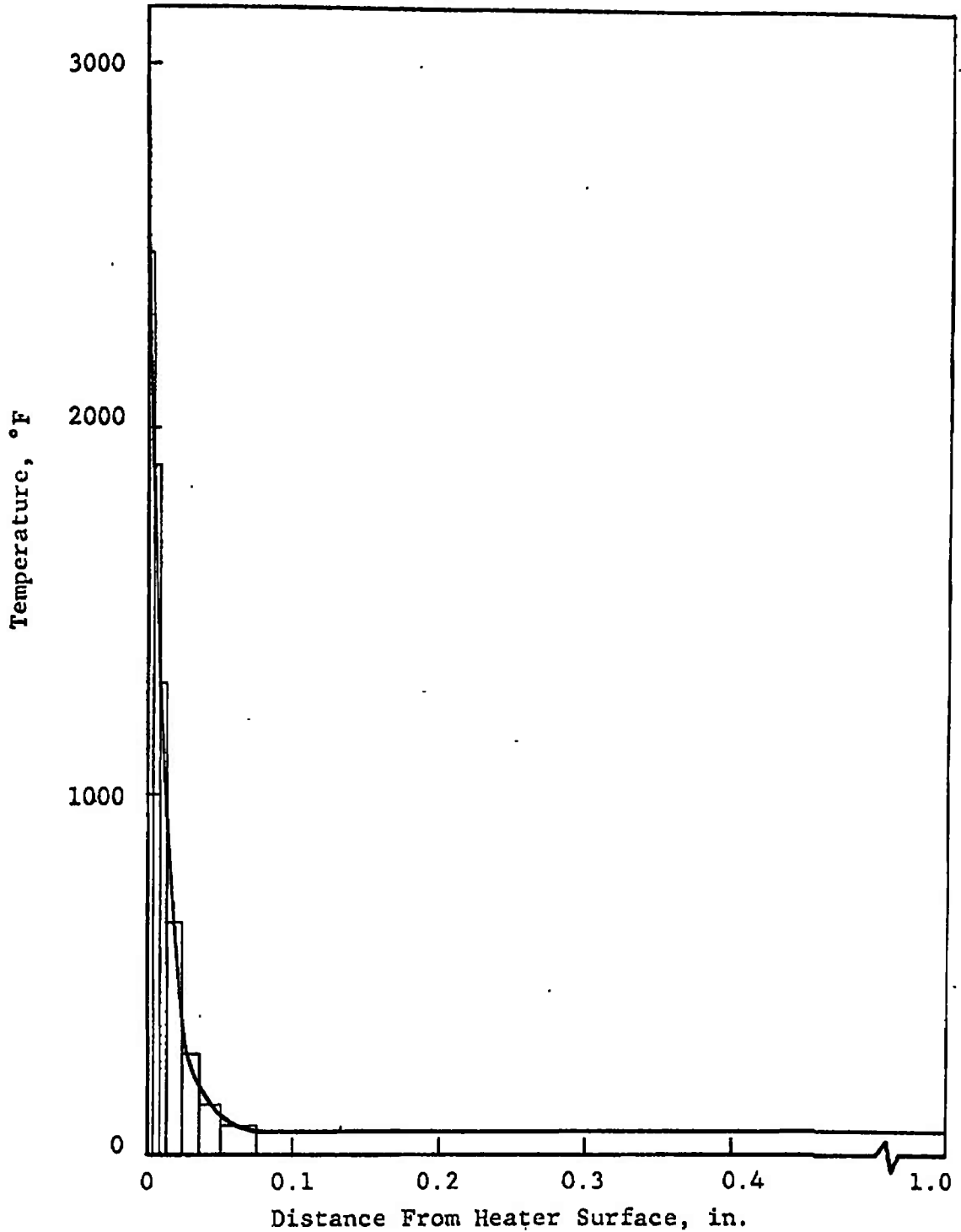


Fig. I-5 PIECEWISE CONSTANT TEMPERATURE APPROXIMATION
FOR TIME = 0.1 SEC (RUN 1)

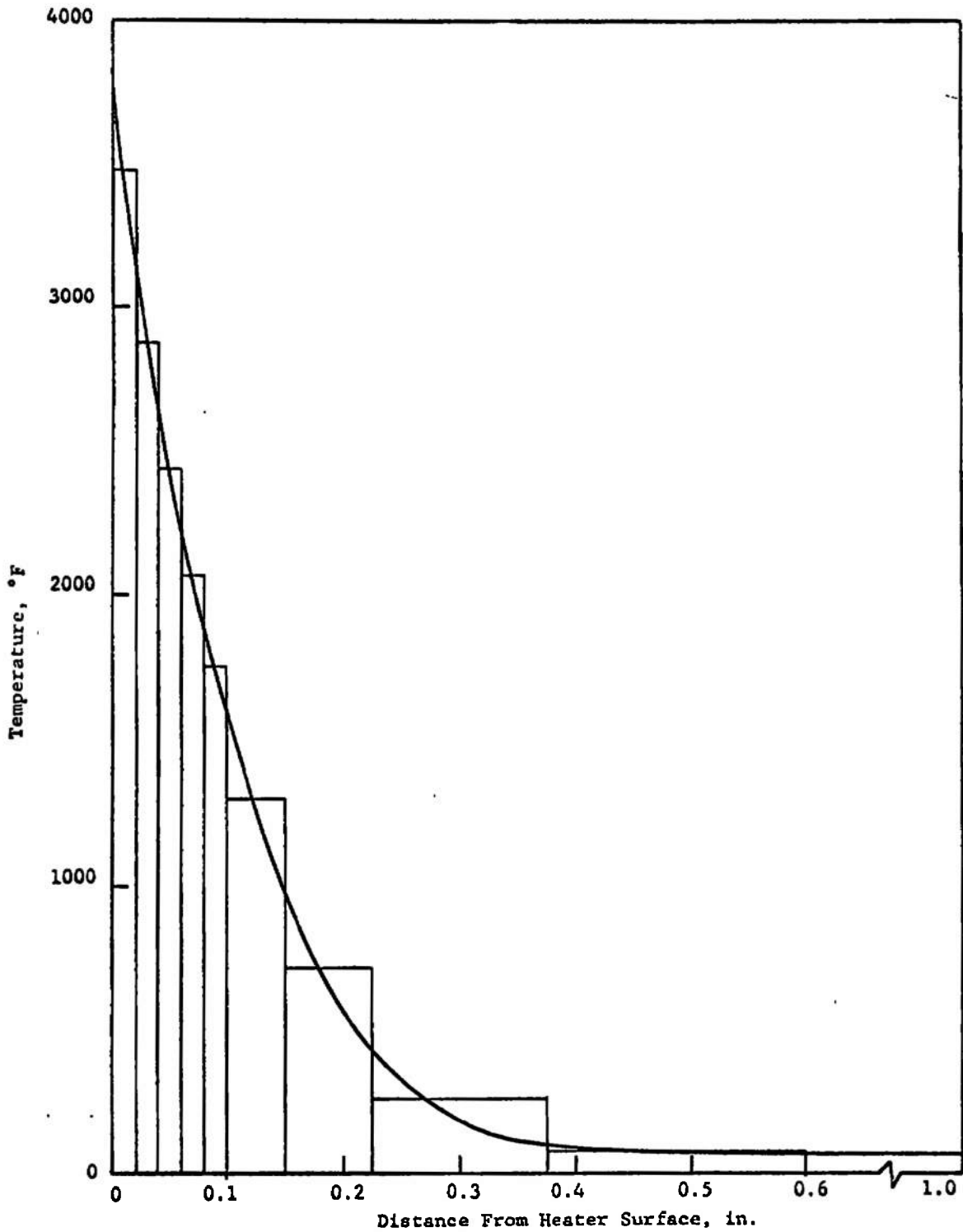


Fig.I-6 PIECEWISE CONSTANT TEMPERATURE APPROXIMATION
FOR TIME = 10 SEC, THICKNESS $t = 1$ IN.
(Runs 2, 4, 5 and 7)

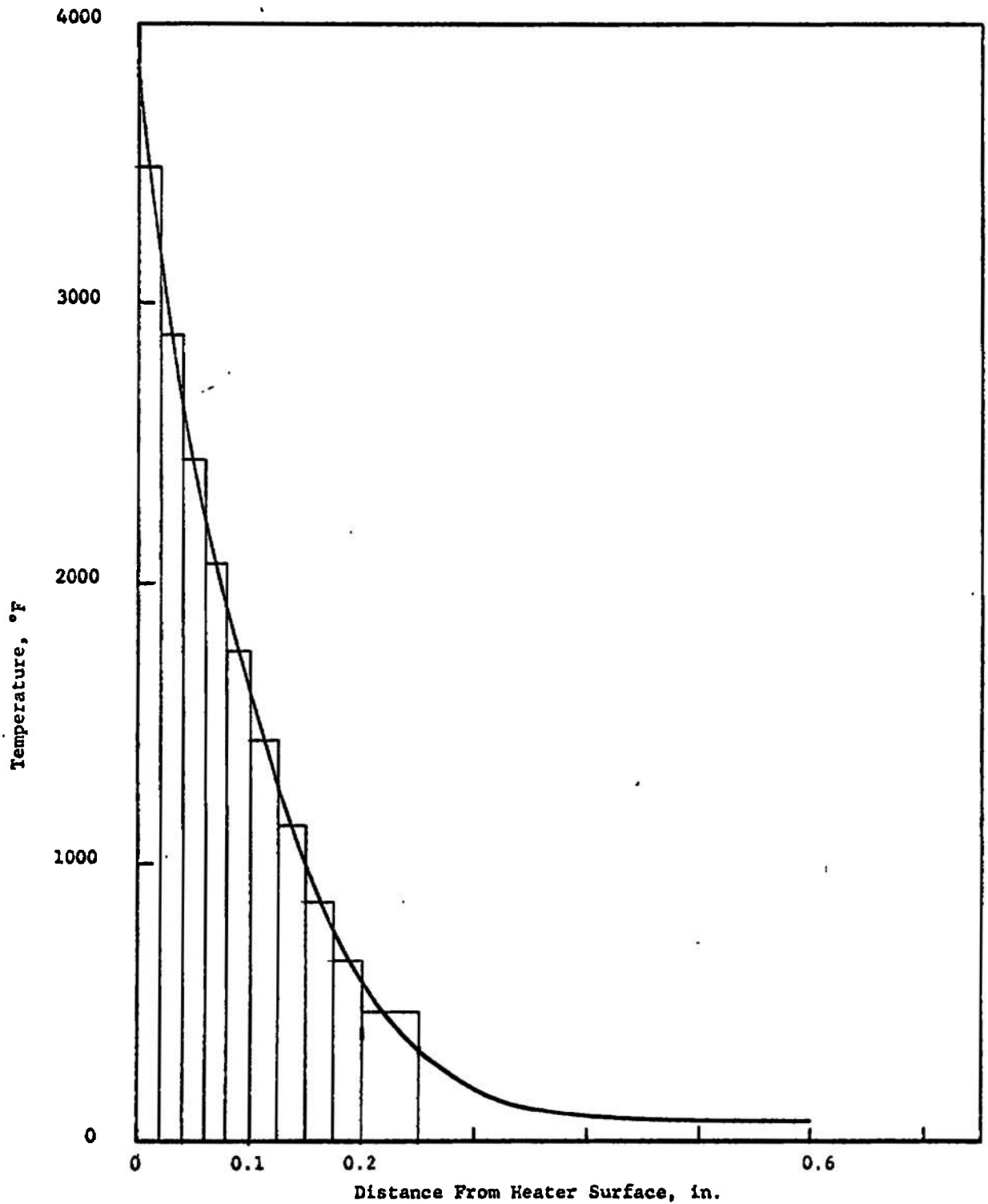


Fig. I-7 PIECEWISE CONSTANT TEMPERATURE APPROXIMATION
FOR TIME = 10 SEC, THICKNESS $t = 0.25$ IN. (Run 6)

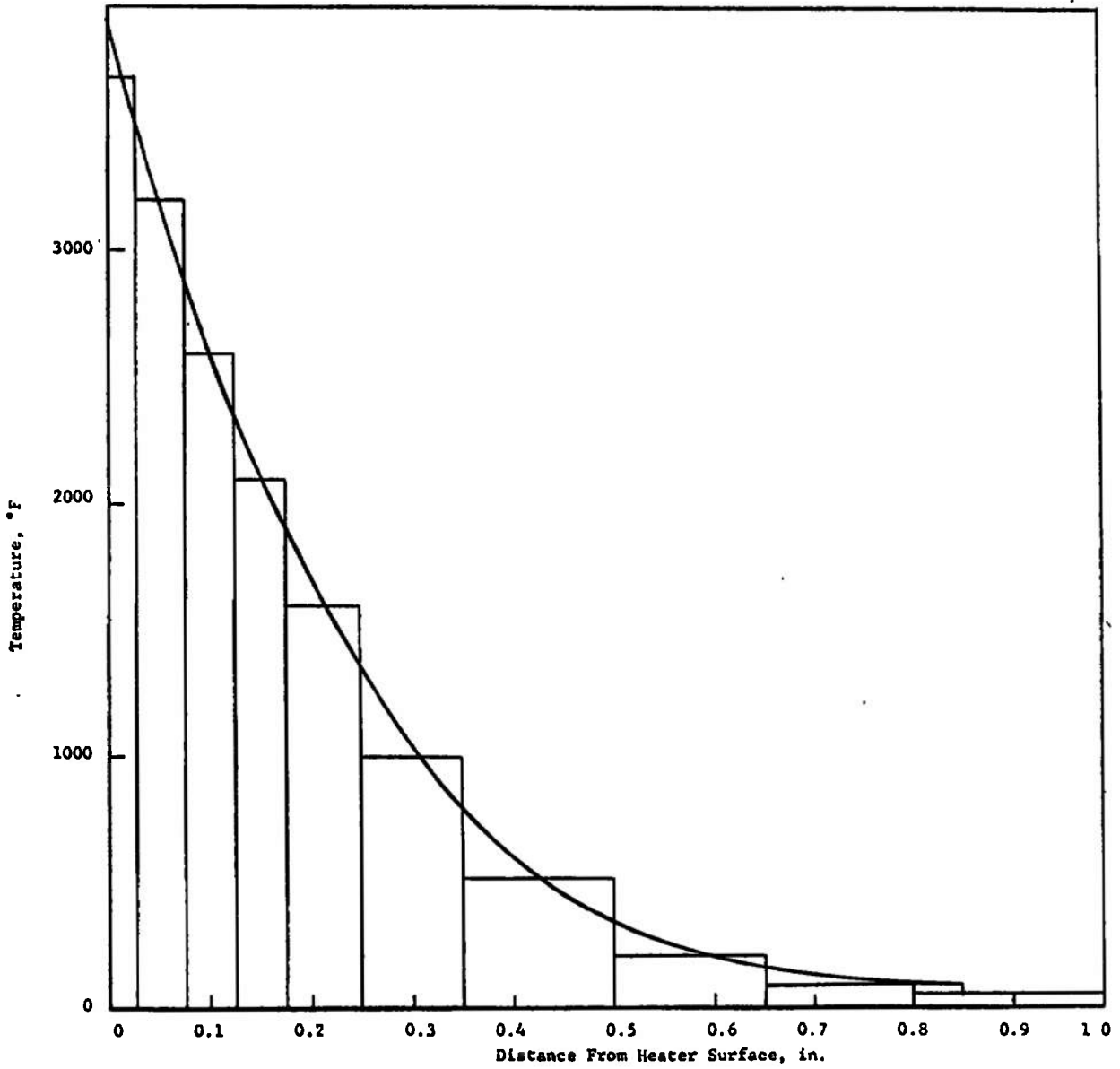


Fig. I-8 PIECEWISE CONSTANT TEMPERATURE APPROXIMATION
FOR TIME = 40 SEC, (Runs 3 and 8)

TABLE I-2
 PROBLEM SPECIFICATIONS FOR RUNS 1 to 8

Run	Condition	Time sec	Dimensions, in.		
			a	b	t
1	Cold Start	0.1	1.0	1.0	1.0
2	Cold Start	10.0	1.0	1.0	1.0
3	Cold Start	40.0	1.0	1.0	1.0
4	Cold Start	10.0	2.0	2.0	1.0
5	Cold Start	10.0	0.5	0.5	1.0
6	Cold Start	10.0	1.0	1.0	0.25
7	Cold Start	10.0	1.0	0.5	1.0
8*	Cold Start	40.0	1.0	1.0	1.0

*The material properties for Run 8 were constant, with the value of each constant at its value at room temperature.

TABLE I-3
DATA FOR RUN 1

Layer No.	Thickness H	Temperature T	Young's Modulus E	Thermal Coefficient α
1	0.005	2480	9.0×10^6	6.8×10^{-6}
2	0.005	1900	21.0×10^6	6.5×10^{-6}
3	0.005	1300	24.5×10^6	6.1×10^{-6}
4	0.010	650	26.0×10^6	5.4×10^{-6}
5	0.010	280	26.4×10^6	4.9×10^{-6}
6	0.015	140	26.5×10^6	4.7×10^{-6}
7	0.025	80	26.5×10^6	4.6×10^{-6}
8	0.125	60	26.5×10^6	4.55×10^{-6}
9	0.300	60	26.5×10^6	4.55×10^{-6}
10	0.500	60	26.5×10^6	4.55×10^{-6}

Cold Start

Time = 0.1 sec

Thickness = 1.0 in.

TABLE I-4
DATA FOR RUNS 2, 4, 5, and 7

Layer No.	Thickness H	Temperature T	Young's Modulus E	Thermal Coefficient α
1	0.020	3480	1.8×10^6	7.2×10^{-6}
2	0.020	2880	4.0×10^6	7.0×10^{-6}
3	0.020	2440	10.0×10^6	6.8×10^{-6}
4	0.020	2070	19.3×10^6	6.6×10^{-6}
5	0.020	1760	22.0×10^6	6.4×10^{-6}
6	0.050	1300	24.5×10^6	6.1×10^{-6}
7	0.075	720	25.9×10^6	5.5×10^{-6}
8	0.150	260	26.4×10^6	5.1×10^{-6}
9	0.225	80	26.5×10^6	4.6×10^{-6}
10	0.40	60	26.5×10^6	4.55×10^{-6}

Cold Start

Time = 10 sec

Thickness = 1.0 in.

TABLE I-5
DATA FOR RUN 6

Layer No.	Thickness H	Temperature T	Young's Modulus E	Thermal Coefficient α
1	0.020	3480	1.8×10^6	7.2×10^{-6}
2	0.020	2880	4.0×10^6	7.0×10^{-6}
3	0.020	2440	10.0×10^6	6.8×10^{-6}
4	0.020	2070	19.3×10^6	6.6×10^{-6}
5	0.020	1760	22.0×10^6	6.4×10^{-6}
6	0.025	1440	23.9×10^6	6.2×10^{-6}
7	0.025	1140	25.0×10^6	5.9×10^{-6}
8	0.025	860	25.6×10^6	5.6×10^{-6}
9	0.025	650	26.0×10^6	5.4×10^{-6}
10	0.050	460	26.2×10^6	5.2×10^{-6}

Cold Start

Time = 10 sec

Thickness = 0.25 in.

TABLE I-6
DATA FOR RUN 3

Layer No.	Thickness H	Temperature T	Young's Modulus E	Thermal Coefficient α
1	0.025	3700	1.4×10^6	7.2×10^{-6}
2	0.050	3200	2.5×10^6	7.2×10^{-6}
3	0.050	2600	6.8×10^6	6.9×10^{-6}
4	0.050	2100	19.0×10^6	6.7×10^{-6}
5	0.075	1600	23.2×10^6	6.3×10^{-6}
6	0.100	1000	25.4×10^6	5.8×10^{-6}
7	0.150	540	26.2×10^6	5.1×10^{-6}
8	0.150	220	26.4×10^6	4.8×10^{-6}
9	0.150	100	26.5×10^6	4.6×10^{-6}
10	0.200	60	26.5×10^6	4.55×10^{-6}

Cold Start

Time = 40 sec

Thickness = 1.0 in.

APPENDIX II
DESCRIPTION OF MODIFIED
THERMAL STRESS COMPUTER PROGRAM, TPA II

Prepared by:
Illinois Institute of Technology Research Institute

November 1968

DESCRIPTION OF TPA II, CDC VERSION

A. INTRODUCTION

TPA II is a version of TPA which has been modified to be compatible with the CDC 6600 system and to extend the problem size capacity. The program obtains thermal stresses created within a rectangular prism by the variation of temperature and material properties in one direction. The governing equations are formulated by means of the finite element method and then solved by the Gauss-Seidel method. The TPA II version can handle problems with up to 20 layers of elements in the direction of the thermal gradient and up to nine elements in each of the other two directions. To facilitate convergence for these large problems, the Gauss-Seidel algorithm has been altered so as to alleviate the difficulties caused by the fixed points and roundoff error.

B. INPUT DATA

Let the direction of the thermal gradient be denoted by x and let the remaining two orthogonal directions be denoted by y and z respectively. The x -direction must correspond to an axis of the prism. Since the prism is symmetric with respect to the x - y and x - z planes, only a quadrant of the prism is considered. The geometry of this quadrant is specified by giving its y and z dimensions and the number of nodes desired in x , y , and z directions. The nodes in the y and z directions will be equally spaced. The spacing between the nodes in the x -direction which corresponds to the thicknesses of the element layers, are specified by the user in the layer cards.

For each layer of elements the user must provide a "layer" card which gives its thickness and the temperature, Young's modulus E , Poisson's ratio ν , and the thermal expansion coefficient α .

The only other required input is composed of two control numbers NUREAD and NUPRNT and the following parameters for the Gauss-Seidel method: the maximum number of iterations NIT, the error printout cycle NPERR, displacement and modified force printout cycle NPOTPT, the tolerance TOL, the initial relaxation factor XFAC and the error parameters, DELERR. The initial relaxation factor should be about 1.5. After the iterative method is started if a given iteration does not reduce the error by a factor of at least DELERR, the relaxation factor is reduced. The Gauss-Seidel method terminates after the error fails to decrease, when the number of iterations exceeds NIT, or if the error meets the tolerance TOL. During the iterations the error and displacements are printed out according to the value of NPERR and NPOTPT, respectively. It is recommended that the displacements not be printed out at all during the solution for larger problems since this output is very time-consuming.

The control number NUREAD determines whether the starting values of the displacements are to be read from an input tape or to be computed. The second control number, NUPRNT gives the user the option of saving the displacements on tape or interpolating to a lattice with a larger number of elements. These options allow the user to run the problem to a certain point, save the displacements on a tape and continue later from the same point by using these displacements as starting values.

The interpolation routine inserts the displacement values for a lattice with n_1 elements in the z-direction, n_2 elements in the y-direction, and m elements in the x-direction to obtain the starting values for $2n_1$ and $2n_2$ by m lattice. When this option is used the second problem is then automatically run with the interpolated displacements as starting values. A detailed description of the input data required is given in Table 1.

C. DESCRIPTION OF OUTPUT

The initial output is an echo of all data. The final output consists of the displacements and stresses. The stresses are computed and printed at the centroids of all elements. The stresses are printed out in the following manner. For each point there are five lines. The first line gives the x, y and z coordinates of the point. The second line gives the xx, yy, zz, xy, xz and yz components of the stresses and the effective stress σ_e . The effective stress σ_e is computed by the formula

$$\sigma_e^2 = (\sigma_{xx} - S)^2 + (\sigma_{yy} - S)^2 + (\sigma_{zz} - S)^2 + 2(\sigma_{xy} + \sigma_{yz} + \sigma_{xz})$$

where

$$S = 1/3(\sigma_{xx} + \sigma_{yy} + \sigma_{zz}).$$

The remaining three lines give the three principal stresses and the corresponding principal directions. If the solutions to additional problems are desired, the data sets are repeated. Any number of problems can be solved in sequence.

TABLE
INPUT DATA FORMAT

Card 1	TITLE CARD (12A6)	
Column		
1 - 72	Any alphanumeric information	
Card 2	PARAMETER CARD (6I5,4F10.0)	
1 - 5	NX	- Number of nodes in x-direction
6 - 10	NY	- Number of nodes in y-direction
11 - 15	NZ	- Number of nodes in z-direction
16 - 20	NIT	- Maximum number of iterations
21 - 25	NPERR	- Error printout cycle
26 - 30	NPOTPT	- Displacement and modified force printout cycle
31 - 40	DIMY	- y-dimension of prism quadrant
41 - 50	DIMZ	- z-dimension of prism quadrant
51 - 60	TOL	- Error tolerance for Gauss-Seidel
61 - 65	XFAC	- Initial relaxation factor
66 - 70	DELERR	- Error parameter δ , if the error for iteration i is ϵ_i and the previous error ϵ_{i-1} , the relaxation factor is reduced if $(\epsilon_{i-1} - \epsilon_i) / \epsilon_i < \delta$.
Card 3	LAYER PROPERTY CARD (15,5E10.0)	
Column		
1 - 5	Layer number	
6 - 15	H	- Thickness of layer
16 - 25	T	- Temperature of layer
26 - 35	E	- Young's modulus for layer
36 - 45	PR	- Poisson's ratio for layer
46 - 55	ALFA	- Thermal expansion coefficient for layer
Card 4	CONTROL CARD	
Column		
1 - 5	NUREAD	- Determines how initial displacements are obtained = 0 calculated = 2 read from tape 8
6 - 10	NUPRNT	- Gives the following options = 0 none of the options used = 1 displacements are saved on tape 10 = 2 displacements are used to interpolate to a larger lattice
Card 5	INTERPOLATION CARD (OPTIONAL) (3I5,2E10.0)	
Column		
1 - 5	I	- Code number; must equal 619 if interpolation is to be performed.
6 - 10	IMAX	- Number of nodes in x-direction for interpolated lattice
11 - 15	JMAX	- Number of nodes in y-direction for interpolated lattice
16 - 20	KMAX	- Number of nodes in z-direction for interpolated lattice
21 - 25	NIT	- Maximum number of iterations to be performed for second problem
26 - 30	NPERR	- Error printout cycle for second problem
31 - 35	NPOTPT	- Displacement printout cycle for second problem
36 - 45	TOL	- Error tolerance for second problem
46 - 55	XFAC	- Initial relaxation factor for second problem
(If interpolation option is used, Card 4 must be repeated after Card 5)		

DOCUMENT CONTROL DATA - R & D

(Security classification of title, body of abstract and indexing annotation must be entered when the overall report is classified)

1. ORIGINATING ACTIVITY (Corporate author) Fluidyne Engineering Corporation Minneapolis, Minnesota		2a. REPORT SECURITY CLASSIFICATION UNCLASSIFIED	
		2b. GROUP N/A	
3. REPORT TITLE STUDY OF AN UNCOOLED NOZZLE THROAT FOR A LARGE HYPERSONIC WIND TUNNEL			
4. DESCRIPTIVE NOTES (Type of report and inclusive dates) Final Report			
5. AUTHOR(S) (First name, middle initial, last name) P. B. Hasselquist, K. W. Smith, and D. G. DeCoursin			
6. REPORT DATE May 1970	7a. TOTAL NO. OF PAGES 137	7b. NO. OF REFS 6	
8a. CONTRACT OR GRANT NO. AF40(600)-1186	8a. ORIGINATOR'S REPORT NUMBER(S) AEDC-TR-70-92		
b. PROJECT NO. 3012	8b. OTHER REPORT NO(S) (Any other numbers that may be assigned this report) N/A		
c. Program Element 62402F			
d. Task 07			
10. DISTRIBUTION STATEMENT This document has been approved for public release and sale; its distribution is unlimited.			
11. SUPPLEMENTARY NOTES Available in DDC		12. SPONSORING MILITARY ACTIVITY Arnold Engineering Development Center, Air Force Systems Command, Arnold Air Force Station, Tennessee 37389	
13. ABSTRACT A study was made of the feasibility of an uncooled throat for a large hypersonic wind tunnel facility using currently available materials. Maximum fullscale stagnation conditions would be 2000psi, 4400°R, 1500 lb/sec air flow, and throat diameter 10.5-inches. The basic throat concept was that of a ceramic insulation layer, composed of small pieces, that would form a protective liner within a metal structure. High resistance to thermal spalling was the material characteristics of greatest importance. Tests were made of several zirconia materials and two zirconium diboride compositions by exposing them to hot air flow in a sonic throat at maximum conditions of 800 psi and 3550°R. Behavior of the zirconia materials ranged from minor cracking to complete fragmentation. The zirconium-diborides did not crack and were oxidation resistant at these conditions. In addition, the thermal stress distribution was studied for the individual blocks that would form the throat insulation. For this purpose the three-dimensional stress distribution was calculated for mechanically unrestrained blocks having one-dimensional temperature distributions. Effects of temperature distribution, block size and block shape were determined. The computer program is included with the report. It was concluded that currently available materials are not satisfactory for a throat that would be used with no cooling. Some of the materials tested may be satisfactory if the thermal shock conditions were reduced by use of film cooling (less than that required for a backside cooled throat) and by preheating with a flow of air through the throat during heater pressurization. A major problem in use of zirconia would be the attachment of the insulation layer to the backup structure. Use of zirconium-diboride would require a design concept that would be compatible with its high thermal conductivity. Both materials might be used to advantage in a single design.			

14. KEY WORDS	LINK A		LINK B		LINK C	
	ROLE	WT	ROLE	WT	ROLE	WT
hypersonic wind tunnels						
hypersonic nozzles						
zirconium oxides						
zirconium borides						
spalling						
cracking (fracturing)						
fragmentation						
temperature distribution						
thermal stresses						